Universidade de Aveiro Departamento de
2020 Eletrónica, Telecomunicações e Informática

Miguel Ângelo
dos Santos Rosa

Controlo de Temperatura de um Gasificador de Biomassa

Temperature Control of a Biomass Gasifier

Miguel Ângelo
Santos Rosa

Controlo de Temperatura de um Gasificador de Biomassa

Temperature Control of a Biomass Gasifier

Dissertação apresentada à Universidade de Aveiro para cumprimento dos requisitos necessários à obtenção do grau de Mestre em Engenharia Eletrónica e Telecomunicações, realizada sob a orientação científica do Professor Doutor Alexandre Manuel Moutela Nunes da Mota, Professor Associado do Departamento de Eletrónica, Telecomunicações e Informática da Universidade de Aveiro e do Professor Doutor Valter Filipe Miranda Castelão da Silva, Professor Adjunto na Escola Superior de Tecnologia e Gestão de Águeda da Universidade de Aveiro.

o júri / the jury

presidente / president

Professor Doutor Telmo Reis Cunha
Professor Auxiliar do Departamento de Electrónica, Telecomunicações e Informática da Universidade de Aveiro

vogais / examiners committee

Professor Doutor José António Barros Vieira
Professor Adjunto do Instituto Politécnico de Castelo Branco

Professor Doutor Valter Filipe Miranda Castelão da Silva
Professor Adjunto na Escola Superior de Tecnologia e Gestão de Águeda da Universidade de Aveiro

agradecimentos / acknowledgements

Aos meus orientadores Prof. Doutor Alexandre Manuel Moutela Nunes da Mota e Prof. Doutor Valter Filipe Miranda Castelão da Silva pela orientação, disponibilidade e acompanhamento ao longo deste trabalho.
Ao Prof. Doutor Miguel Lienhard Mendonça pelo apoio e disponibilidade.
Aos meus colegas João Patela e José Antunes pela ajuda prestada em todos os momentos nos quais esta foi procurada.
Aos amigos que me acompanharam ao longo de todo o meu percurso.
Aos meus Pais e Irmão pelo apoio, sempre incondicional.

Palavras-Chave Gasificador Downdraft, Biomassa, MPC, Identificação de Sistemas, Instrumentação

Resumo

O desenfreado crescimento da crise ambiental e uso insustentável de combustíveis fósseis vivido nas últimas décadas tem vindo a tornar-se num catalisador na busca de soluções carbonicamente neutras de produção de energia.

Este facto levou ao ressurgimento dos processos de gasificação, principalmente de biomassa, como um tema na comunidade de pesquisa e desenvolvimento. Esta tecnologia foi predominante durante a segunda guerra mundial, período no qual a dificuldade de obtenção de petróleo levou acréscimo da sua necessidade, sendo carvão o combustível utilizado. Com o fim da guerra, veio também o fim do seu desenvolvimento.

Inicialmente, será realizada uma revisão de literatura que culminará na escolha dos instrumentos de medição e atuação necessários para proceder à monitorização e controlo dos parâmetros operacionais do processo de gasificação. De modo a facilitar a analise dos dados presentes nestes sensores foi desenvolvida uma aplicação de visualização de informação.

Findada esta etapa procedeu-se a uma nova revisão da literatura focada na procura de um modelo para o processo de gasificação. Esta revisão revelou as redes neuronais como sendo a melhor topologia para descrever o processo. Utilizando dados disponíveis na literatura procedeu-se à identificação do sistema em causa. O modelo desenvolvido foi utilizado para estabelecer um ambiente de simulação e desenho de controladores e assim, desenvolver um controlador preditivo baseado em modelo para controlar a temperatura dentro do gasificador.

O modelo desenvolvido apresenta um grande potencial como modelo de predição, apesar da deterioração do seu desempenho quando usado como simulador. O controlador desenvolvido foi capaz de estabilizar a saída gerada pelo modelo de simulação para todos os *set-points* testados. O trabalho desenvolvido constitui uma base de trabalho bastante completa que deverá facilitar desenvolvimentos futuros.

Keywords Downdraft Gasifier, Biomass, MPC, System Identification, Instrumentation

Abstract

In recent history, the growing environmental crisis and the unsustainable overuse of fossil fuels have become a catalyst for the development of environmentally friendly or carbon neutron energy sources.
Such fact lead to the reemergence of gasification in the research and development community. This technology was prominent during World War II due to the unavailability of oil existent at that time, mostly using coal as fuel. With the end of the war, so came the end of its development.
Initially, the literature will be reviewed in order to assess the instrumentation technologies needed to measure the gasification process' operational parameters, and thus, allow its monitoring and control. In order to facilitate the analysis of the data from the developed instrumentation system, a visualization tool was developed.
The literature was then reviewed again in order to find the most suitable model topology for the gasification process. This revealed neural networks as the most reliable model architecture for such endeavor. A gasification model was then devised using experimental data present in the literature. The devised model was then used to establish a simulation and controller design environment. This enabled the development of Model Predictive Controller to control the temperature inside the gasifier.
The devised model showed great potential as a prediction model, in spite of the deterioration presented when used as a simulator. The developed controller was able to stabilize the model generated output for all tested set-points. The develop work constitutes a solid ground for future work.

List of contents

List of figures

List of acronyms

ADC	Analog-to-Digital Converter
BFB	Bubbling Fluidized Bed
BLDC	Brushless Direct Current
CFB	Circulating Fluidized Bed
CFD	Computational Fluid Dynamics
CGE	Cold Gas Efficiency
EC	Electronically Commutated
EMF	Electromotive Force
ER	Equivalence Ratio
ESTGA	Escola Superior de Tecnologia e Gestão de Águeda
GPC	Generalized Predictive Control
GSTC	Global Syngas Technologies Council
I^2C	Inter-Integrated Circuit
IC	Integrated Circuit
LHV	Low Heating Value
MISO	Multiple Input Multiple Output
MPC	Model Predictive Control
MSE	Mean Squared Error
NARNN	Nonlinear Autoregressive Neural Network
NARX	Nonlinear Autoregressive with Exogenous inputs
NARXNN	Nonlinear Autoregressive with Exogenous inputs Neural Network
NMSE	Normalized Mean Squared Error
NTC	Negative Temperature Coefficient
PCA	Principle Component Analysis
PID	Proportional Integral Derivative
PWM	Pulse Width Modulation

RTD	Resistance Temperature Detector
SPI	Serial Peripheral Interface
SRAM	Static Random Access Memory
SVG	Scalable Vector Graphics
UART	Universal Asynchronous Receiver-Transmitter

CHAPTER 1

Introduction

1.1 Motivation

The growing environmental crisis, scarcity of fossil fuels and the consequential instability of their price has propelled the renewable energy market into unforeseen proportions. At the present day, nearly 82% of the world's energy requirements are supplied by the big three fossil fuels: oil, coal and natural gas. The next biggest contribution, at about 10% is derived from biomass. In developing countries, the contribution of biomass in energy requirements rises to 35% with over 90% being used in the form of traditional fuel [1].

Biomass resources are prominently solid, thus being unfit for utilization in many sectors, such as transport and domestic. As so, a special interest arises in methods that are able to convert biomass into liquid or gaseous fuels, namely gasification.

Gasification has been used for over 200 years in electricity and heat production. This technology was extensively used in Europe from 1940 to 1975 with its gas being serving as fuel for combustion engines and as feedstock for synthetic fuels. Ground transportation saw a massive use of gasifiers during this period, however, the end of world war II and the resulting high availability of oil fostered a loss of interest in this technology. This was, nonetheless, the time when some countries, mostly developing, started seeing gasification as an alternative for less resourceful citizens.

Nowadays, gasification is again seeing further research and commercial investment with the premium shifting to the gasification of biomass and waste material. In addition to providing syngas for subsequent biofuel synthesis, gasification of biomass and waste has proven to have a higher efficiency in electricity generation when compared to more conventional methods such as incineration.

Some technological challenges remain unsolved and currently block the way for a robust market penetration to happen. One of the challenges is the optimization and understanding of the reactor's behaviour which constitutes the lowest efficiency point in a gasification system. Another challenge is the development of cost effective gas cleaning systems. These are needed to prevent environmental hazards and make the produced fuel fit for most applications.

1.2 Objectives

This dissertation will focus on the design of the instrumentation, visualization and control layers of the gasification system developed by the University of Aveiro - Águeda School of Technology and Management, ESTGA [2, 3]. This will allow supervised operation and control of the system which will be needed for its future optimization. After the conclusion of this project the following objectives should be achieved:

- Definition of the key parameters that need to be measured;
- Instrumentation proposal to achieve these measurements;
- Implementation of a visualization tool to monitor such parameters;
- Definition of the best modelling approach for system identification;
- System identification with Neural Networks;
- Temperature control of the devised system with a Model Predictive Controller.

1.3 Metodology

As gasification is a complex process [4], this dissertation will start with a research of its operating principles. The know-how gained at this point should allow timely discrimination of the problems that may arise from the subsequent steps.

This will be followed by research in the instrumentation field as to get a grasp of the current technologies available to quantify the operating parameters of a gasifier. The outcome should consist of a list of sensors and actuators that corroborate the constraints disseminated in the previous step and the products of similar research. Development of a visualization software application will then take place. The aim of the software is to monitor the operation of the gasifier whilst providing a simple post operational data analysis tool. As so, it was devised taking into consideration the user's needs and potential problems determined in the second Chapter.

As current conditions do not enable the depuration of the previous steps, a study of the modelling approaches used in the literature will follow. The study will be composed by a description and critical comparison between the available options. Using the appropriate model topology, system identification will follow endeavoring the implementation of a simulation environment, in which a temperature controller may be designed. The dissertation will then be concluded with the implementation of a Model Predictive Controller.

1.4 Structure

This dissertation is composed of eight chapters where the work developed is explained. A short overview of these Chapters is here presented:

- In Chapter 2: The Gasification Process, an explanation of the gasification process and its governing parameters will be given;
- In Chapter 3: Instrumentation Principles, an exposition of the available technologies will take place along with the analysis of its advantages and disadvantages;
- In Chapter 4: Instrumentation System, the chosen sensors and actuators and the underlying reasons for such choices will be assessed along with the development of the visualization tool;
- In Chapter 5: System Identification: Model Comparison, a description and comparison of the modelling topologies used in the literature will be given;
- In Chapter 6: System Identification, the devised system identification procedure will be assessed;
- In Chapter 7: Temperature Control, the implementation of a Model Predictive Controller will take place;
- In Chapter 8: Conclusion, the final assessments derived from the elaboration of this dissertation will be documented in conjunction with proposals for its continuation.

CHAPTER 2

The Gasification Process

Gasification is a thermochemical process that converts a solid or liquid substance of carbonic composition into a gaseous fuel by providing it with a gasifying agent. It differs from typical burning for maintaining the amount of oxygen present in the process at lower quantities than those needed for combustion. In its raw form, the gas generated is known as producer gas but by ridding it of its impurities, synthesis gas is formed, ideally comprised of carbon monoxide and hydrogen.

The process is characterized by four different sub-processes: drying and heating, pyrolysis, combustion or oxidation and reduction or gasification.

2.1 Drying and heating

The first step in any thermochemical process is the heating of the fuel particles up to system temperature. The heating rate of such process can vary from 100ºC/s to 1000ºC/s depending on the type of gasifier.

Concurrently to the heating, water present in the biomass' surface and pores evaporates, typically reducing the moisture content in biomass below 5%. The evaporation consumes energy forcing a decrease in the heating rate. Because of this, humidity in biomass is a major factor in the gasification process and, past certain values, biomass needs to be dried before being used as fuel [5].

Some authors choose not to include drying and heating in the phases of the gasification process as no real chemical reactions take place but it is nonetheless, always present.

2.2 Pyrolysis

Pyrolysis is the name given to the degradation of material caused by heat [6]. It is an intricate process as products differ depending on temperature, pressure and heat losses. Below 200ºC, only water is driven off. From 200ºC to 280ºC acetic acid and water are produced. In the 280-500ºC range, real pyrolysis occurs producing large quantities of tar and gases containing CO_2. In the range 500-700ºC, gas production is small and contains Hydrogen

[7]. Another variability inducing factor is the biomass' composition, depending on which the process may be considered slightly endothermic or exothermic [8].

In the range of interest, from 280ºC to 500ºC, the process is described as follows.

Initially, fuel particles start dehydrating, generating water vapor, carbon dioxide, formic acid and acetic acid. Complex reactions occur at this stage due to thermal decomposition and the cracking of organic matter. The quality of biomass, and its heat transferring capacities, influence the reaction's conversion time and, inevitably, the quantity of products generated. Before leaving the pyrolysis zone, exothermic reactions between the previous products takes place forming charcoal and more volatile gases.

Some of these volatile gases cool down and condensate forming a liquid material. This material is comprised of two phases, an aqueous one with organic compounds of low molecular weight, and a non aqueous phase containing organic compounds of high molecular weights, known as tars.

The overall process may be generalized by the following equation [9]:

$$Solid\,fuel \rightarrow aCO + bCO_2 + cCH_4 + dH_2 + eH_2O + fTar + gChar \tag{2.1}$$

Where a to g describe the stoichometric amount of each individual species.

Liquid tar is one of the major concerns in biomass gasification and often catalyses the failure of gasification projects [10]. Pressure and temperature should be optimized to prevent generation of high quantities of this substance. Compulsorily, the amount of non condensible gases: carbon dioxide (CO_2), carbon monoxide (CO), methane (CH_4), nitrogen (N_2), a small amount of hydrogen (H_2) and light hydrocarbons should be maximized.

2.3 Combustion

At this phase, an externally supplied oxidation agent reacts with the volatile gases and charcoal generated in the pyrolysis phase. Combustion is the net exothermic process of all processes in gasification. Meaning it is the main energy source of the system. It constitutes the part of the gasifier with highest temperatures, with particular designs reaching values of up to 1700ºC. It is important, in this phase, to get a good mixing and high enough temperature so that the tar gases from pyrolysys can be used to generate heat. Both reduction phase and char bed contribute relatively little in the conversion of messy tars to fuel. Consequentely, in case of failure, aside from squandering the attainable heat from tars, these will mostly likely be present in the syngas. Solving the tar problem is mostly an issue of tar cracking in the combustion zone [11].

The following reactions may occur in the combustion zone [12].

$$C + O_2 \rightarrow CO_2 - 392.5KJ/mol \tag{2.2}$$

$$C + \frac{1}{2}O_2 \rightarrow CO - 110.5Kj/mol \tag{2.3}$$

$$CH_4 + 2O_2 \Longleftrightarrow CO_2 + H_2O - 803Kj/mol \tag{2.4}$$

$$2H_2 + O_2 \rightarrow 2H_2O - 242Kj/mol \tag{2.5}$$

The typical oxidation agents are: air, pure oxygen, and water vapor. Depending on the amount of oxygen, volatile gases may combust, reacting with char, into carbon dioxide or monoxide, equation 2.2 and 2.3. In the presence of water vapor, endothermic, homogeneous reactions take place culminating in the formation of H_2, CO and CH_4, equations 2.4 and 2.5.

Heat production purposes makes the control of this process relatively lax as only sufficiently high temperature and an over stoichometric amount of oxidation agent need to be ensured. This is, however, not the case of the endeavour is to create fuel gas. The combustion of charcoal is one of the most important phases of gasification as it ensures there is enough thermal energy for the reduction reactions to occur.

The main factors governing this process are temperature, residence time and turbulence. Temperature affects reaction kinetics, residence time influences the degree of conversion of fuel into products and turbulence ensures an effective mixing between biomass and the oxidation agent [5].

2.4 Reduction

Reduction or gasification is the phase where a series of mostly endothermic reactions take place creating fuel rich in combustible gases such as carbon monoxide, methane and hydrogen. This fuel, when compared to solid fuels, allows cleaner combustion, is more efficient, and more environmentally friendly as less pollutant gases are set free into the atmosphere.

The main equations that occur in this phase are:

Boudouard equation [12]

$$C + CO_2 \Longleftrightarrow 2CO + 172MJ/Kmol \tag{2.6}$$

Water-gas reaction

$$C + H_2O \Longleftrightarrow CO + H2 + 131MJ/Kmol \tag{2.7}$$

Water-gas shift reaction

$$CO + H_2O \Longleftrightarrow CO_2 + H_2 - 41.2MJ/Kmol \tag{2.8}$$

Methane formation

$$C + 2H_2 \Longleftrightarrow CH_4 - 74.8MJ/Kmol \tag{2.9}$$

Reforming with vapor. [13]

$$CH_\alpha + (1-\beta)H_2O \rightarrow CO + (1 - \beta + \frac{\alpha}{2})H_2 \tag{2.10}$$

Reforming with hydrogen. [13]

$$CH_\alpha + (1 - \frac{\alpha}{2} + \beta)H_2 \rightarrow CH_4 + \beta H_2O \tag{2.11}$$

Reforming with CO_2. [13]

$$CH_\alpha + CO_2 \rightarrow 2CO + \beta H_2O + \frac{\alpha}{2} - \beta)H_2O \tag{2.12}$$

The reforming equations can be generally described by the equations 2.10 to 2.12, where α and β describe the variability existent in their stoichometry.

At temperatures above 725ºC it is common for carbon to react with carbon dioxide as described by the boudouard equation. This reaction is however, inhibited by the presence of CO. The water gas reaction usually occurs if the environment has a high temperature and a low pressure. An increase in temperature may also give place to an unbalance between CO, H_2, CO_2 and H_2O resulting in the water-gas shift reaction which, in spite of being exothermic, has a negligible effect on the energy balance. It does nonetheless incur an alteration in the gaseous mixture, having a significant toll in the ratio between H_2 and CO. Both the methane formation reaction and the reforming with hydrogen reaction, also known as methane reforming reaction are very slow, only being influential at high pressures.

The tars formed in the pyrolysis stage also undergo secondary cracking in this phase [10].

2.5 Types of gasifier

Gasifiers may be differentiated according to many factors including gasyfing agent, heat supply, pressure profile or design. In spite of this, four major types of gasifier dominate the industry: updraft or downdraft from the fixed bed category and bubbling or circulating from the fluidized bed category [14].

Fixed bed gasfiers are the simplest to develop and are classified according to the direction of fuel flow relative to the direction of gasifying agent flow. Normally the fuel is fed from the top of the gasifier, and hence, when the gasifying agent is supplied from the bottom, the gasifier is called counter-current or updraft whilst if the agent is supplied above the reduction zone, the gasifier is called co-current or downdraft.

Updraft gasifiers, figure 2.1 (left), regardless of the triviality in its design, are among the most efficient of gasifiers. This makes them one of the most widespread technologies, specially used in the gasification of coal. Their advantages include a high charcoal burn-out and high internal heat exchange which permit the use of fuel with moisture contents up to 60% and small particle size. Furthermore they operate properly even with variations in the feed-stock size.

The problems of this design is the high amount of tar and pyrolysis products, which is not problematic for heat generation purposes as these are simply burnt. As a matter of fact, condensable tars are a high energy fuel and greatly enhance the amount of energy per volume of biomass [15]. On the contrary, for power generation, extensive gas cleaning is required, outweighing the gasifier's efficiency.

Downdraft gasifiers, figure 2.1 (right), do not suffer from this as they are known to produce the lowest quantities of tar, with some implementations reporting values close to 0% tar content, a significant decrease from the 5 to 20% produced by updraft gasifiers [15]. Unlike in their updraft counterpart, where temperature monotonously decreases with the height of the gasifier, these feature a change in relative position between reduction and combustion zones leading to the consequent changes in the temperature profile along the height of the gasifier. The major drawback of the downdraft technology is its scalability limitations. The problem can be described as follows. At low loads, temperature is lower leading to less efficient tar cracking but lesser amounts of particles in the gas. Increasing the loads provokes more efficient tar cracking, and thus, less tar content at the cost of higher amounts of particles in the gas. These particles, ash and dust, induce a higher temperature in the outgoing gas which amounts to a lesser efficiency. Furthermore, regular flow requires strict biomass properties, moisture levels must be kept under 25% and feedstock size should be regulated between 4 to 10cm.

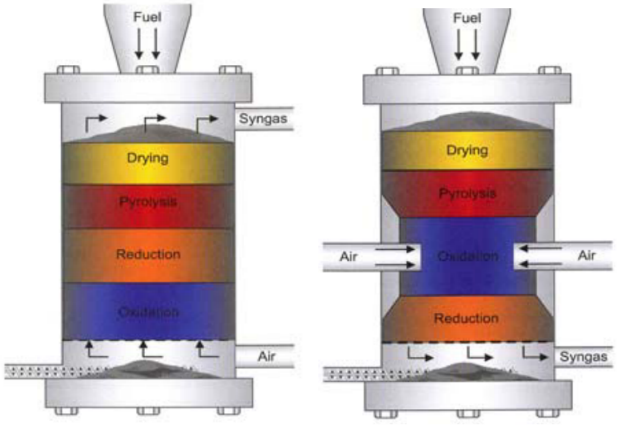

Figure 2.1: Main zones of the updraft, left, and updraft gasifiers, right [16].

Fluidized beds are cylindrical columns containing particles and through which a gaseous or

liquid fluid flows [1]. At a certain fluid velocity, the particles become suspended. This happens when the fluids ascending force equals the particles' weight, at which point the particles are deemed fluidized and the velocity is called minimum fluidization velocity. The outcome is a high surface area to make contact with the fuel, this being the highest advantage of this category.

Comparing figures 2.1 and 2.2, an obvious difference between fluidized and fixed bed gasifiers can be seen. Due to the intense mixing of the difference zones, no distinction between the phases of the gasification process can be made and the temperature along the bed is uniform.

The difference between the bubbling and circulating fluidized bed archtypes is the fluid's velocity, being higher in CFB which also requires the inclusion of a cyclone separator to bring elutriated bed material back to the gasifier. From an empirical point of view CFB feature an increment in gasification rate, conversion rate of tar, carbon burnout and are more suitable for large scale applications.

Comparing them to fixed bed gasifiers, they boast of higher heat exchange and reaction rates, flexible biomass properties and relatively low ash melting points. Their disadvantages are: high tar and dust content in the gas, existence of alkali metals in the vapor state, complex operation as both fuel supply and temperature need to be controlled and the need of power consumption for the compression of gas stream. [16]

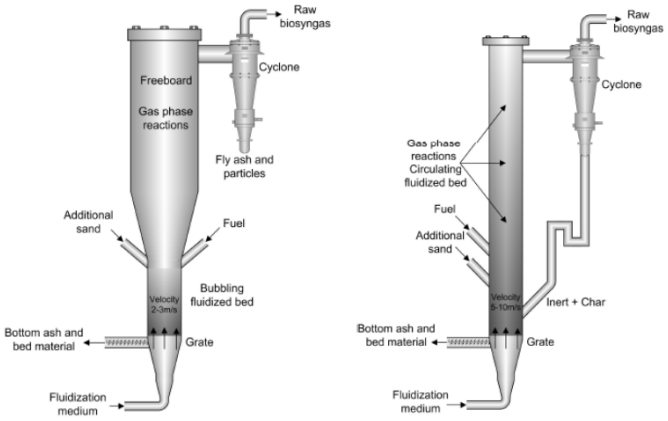

Figure 2.2: Diagram of bubbling fluidized bed, left, and a circulating fluidized bed, right [16].

To conclude this section it can be stated, according to [1] that the scalability and the investment cost of external gas cleaning devices puts fluidized bed gasifiers among the most promising candidates for biofuel production plants. Meanwhile, downdraft gasifiers have established themselves has the most suitable technology for small scale distributed power generation.

2.6 Process Parameters

In this section a description of the gasification process parameters will take place. It will start with equivalence ratio, the characteristic that differentiates gasification from simple burning.

2.6.1 Equivalence Ratio

ER describes the relation between the oxygen present in a process and the stoichometric amount of oxygen that leads to combustion. It may be calculated according to the following equation [13].

$$ER = \frac{mass\,flow\,rate\,of\,air}{mass\,flow\,rate\,of\,fuel} \Big/ \frac{mass\,flow\,rate\,of\,air}{mass\,flow\,rate\,of\,fuel}\Bigg|_{stoichmetric} \tag{2.13}$$

The quality of producer gas is strongly dependent on equivalence ratio. Typical values go from 0.2 to 0.3 [17]. Below this range the conversion of charcoal is incomplete and the system is prone to the formation of tars and producer gas with low energy. On the other hand, values above this range foster the formation of combustion gases in detriment of CO and H_2. The reason for this is that, besides governing the amount of fuel available, ER also strongly influences the temperatures inside the gasifier.

Meanwhile at low ERs, the decrease of temperature favors the occurrence of the methane formation reaction, leading to an increase in the concentration of CH_4 producer gas. In both conditions, the inert[1] gas N_2 sees an increase in its relative concentration as the overall concentrations of other species diminishes.

2.6.2 Gasifying Agent

Air, pure oxygen and water vapor are the three gasifying agents used. A mixture between them may also be employed. When gasification is done with air or pure oxygen, it is labeled direct, as the oxygen will enhance oxidation and thus provide the energy needed for the system to operate [15]. Gasification with air is cheaper while pure oxygen generates a gas of higher calorific values. Water vapor for one, produces the gas with the best chemical compostion, and highest calorific value while still being cheaper than pure oxygen and countering the hindraces caused by nytrogen in atmospheric air. The problem is that the process becomes highly endothermic requiring extra measures for correct functioning.

In [10] a kinetic gasification model was created and used to research the effect of mole fraction of oxygen in the gasifying agent. The results showed that a slight increase in O_2 concentration leads to an increase in the CO/CO_2 ratio and a decrease in the tar yield. This counters the effects of increasing oxygen by manipulating air flow, and thus ER. The difference

[1] An inert gas is a gas that does not undergo chemical reactions under a set of given conditions

is that, unlike increasing flow rate, increasing O_2 concentration does not increase superficial velocity or hearth load. As so the residence time remains unchanged and does not hinder the occurrence of reactions in the chamber bed.

Superficial velocity(m/s) is defined as the ratio of gas production rate to the smallest cross-sectional area of a gasifier, neglecting the presence of fuel. For downdraft gasifiers its is more common to define hearth load ($Nm_3/h/cm^2$), which corresponds to the ratio of producer gas generated to the gasifier's throat, or hearth, area, normally corresponding to the smallest passage area in the gasifier. Typical values of hearth load tend to be confined between 0.3 and 0.9 $Nm^3/h/cm^2$. Operating outside of this range normally produces results similar to operating outside of the recommended ER range [15, 18].

2.6.3 Residence Time

Burnout time is the time needed for a particle to change into gaseous form. For combustion to be complete, residence time must be higher than the particles' burnout time [5]. It depends on the particles oxidation rate, combustion temperature, reactivity, particle's size, particle's surface area and reactivity. In the particular case that is gasification, the objective is to convert the particles to gaseous form while creating combustion gases. All of the properties stated are tightly dependent of the type of feedstock used. Residence time plays an important role in the reduction of impurities, like sulfur and tar, as higher residence time is required for it to happen [5].

2.6.4 Moisture Content

The phenomenons that occur in the drying and heating phase have two major, concurrent, consequences in the overall gasification process: reduction of the temperature in the oxidation zone, due to the increased drying energy requirement, and steam auto generation which acts as a reactant in the decomposition of volatile gases and char [19].

At low moisture levels, the temperature of the reduction zone remains close to constant favoring the creation of products in water gas reactions and therefore increasing the amounts of CO and H_2. As moisture increases, the second effect starts gaining prominence. What happens next is an increase in H_2 due the decomposition of char and volatile gases and a further increase in CO is enhanced by the decrease in temperature as the water gas shift reaction is exothermic. The problem is the methanation reaction, also exothermic, in which the increased quantities of H_2 and CO will react to form CO_2 and CH_4. The overall conclusion, derived from the outgoing gas composition, is that as moisture level increases, the low heating value of producer gas decreases.

Having said this, studies performed by Narváez et.al. [20] have shown the use of small amounts of water in feed-stock improves syngas calorific power due to its effect in "reforming with vapor", gasification of charcoal, water-gas and water-gas shift reactions. In 2011, a

modified equilibrium model was developed by Arnavat [14] and used to study the utility of increasing the moisture level from 20% to 25%. This further enhanced the conclusion that the low heating value, LHV, decreases with moisture level as the increase in H_2 revealed was overshadowed by a more significant decrease in CO concentration. It was also stated in this document that an increase in moisture should be compensated with an increase in ER, so as to maintain the gasifier's temperature.

Another important conclusion is that, despite of the increase in power achieved though drying of biomass, this should only be attempted in scenarios where it can be carried out naturally using sunlight or through energetically cheap artificial methods. The reason for this is that to cost of others measures outgrows the efficiency increase mentioned [19].

2.6.5 Air preheating

Air preheating is a cost efficient way of increasing efficiency in gasifier systems. The sensible heat in the inlet air causes an increase in gasification temperature, this is caused by an increase in the enthalpy of oxidation reactions [19]. Its increase allows an increase in H_2 and CO whilst decreasing the concentration of CO_2 and CH_4 in syngas.

In [21] it was found that gasification temperature increases almost linearly with the temperature of inlet air for all ER. However it was also found out that, after a certain temperature, which, in the study's conditions, corresponds to 550^{o}C, further preheating has little to no effect on syngas composition.

A 100kW pilot scale, two stage gasifier developed in the technical university of Denmark has achieved 92% to 97% cold gas efficiency[2] by using the heat liberated from cooling the exhaust gas to pyrolyse the fuel and preheat the air. In 2017 this was approximately 10-20% higher than other known gasification facilities [10].

2.6.6 Grate shaking

As gasification proceeds the char in the reduction zone will eventually turn to dust containing ashes and carbon. Some of this dust is carried by the gas while the remaining will eventually plug the gasifier. Fixed bed gasifiers, due to the downward motion of feed stock also suffer from bridging and channeling. Channeling is the formation of air channels amidst the gasifier's load. Bridging happens when the biomass get stuck in a constriction, such as the throat of a downdraft gasifier, preventing its flow. These phenomenons should be reflected in the gasifier's pressure profile.

Biomass with low bulk density normally aggravates these issues. Bulk density describes the relation between biomass weight and occupied volume when packed loosely inside a gasifier [15].

[2] Percentile ratio between the heating value of product gas and the heating value of the feedstock.

In [22], a novel approach consisting in the usage of metal scraps atop the fuel load is used to enhance the gravitic force and thus regulate the fuel flow. The most typical techniques however, include pelletizing or bricketing of the feedstock before its use, which is also helpful in reducing the moisture content in the biomass, or the incorporation of a shaking mechanism in the design.

According to [23] in which a vertical motion shaker was developed and tested, a decrease in tar content was effectively induced by the grate shaking mechaninsm. This was attributed to an increase in the area occupied by the combustion zone, and therefore, an increase in the reduction zone's temperature coupled with an increase in the char's residence time, enhancing the tar cracking reactions. It was also implied in this study that further enhancements could be achieved by optimizing the grate shaking frequency which was further researched in [7] where it was concluded that the CO/CO_2 could be controlled by adjusting the grate shaking frequency.

2.6.7 Temperature

Temperature plays a crucial role in gasification. It influences all the reactions involved in the process [5] as it is strongly correlated to reaction rates, reaction equilibrium constants, pressure, superficial velocity and residence time [10].

It is dictated by the biomass' properties, gasifying agent, energy losses in the gasifier, and most importantly, equivalence ratio as was described in the previous sections.

The higher the ER, the higher the temperature as there will be an increase in the products of complete combustion. A high temperature enhances tar cracking, and thus decreases the amount of tars in the producer gas, possibly the most important characteristic in power production gasification plants

2.6.8 Tar Content

Global progress of gasification is highly deterred by the formation of tars and the high cost of its removal. Tars carried by the gas stream may agglomerate in though the pipework, causing blockages, system failures and component damage [24].

To further exalt this issue, the thoughts of Thomas Reed [25] are shared here: "While a great deal of time and money has been spent on biomass gasification in the last two decades, there are very few truly commercial gasifiers, operating without government support or subsidies, day in, day out, generating useful gas from biomass. The typical project starts with new ideas, announcements at meetings, construction of the new gasifier. Then it is found that the gas contains 0.1–10% 'tars.' The rest of the time and money is spent trying to solve this problem. Most of the gasifier projects then quietly disappear. In some cases the cost of cleaning up the experimental site exceeds the cost of the project! Thus 'tars' can be considered the Achilles heel of biomass gasification. In the gasification of coal, a more mature technology,

the 'tars' (benzene, to-luene, xylene, coal tar) are useful fuels and chemicals. The oxygenated 'tars' from biomass have only minor use. With current environmental and health concerns, we can no longer afford to relegate 'tars' to the nearest dump or stream."

Ultimately, the performance of a gasification system is constrained by the tar acceptance limits of its downstream systems and/or applications. These limits were resumed in [24], as shown in figure 2.3.

Application	Tar acceptance limit (g/Nm^3)
Direct combustion	No limit
Gas turbine	0.05-5
IC engine	50-100
Pipeline transport	50-500
Fuel cells	<1

Figure 2.3: Tar limitations for syngas applications. [24]

Figure 2.3 also highlights a clear difference between direct combustion, normally used for heat or steam generation [26], and power production applications, as tars do not constitute an issue in the previous.

2.7 State of the art

According to data collected by the GSTC, global syngas technologies council, there were, in 2017, a total of 1099 gasification projects with its vast majority being developed in China. Data related to the number of projects with commercial purposes can be seen in figure 2.4. Figure 2.5 indicates the average values of power generated by these plants.

Commercial	Projects	Gasifiers	GWth Syngas
Operating	379	938	173
Construction	131	348	108
Planned	146	734	116
Total	656	2,020	398

Figure 2.4: Empirical world wide gasifier data [27].

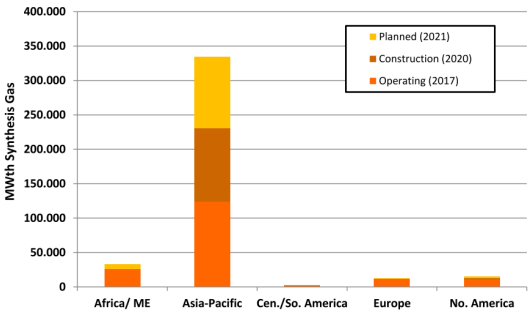

Figure 2.5: Gasification power production per region [27].

When it comes to feedstock, coal has clear dominance over the market as can be seen in fig 2.6. Biomass gasification is still in an immature state and is yet to make a commercial break-trough [28].

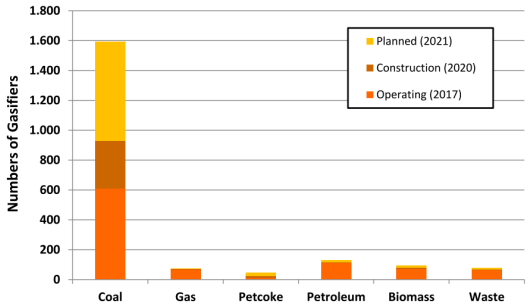

Figure 2.6: Number of gasifiers per feed stock [27].

In this field of research, Europe emerges as the biggest investor with a total of over 60 projects expected for 2021, figure 2.7.

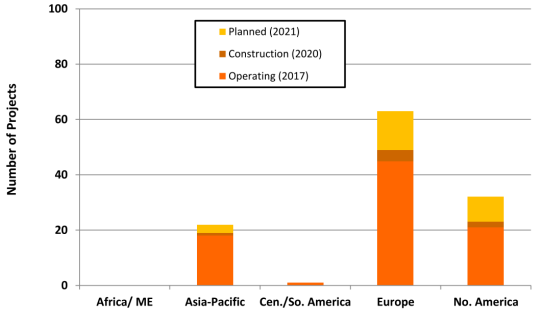

Figure 2.7: Number of biomass gasification projects per region [27].

The table in figure 2.8 shows an overview of the top gasification plants in Europe, 2016.

Site gasification plant	Input	Product	Output	Technology
Skive, Denmark	Lignocellulosics; wood pellets	Heat; power	11 MWth; 5,5 MWel	CHP conversion
Harboøre, Denmark	Lignocellulosics; wood chips	Heat; power	3,5 MWth; 1 MWel	CHP conversion
Barrit, Denmark	Lignocellulosics; wood chips	Heat; power	140 kWth; 35 kWel	CHP conversion
Kgs. Lyngby, Denmark	Lignocellulosics; wood chips	Heat; power	140 kWth; 35 kWel	CHP conversion
Cumbria, United Kingdom	Lignocellulosics	–	1 MWel	CHP conversion
Mossborough, United Kingdom	Lignocellulosics; wood chips	–	250 kWel	CHP conversion
Neunkirchen, Austria	Lignocellulosics; waste wood, clean wood, biomass	Heat; power	620 kWth; 300 kWel;	CHP conversion
Güssing, Austria	Lignocellulosics; wood chips	Heat; power	4.5 MWth; 2.0 MWel	CHP conversion
Oberwart, Austria	Lignocellulosics; wood chips	Heat; power	1–6 MWth; 2.7 MWel	CHP conversion
Neumarkt, Austria	Cleanwood, biomass	Heat; power	580 kWth; 240 kWel	CHP conversion
Sulzbach-Laufen, Germany	Other; wastewood, biomass	Heat; power	280 kWth; 130 kWel	CHP conversion
Neufahrn bei Freising, Germany	Lignocellulosics; waste wood, clean wood	Heat; power	250 kWth; 110 kWel	CHP conversion
Langballig, Germany	Lignocellulosics; wood chips	Heat; power	280 kWth; 70 kWel	CHP conversion
Carlow, Ireland	Lignocellulosics; wood chips	Heat; power	140 kWth; 35 kWel	CHP conversion
Wila, Switzerland	Lignocellulosics; dried chips from waste wood	Heat; power	425 kWth; 350 kWel;	CHP conversion
Stans, Switzerland	Lignocellulosics; dried chips from demolition wood	Heat; power	1.2 MWth; 138 kWel	CHP conversion
Geertruidenberg, Netherlands	Wastewood; demolitionwood	Heat; power; gas for coal-fired boiler	30 MWel	Co-firingconversion
Buggenum, Netherlands	Biomass /biomasscoalblends	Power	280 MWth	Co-firingconversion
Lahti, Finland	Lignocellulosics; wood chips, wood waste, plastic waste	Fuel gas	40–90 MWth	Co-firingconversion
Värö, Sweden	Lignocellulosics; bark	Heat	35 MWth	Co-firingconversion
Varkaus, Finland	Other; wood fibre, plastic, aluminium	FT-liquids; heat; aluminium	14 t/d; 50 MWth	Synthesisconversion
Groningen, Netherlands	Other; from biodiesel and oleochemicals	Methanol	200 000 t/a	Synthesisconversion

Figure 2.8: Characteristics of gasification plants in Europe [29].

As can be seen, there were, in 2016, 22 functioning gasification plants, with 7 companies having the know-how required for their construction [29].

2.8 Conclusion and Future Work

Throughout this Chapter, most gasification parameters were addressed and explained. The goal of this dissertation is the design of a temperature controller for a downdraft biomass gasifier. Ideally, this step would be preceded by identification of the system to be controlled. For this reason, a study of the gasification process was done in order to assess which of the enumerated parameters could, or would need to be measured in order to achieve this endeavor. Furthermore, this dissertation is part of the beginning stages of a full gasification project, and besides identification or control, it will incorporate the design of the instrumentation system needed for its developers to investigate the inner workings of the gasification process.

Online measuring the concentration of the different species is optimal for control of the gasifier. This task was, however, undertaken by other members of the project and was not an option during development of this dissertation. As so, it will receive no further mention.

There is no simple way of measuring static parameters like biomass composition, size or shape. These are highly influential in the process. They directly influence the stoichometric air-to-fuel ratio, and thus ER, for example. At this stage, to reduce the process' variability, wood pellets with known, controlled properties will be used. It was also decided that the gasifying agent would be natural air. Furthermore, in order to simplify the initial construction,

grate shaking will be performed manually, and thus, no automated mechanism will be constructed.

Temperature seems to emerge as the most important parameter on a gasification system. It is common procedure in the literature to measure temperature at multiple heights of the gasifier. At a bare minimum, temperature should be measured at each of its zones: Drying, Pyrolysis, Combustion and Reduction.

Pressure inside a gasifier is also an important monitoring parameter having proven to be helpful in diagnosing constrictions and energy loss problems.

After the undertaken literature review, it would seem that the best stratefy for controlling the operation of a gasifier, and its temperature, would be through direct actuation of the equivalence ratio. The simplest way of extrapolating this variable is through the formula shown in equation 2.13, calculating it through a direct relation between stoichometric and actuated air-to-fuel ratio. This would imply, aside from the already assumed constant biomass properties, measurement of the flow of air entering the gasifier and measurement of the flow rate of biomass fed through it. This approach is however, not possible for this dissertation as, in its beggining stage, the gasifier will be operated as a batch reactor. As only air flow can be actuated, it was decided that the mass of products inside the gasifier would also have to be measured in order to control the operation of the gasifier, as done in [9, 30]. This is considered, however, sub-optimal as when the ER fluctuates, changes in the proportions of fuel, char and ash will change accordingly, which may not be reflected in the height of the fuel pile [31]. A weighting system should, nonetheless, prove further usefulness in future iterations of the project in order to measure feeding rate, and optimize bed height when continuous feeding is installed.

Tar content is the single weakest point of the gasification system. Unfortunately, there is no established technology that can be used for online tar measurements. In order to estimate its concentration in syngas, complex sampling systems have to be devised with the samples being sent to specialized laboratories for measurement. Resulting in a very time consuming process [24].

CHAPTER 3

Instrumentation principles

The research undertaken in the previous Chapter revealed the need to measure: temperature, pressure, mass and air flow, along with actuation of the latter. In this Chapter a description of the instrumentation technologies available for such endeavor will be addressed.

3.1 Ventilation systems

Ventilation systems may be deemed forced or natural. In the natural category, air is allowed into the system though orifices and its movement is caused by changes in pressure inside the system. For the forced case a fan is either positioned in the inlet and/or outlet of the system. For a fan to be properly sized, two main parameters must be taken into account: the pressure losses inside the system and the nominal flow rate. The dependence of the pressure losses in a system with flow rate is known as the system's characteristic.

The operating point of a fan in a system is represented by the intersection of the system's characteristic and the fan's characteristic, as shown in figure 3.1.

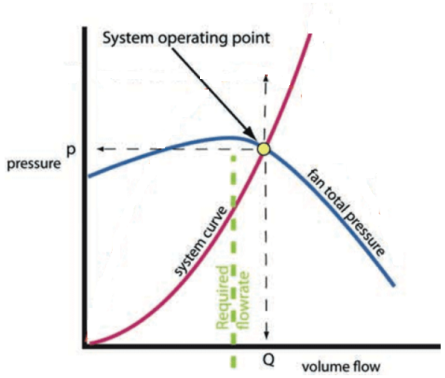

Figure 3.1: Representation of a fan's operating point.

Obviously, changes in air flow and systems pressure will incur changes in the fan's operating point. Consequently, if flow is to be changed during operation, its range must be to the left or right of the operating point depending on the type of control utilized. For fans of relatively

small size, speed control is the most economical technique and the flow range should be left to the fan's optimal operating point.

This section will now describe the different motor technologies used to drive a fan's helix. This description will restrict itself to the main categories of motors, namely: brushed DC, brushless DC and induction AC motors.

3.1.1 DC Motors

As the name implies, DC motors are devices that transform electrical into mechanical energy when actuated with direct current. The simplest, and oldest, iteration of these category is that of Brushed DC motors, illustrated in figure 3.2.

Figure 3.2: Illustration of a brushed DC motor [32].

These motors are composed of the stator, a permanent magnet, and the armature, formed by an arrangement of coils. The coils are connected through brushes to a DC power source. With this configuration, when activated, the coils will be run through with a current as indicated in figure 3.2 by blue arrows. According to the Lorentz law, this will create a force that is perpendicular to the armature, forcing it to rotate.

The speed of rotation may be controlled by simply altering the amount of current provided to these motors. The main disadvantage of these motors is the friction caused on the brushes by the rotating coils making them prone to deterioration.

Another category of DC motor is that of brushless DC motors, or BLDC, figure 3.3. Like their counterpart, a permanent magnet is involved, but in this category, it corresponds to the rotary part of the motor, or rotor.

These stator is now formed of a coil arrangement, where opposite windings are connected forming three separate coils. When each of these coils is subject to a current, an electromagnet is formed, which will force the movement of the surrounding rotor. The operation of such motors consists in the actuation of a single coil arrangement when the rotor nears the previous one. As only the coils are actuated, the need for brushes is now forfeit. However, it is now necessary to know the position of the rotor in order to operate it, which is normally achieved through an electronic controller.

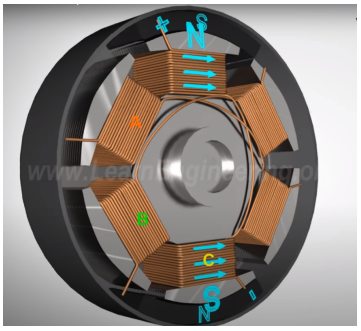

Figure 3.3: Ilustration of a brushless DC motor [32].

3.1.2 AC Motors

AC motors, more concretely, induction AC motors, are the most used type of motor in the industry, illustrated in figure 3.4. The justification for this lies in the absence of: permanent magnets, brushes, commutator rings and position sensors.

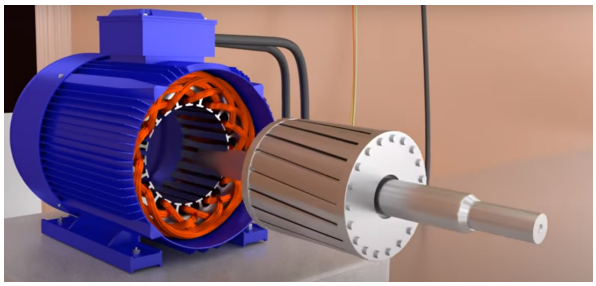

Figure 3.4: Illustration of an induction AC motor [32].

Like DC motors, induction motors are composed of two main parts, a stator and a rotor. The stator is formed of 3 coils, 120^{o} apart, connected at one end. When a three phase power input is applied to this arrangement, a rotational magnetic field, RMF, will be created centered in the rotor. In figure 3.4, a squirrel cage type rotor is shown. In this case the RMF will induce a current in the cage's bars, forcing it to rotate. As current is induced in the rotor through electromagnetic induction, no direct connections are needed.

Another strong point of this type of motor is its speed control. This is achieved by controlling the frequency of the AC power signal, normally with a variable frequency drive.

3.2 Valves

A broad array of options exists in the flow control industry. This dissertation will focus on solutions that are commonly used in gasificaton systems.

3.2.1 Solenoid valves

Solenoid valves are electrically actuated valves commonly used in hydraulic applications to control the flow and direction of liquids or gases. Their main component is a solenoid, which consists of a coil with a movable, ferromagnetic core in its center. When an electric current runs trough the coil, a magnetic field is created exerting a force on the core, often called plunger. By energizing the plunger, a small orifice is opened or closed depending on the resting position of the valve. These valves can be divided into three groups, categorized by their point of operation as: direct operated, indirect operated and semi direct operated [33, 34].

Direct operated, figure 3.5, are the simplest of solenoid valves where a rubber gasket is fitted into the bottom end of the plunger in order to seal the valve's orifice. On normally closed valves the plunger is held down by a spring, restraining the flow when the coil is not energized. Applying a current trough the coil forces the plunger to retract allowing the medium to run trough. The limits of operating pressure are directly related to the size of the orifice and the strength of the magnetic field.

Direct operated valves do not require a minimum operating pressure or pressure difference to work and are suitable for systems with minor flow values [33, 34].

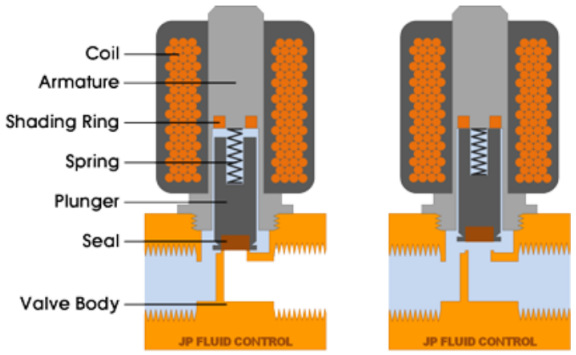

Figure 3.5: Diagram of a direct operated solenoid valve [33].

In the indirect operated category, figure 3.6, the differential pressure between the valve ports to used to operate it. A minimum pressure around 0.5 bar is needed for proper function of the valve which makes it more suitable for processes that always have media pressure in the pipeline. In a two way valve, both ports are connected by a rubber membrane, separating the valve body in two compartments. By allowing medium to flow though the inlet port into the upper compartment, an increase in pressure is forced upon the diaphragm sealing the orifice.

The upper chamber is also connected to the outlet port with a small pilot orifice. This connection is, however, constrained by the solenoid's plunger. By actuating the solenoid the pilot orifice is unsealed, allowing the medium to flow into the outlet port. As so, a pressure difference is created between the two ports, lifting the diaphragm and allowing the medium

through.

The fact that the medium serves as a pilot for the valve's operation allows the control of higher flow rates with smaller solenoids culminating in low power consumption and increased efficiency. These are the most cost-efficient of the solenoid valves [33–35].

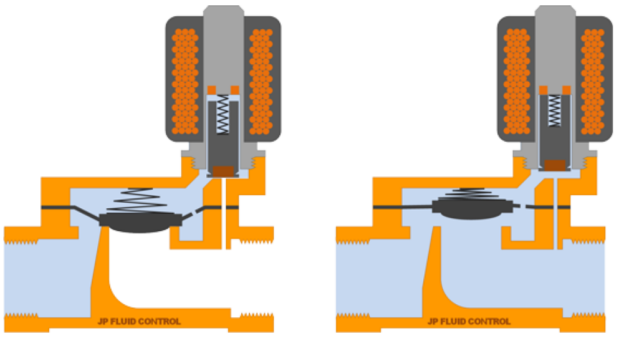

Figure 3.6: Diagram of an indirect operated solenoid valve [33].

The construction of the semi direct category, figure 3.7, is similar to that of indirect operated valves. A diaphragm is, again, employed to connect both ports of the valve, the difference is that the plunger is positioned directly above the diaphragm, and tied to it. Therefore, when the plunger is lifted the membrane is directly dragged with it. This causes the pressure in the upper chamber to drop, creating a pressure difference and consequently assisting in the membrane's rising. For this reason semi-direct operated valves are also called assisted-lift valves.

The configuration described allows the valve to function from zero bar differential pressure and still accommodate high flow rate values.

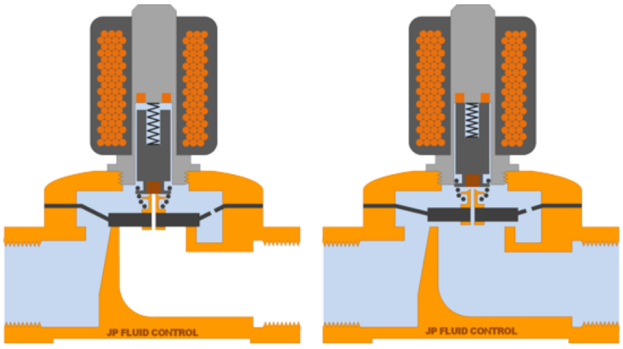

Figure 3.7: Diagram of a semi-direct operated solenoid valve [33].

3.2.2 Butterfly Valves

Butterfly valves are quarter turn rotary valves that can be used to stop, regulate and start flow. Normally set between pipe flanges, they are composed by a round disc surrounded by a circular short body and connected to an actuator that runs through it, as shown in figure 3.8. The disk is normally of the same size of the pipe and is able to rotate in a vertical or horizontal axis. When the disk is parallel to the pipe length, flow is allowed through, and thus, the valve is fully opened. If it is perpendicular to the pipe run the flow is shut off. Intermediate positions can be achieved for the case of throttling flow. In older construction models it was impossible to completely constrict the flow with this kind of valve, however more recent manufacturing strategies have allowed tight sealing through the use of rubber or elastomeric materials. Its shut off performance is now close to that of other valves.

Actuators for butterfly valves can be designed to remain open on failure, in which case they are called *"fail-open"*, or remain closed on failure, being called *"fail-closed"*. Three different principles may be followed to achieve automatic actuation:

- Electric: Uses a torque or servomotor to turn the disc;
- Pneumatic: Uses compressed air to move a piston or a diaphragm;
- Hydraulic: Uses hydraulic pressure to move a piston or a diaphragm.

Savings in weight, size, cost and good performance at low pressure drops are among the main advantages of this type of valve. These characteristics make them suitable for systems with high flow rates and large pipe diameters. In spite of this, the tendency of these valves to suffer from cavitation[1] and choked flow should not be overlooked, just as the fact that disc movement may be affected by flow turbulence [33, 34, 36].

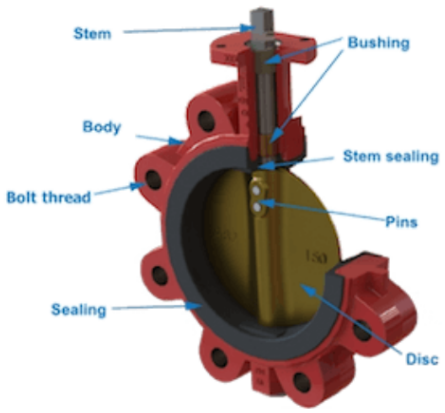

Figure 3.8: Diagram of a butterfly valve [33].

[1] Vaporization of liquids due to low pressure in the environment

3.2.3 Needle Valves

Needle valves, figure 3.9 are a typical choice in control systems due to their capacity of accurately regulating water or gas flow [37].

These are easily recognizable for the use of a small plunger akin to the shape to a needle. A handle, known as handwheel is used to adjust the position of the needle. When closed, the needle is fully elongated and tightly fits a structure named seat.

A large amount of turns is needed to create enough space between the needle and the seat for a minimal amount of substance to pass through, and thus, gradual position changes are achieved allowing precise control.

Similarly to their butterfly counterpart, needle valves may substitute the handle with an electric or pneumatic actuator if unmanned control of the plunger is desired.

The main disadvantage of this instrument is the high pressure drop needed for correct operation. They are generally only used in applications with low flow rates [34, 37].

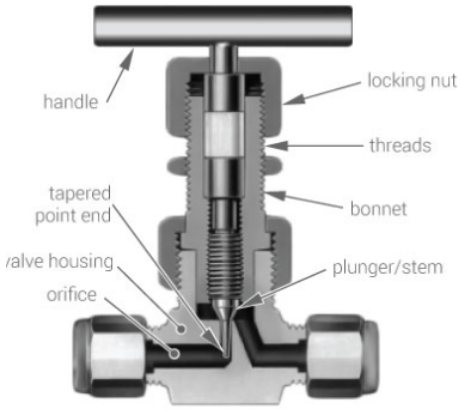

Figure 3.9: Diagram of a needle valve [38].

3.2.4 Valve Sizing Considerations

The information present in this section derived from an article written by Jon Monsen and published by Flow Control Magazine in 2015 [39–42].

If good performance is to be achieved on flow systems, a number of considerations must be taken into account. In this section, an overview of these considerations will be discussed.

The first is flow characteristic, corresponding to the relation between the valve's flow capacity and its position. This property is divided into two categories: the inherent and the installed characteristic. Inherent characteristic refers to the relation between flow and position if there were no system effects involved in the process, meaning that the pressure drop across the valve would remain constant along the experiment. Installed characteristic refers to the real case, after the valve is incorporated in the system.

The typical behaviour of inherent characteristics is shown is the figure 3.10.

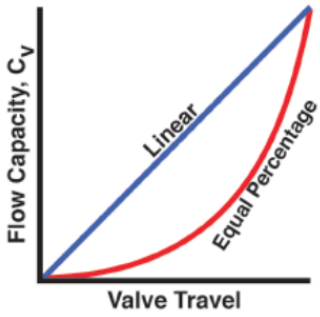

Figure 3.10: Valve characteristics [39].

The name equal percentage derives from the fact that percentile changes in valve's position induce equal percentage changes in the flow rate.

Linear characteristics may seem more appealing than its counterpart. However, linear inherent characteristics do not lead to linear installed characteristics. Most fluid process systems include a considerable amount of piping and other pressure consuming elements. Figure 3.11 shows an overview of the typical relation between flow and differential pressure.

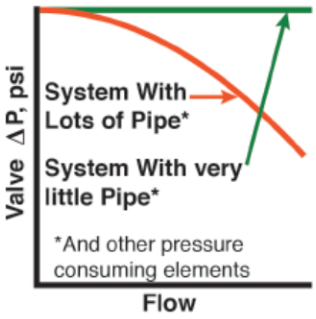

Figure 3.11: Valve pressure changes with relation to flow [39].

A quick overview of the graph in figure 3.11 allows the inference that when the valve moves towards the closed position, decreasing the flow, an increase in differential pressure occurs, resisting the decrease in flow. Coupling the typical system behaviour with that of the equal percentage curve, figure 3.12, creates an approximately linear installed characteristic making valves with this characteristic widely popular in the industry.

After exposing this problem it can be concluded that systems with significant amounts of pressure consuming elements should opt to use equal percentage valves while systems that can maintain a constant pressure difference between valve ports should opt to use linear characteristic valves. A poorly chosen characteristic will probably lead to a system with a control loop that only allows good control on one end of its range, while the other end of its range is sluggish and might even become unstable.

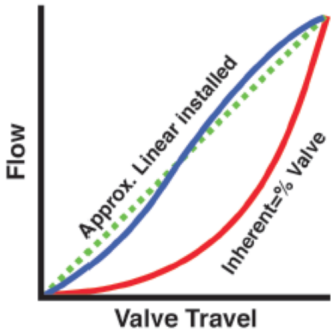

Figure 3.12: Comparison between installed and inherent characteristics [39].

The next consideration that will be addressed is valve size.

Two scenarios might occur in case of improperly sized vales. First is the case of undersized vales, which simply results in a system that cannot reach the desired flow rate. The second and most common is the oversized case. This will result in, apart from unnecessarily high financial investments, overly sensitive valves, meaning small changes in valve position will amount to large changes in flow rate. Valves also exhibit a certain amount of stickiness that only increases with time, it is not uncommon for valves' position increments to be limited to 1% after a prolonged life cycles.

The rule of thumb here is to size the valve to allow passage of the maximum flow rate at openings between 60% and 80%, while sizing the minimum opening at 20% openings. This guidelines amount to an adequate safety factor while allowing the use of most of the valve's control range.

Having said this, it is not uncommon for valve producers not to directly specify the flow rates of a valve for a given opening. The common specification is what is know as flow capacity, C_v, which represents the volume of water, in US gallons, that will flow through the valve during one minute, at a temperature of 60^{o}F and a differential pressure of 1psi.

It can be calculated by using the following formula:[34]

$$C_v = Q * \sqrt{\frac{S_g}{\Delta\rho}} \tag{3.1}$$

Where $\Delta\rho$ is the differential pressure across the valve, Q is flow rate and S_g is specific gravity. A few variations of this expression exist, so the best approach is to use the one normally provided by the valve supplier. Although not a rule of thumb, it is common for properly sized butterfly, ball and segment valves to be two sizes smaller than the pipe line.

Valves suffer from dynamic and static friction. Because of static friction, a valve tends to stay in place until enough pressure is built up, and when it does, it quickly moves onto the desired position. Valve resolution is the smallest movement a valve can make in the same direction and normally manifests itself as the amount of percentile control signal steps needed

to make the valve move from a stationary position.

Another property needed to assess the performance of a valve is the static dead band. This dead band can be seen upon reversal of the direction in the valve's motion. This factor will manifest as dead time in a process loop.

The simplest way to showcase the hazards that can be caused by these properties is to analyse the performance of a proportional integral controller in a situation where friction has reached significant proportions. Lets suppose that a valve is stuck and its position is above the desired set-point. In this situation the integral action of the controller will keep ramping up the control signal until the induced pressure is big enough to overcome the static friction. Now, since dynamic friction is much smaller that static friction and enough pressure has built up, the valve will quickly move beyond the set-point. The controller will now try to invert the movement, but as the valve stops, it get stuck again and the process will repeat itself.

In the situation described the output signal will take the shape of a square wave whilst the control signal takes the shape of a sawtooth. This is commonly referred to as a "limit cycle", figure 3.13, and the only solutions for it are to replace or repair the valve.

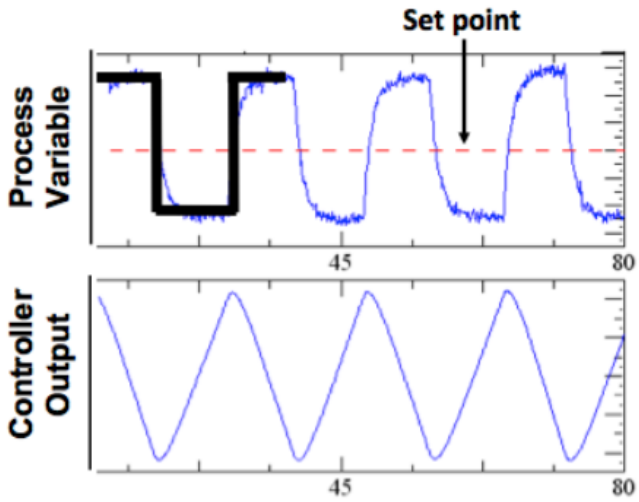

Figure 3.13: Signals in a limit cycle [40].

In order for good control to be achieved, both resolution and dead band should be kept below 0.5%.

Speed of response to step changes is also an important parameter in valve sizing. This is normally expressed in terms of: dead time, settling time, and Tx. Tx amounts to the time required for the valve to reach x% of its final position. T63 is normally chosen in order mimic the time constant of a first order system. The term time constant is not employed because a valve's response is rarely first order.

The rule of thumb is to size the valve so that its response is five times faster than the

desired closed control loop, making it negligible to the process. Empirically speaking: dead time should be below 20% of closed loop time constant, T86 should be below 40% of closed loop time constant, and settling time should be below the closed loop time constant. Overshoot should also be below 20%. This scenario is illustrated in figure 3.14 where the bright red, blue and dark red signals correspond to a step input, open loop response and closed loop response, respectively.

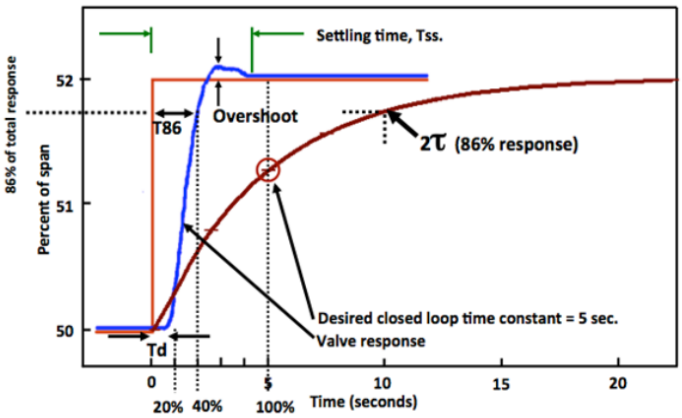

Figure 3.14: Step responses of a properly sized valve [40].

3.3 Temperature Sensors

This section will address the most common temperature measurement technologies.

3.3.1 Thermocouple

A thermocouple is a temperature sensor that functions based on the seebeck effect, which states that a closed circuit formed by the junction of two different metals is run trough with a current induced by an electromotive force, EMF, that is proportional to the temperature difference between the metals.

The usage of this temperature revolves around the measurement of this temperature induced potential difference. Inevitably, when doing so, the thermocouple must be connected to a voltmeter with wires, which are made of specific metals. As so, two new metal junctions are created.

Because of this, thermocouples do not measure absolute temperature but a gradient between a reference junction, called cold junction, and the junction of which a temperature measurement is desired, called hot junction. A representation of the thermocouple is illustrated in figure 3.15.

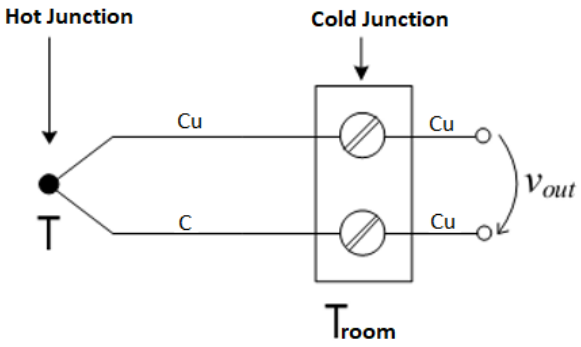

Figure 3.15: Representation of a thermocouple. Adapted from [43]

Since absolute temperature is normally wanted, the temperature of the reference junction must be known and subtracted from the thermocouple's measurement. This is called cold junction compensation and may be achieved through software or hardware techniques. The common procedure is to use another type of sensor to measure the temperature at the cold junction making thermocouples especially suitable in scenarios where the temperature range of other sensors is unfit.

Thermocouples are classified according the metals that comprise them. The different configurations allow measurements from -200ºC to over 2000ºC. Their broad limits makes them the most used sensors in industrial applications.

3.3.2 RTD

Resistance temperature detectors (RTD) are sensors that measure temperature based on the dependence of resistivity with temperature. For its construction a thin film of conductor is mounted on a ceramic substract. An eletric conductor, of length l and section area A composed of a material with resistivity ρ has a resistance that can be calculated by:

$$R = \rho \frac{l}{A} \tag{3.2}$$

The resistance's dependence with temperature can be modelled by a polynomial of the following type:

$$R = R_0[1 + a_1(\theta - \theta_0) + a_2(\theta - \theta_0)^2 + a_3(\theta - \theta_0)^3] \tag{3.3}$$

Where R_0 is the resistance value at temperature θ_0.

The above equation is normally approximated to fit that of a linear model. As so, by eliminating the terms with order higher than, the following equation is attained

$$R = R_0[1 + \alpha(\theta - \theta_0)] \tag{3.4}$$

Where α is a given metal's temperature coefficient.

Diverse types of metal can be used with the most prominent one being platinum (pt) for presenting the best quality in terms of linearity, which makes it suitable for the development of high precision sensors.

The most used RTD is the PT100, a platinum based sensor whose resistance at 0^{o}C is 100Ω.

The simplest way measuring the resistance of such sensors is trough the use of a current source. Running the RTD with a known current makes it possible to calculate its resistance through Ohm's law.

3.3.3 Thermistor

Thermistors are semiconductor based temperature sensors whose resistance, similarly to RTDs, is a function of temperature. The most used sensor in this category is the NTC (negative temperature coefficient), which, as the name implies, exibits a resistance characteristic that decreases with temperature. Inspite of being the most non-linear of temperature sensor, the exponencial characteristic of these sensors also makes them the most reliable in terms of accuracy. Their applicable range goes from -100^{o}C to 300^{o}C.

In order to linearize the NTC's characteristic the steinhart equation is used.

$$\frac{1}{T} = A + Bln(R)^2 + Cln(R)^3 \tag{3.5}$$

The coefficients values are normally provided by the suppliers but they may be obtained though calibration of the sensor. Unlike their counterparts, thermistors are quite fragile and are prone to overheating problems.

3.3.4 Integrated Circuit Temperature Sensors

Integrated circuit sensors exist and have current and voltage outputs that are directly proportional to temperature variation.

IC sensors with current outputs are widely popular since they circumvent the problems caused by wire resistance. There are also some variants with digital outputs.

Despite having a very straight forward use procedure these are restricted to temperature ranges between -50^{o}C and 150^{o}C making them unsuitable for many applications.

3.4 Pressure Sensors

The information written in this section is mostly based in the explanations given in [44]. Depending on the application, three types of pressure may be measured: gauge pressure, absolute pressure and differential pressure.

In the case measurements should not be influenced by changes in atmospheric pressure, absolute pressure is proper choice. This measures pressures relative to zero pressure, similarly to kelvin in temperature.

If the endeavor is to measure pressure variations relative to atmospheric pressure, gauge pressure is the appropriate solution.

And finally if the endeavor is to measure pressure across two points in a system, differential pressure sensors are the correct choice. These are frequently used to diagnose constrictions in piping systems.

This section will describe some of the technologies used to quantify pressure.

3.4.1 Piezoresisive Pressure Sensors

Some materials, like quartz and tourmaline, are able to create eletric charge when under pressure. This charge is called piezoeletricity.

Piezoeletricity can be measured as a voltage proportional to the pressure applied in a crystal. A static force will yield a corresponding voltage drop in the material, however, this voltage tends to leak away due to imperfect insulation, the crystal's internal resistance and the peripheral circuitry. Thus this type of sensor is not suitable for measuring constant pressure.

Having said this, their good sensitivity to dynamic changes makes them able to measure small changes in pressure, even at high pressures. Piezoresitive sensors are able to function properly at temperatures upwards to 1000^{o}C, although the same cannot be said about its surrounding hardware. The high availability of its materials also makes them quite cheap. They offer a linear output in a 0.7Pa to 70MPa range with an accuracy of around 1%.

3.4.2 Capacitive Pressure Sensors

Two operating principles may be used to model pressure changes through capacitve sensors. The first in the variation of dielectric constant of gases, liquids and solids with pressure [45]. The second, and most prominent, is the change in capacity with changes in the spacing between plates. These principles are inherently intertwined and tend to interfere with each other, which should be taken into consideration.

The capacitance, C, of a parallel plates capacitor is given by:

$$C = \epsilon_r \epsilon_0 \frac{A}{d} \tag{3.6}$$

Where ϵ_r is the relative dielectric constant, ϵ_0 is the dielectric constant of vacuum, A is the area of the plates and d is the distance between them.

In the second, and most common, case pressure sensors may be constructed by turning one, or both, of the capacitor's plates into a diaphragm that deflects itself with changes in pressure. An example of this type of implementation is given in figure 3.16.

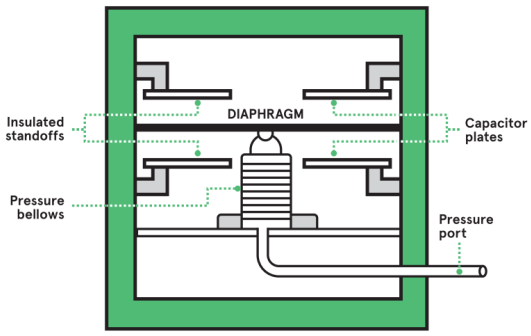

Figure 3.16: Example of a capacitive pressure sensor [44].

To facilitate the measurement of capacitance the sensor is normally incorporated in a tuned circuit. This is a frequency dependent circuit in which changes in capacitance will amount to changes in the resonant frequency. Either an oscillator or a LC circuit may be used, but the oscillator will require a power supply while the LC circuit is passive.

They can be used in differential, gauge, relative and absolute pressure measurements.

In spite of their non linear output these sensors offer good repeatability, furthermore, their ability to withstand temporary over pressure conditions makes them suitable for harsh environments

3.4.3 Optical Pressure Sensors

Optical pressure sensors relate changes in pressure to changes in light. The simplest configurations consists of a mechanism where light will be progressively blocked as pressure increases. This light can be measured by a photodiode as is the case in the example described in figure 3.17.

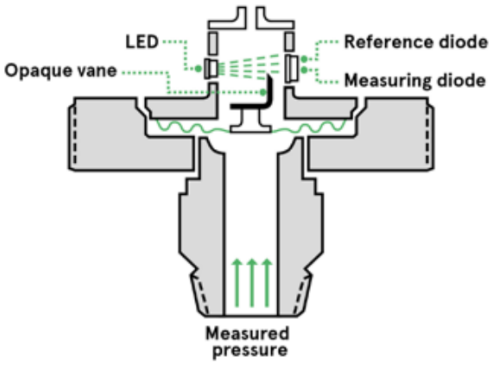

Figure 3.17: Example of a optical pressure sensor [44].

In this case, a reference photodiode that is never blocked by the vane is needed. Its purpose

is to correct variations forced by aging of light source and fluctuations in the supply voltage, among others.

Smaller optical sensors with more reliable measurements have been devised with fiber optics sensors. These utilize interferometry to measure changes in the path length and the phase of light to measure pressure. Two designs are commonly used, figure 3.18: the Fabry-Pérot with a cavity formed of two parallel reflecting surfaces placed on the tip of an optical fiber, and Bragg grating which forces a series of periodic changes in the refractive index of the fiber.

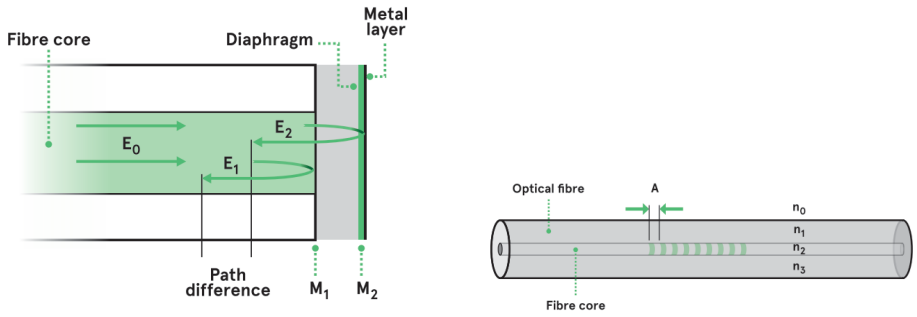

Figure 3.18: Fiber optics pressure sensors. Fabry-Pérot, left, and Bragg grating, right [44].

This is one of the best pressure sensing technologies as it is simple, accurate and easily scalable. Their freedom from electromagnetic interference also makes them suitable for harsh environments. The disadvantage of these sensors lies in the fact that their small size also makes them relatively fragile and their high sensitivity makes them susceptible to acoustic or mechanic vibrations.

3.5 Mass sensors

The most common way of measuring mass in industrial environments is through the use of load cells. These may be conceived through several approaches. In spite of this, only the most prominent type is mentioned here, which is based on the usage of strain gauges.

Strain gauges are transducers consisting of a resistive wire element that changes its resistance with the length of the wire. The strain gauges can be bonded with another solid shape, that will shorten when compressed, and lengthen when stretched. As the wire element is bonded with such shape, it will contract and expand with it, altering its resistance, which can be measured and converted into mass by a readout device.

3.5.1 Load Cells

Load cell is the name given to a structure comprising of four strain gauges in a Wheatstone bridge circuit configuration. These can have many forms, figure 3.19, suitable for different applications, including [46]:

- Single point load cells, capable of measuring off centre loads which is useful for building scales. They are often used in low capacity weighting systems.
- S-Type load cells offer high endurance and compact designs, making them suitable for tight environments with hazardous conditions.
- Tension/Compression load cells, offering high accuracy in applications where high loads are expected, making the suitable for industrial processes.
- Sheer beam and bending beam load cells can be integrated in restricted areas despite being very cost efficient and well suited to harsh environments. These are often used in multiple cell configurations such as tank weighting and industrial process control.

Figure 3.19: Type of load cell: Compression, top left, bending beam, bottom left, single point, top right, s-type, bottom right. Adapted from [46]

Many specifications are normally provided in a load cell's datasheet, however for mass measuring in batch reactors, three parameters stand out: non-repeatability, creep error and temperature induced error.[47] Creep error is specified as the deviation in the measured value after five minutes of operation. These may be summed quadratically to the transmitter's accuracy ratings to calculate the expected accuracy. The final value may be nonetheless affected by both mechanical and operational factors and as a rule of thumb, it is advisable to select load cells with expected accuracies ten times better than the desired system accuracy [47].

3.6 Flowmeters

Flowmeters take advantage of a wide variety of technologies in order to measure flow. They are grouped into four classes according to their structure, which is helpful in describing some of the factors involved in flowmeter selection. These are [48]:

- I. Flowmeters with wetted moving parts;

- II. Flowmeters with no wetted moving parts;
- III. Obstructionless flowmeters;
- IV. Flowmeters with sensors mounted external to the pipe.

The first class refers to flowmeters whose operation and performace depend on high tolerance machined moving parts. These are subject to wear and damage which can result in severe or partial failure. Any alteration to the properties of these parts, geometry for example, will amount to an increase in the uncertainty associated with its measurements. This category of flowmeter is normally only appliable to clean fluids.

Unlike their counterpart, flowmeters with no moving parts should not suffer from severe failure. They may however, be affected by plugging or excessive pressure drops. They are suitable to a broader array of applications, however flows with very dirty or abrasive fluids may pose long term problems.

Class III flowmeters are a subset of class II, with the added advantage of not constricting the flow that passes though them. These are offer prolonged life cycles, even in the presence of corrosive fluids.

Class IV flowmeters are a subset of class III with external transducers mounted on them. These don't require any kind of compatibility with the fluid that is being measured.

Flowmeters can also be grouped according to what they measure specifically.

- Volumetric flowmeters. Volume is measured directly, normally by trapping known quantities of fluid;
- Velocity flowmeters. Total flow is calculated by taking into account the cross section of the pipe;
- Inferential flowmeters if some physical process is used to infere flow;
- Mass flowmeters if mass is measured directly.

3.6.1 Thermal Flowmeters

Thermal flowmeters are sensors that use the thermal properties of the fluid to measure either velocity, or mass flow. This allow application on fluids that are not dense enough to instigate the mechanical parts of a sensor.

Hot wire anemometer is the name given to the normally used working principle of these sensors. It consists in the insertion into a pipe of two probes connected to a bridge circuit. One of the probes is eletrically heated to be at a fixed temperature above the second. The higher the flow, the higher the current needed to maintain the temperature of the probe which is an indicative of the flow through the pipe.

Temperature sensors are needed to control the temperature of the probes. Some approaches include, the use of RTD as the heated elements, from which temperature values may be attained by measuring resistance, while others use semiconductors as the heated elements, from which temperature may be calculated from the dependence of the voltage across a diode with temperature.

It should be noted that this principle relies on the assumption that thermal conductivity and heat capacity[2] of the fluid remain constant during the process.

3.6.2 Coriolis Flowmeters

Unlike thermal flowmeters, coriolis flowmeters are true mass flowmeters which makes them virtually independent of the fluid propertied. This, along with trivial installation and sizing makes these quite appealing to almost every application. The same cannot be said, however, about their cost.

Their operation is based on the conservation of angular momentum during the coriolis acceleration of a fluid. Succinctly, coriolis is the force that describes an increase in tangential velocity, when an object that is performing a circular movement at constant angular velocity moves away from the center of the circle.

Coriolis flowmeters consist of vibrating tubes, in which coriolis acceleration is forced and measured. One or two tubes may be employed in a U or even helix structure, figure 3.20, among others. The inlet and outlet ports are held stationary while sinusoidal vibration is induced in an axis between the ports. In half of the tubes, fluid flows away from the center while in the other half it flows toward the center. This makes it so the forces created by coriolis acceleration have opposite directions, which will twist the pipes. The twist is directly proportional to mass flow.

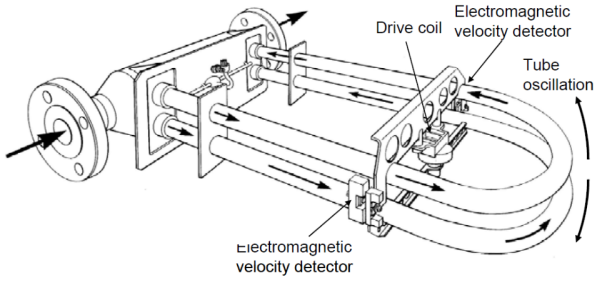

Figure 3.20: Example of a coriolis flowmeter design [48].

The application of this technology to gases may present problems related to pressure required to correctly operate it. The elimination of the need to compensate for pressure and temperature variations does, nonetheless make this flowmeters quite suitable for most applications, as does its high accuracy.

[2] The quantity of heat that a given mass requires to raise its temperature.

3.6.3 Differential Pressure Flowmeters

Due to their versatility, cost and simplicity, differential pressure flowmeters are one the most used flowmeter technologies.

These utilize empirical correlations to quantify the relation between differential pressure and the volumetric flow through a carefully designed constriction in a pipe [48].

The basis of these flowmeters' functioning is the Bernoulli equation which states the the sum of static energy, kinetic energy and potential energy, E_p remains constant in the constriction of a pipe. It can be written as:

$$\frac{P}{\rho g} + \frac{v^2}{2g} + E_p = constant \tag{3.7}$$

Where P is pressure, ρ is density, v is velocity and g is the acceleration of gravity.

For incompressible fluids, the flow can be related to velocity by using the continuity equation.

$$Q = A_1 v_1 = A_2 v_2 \tag{3.8}$$

Where A_1 and A_2 are the cross sectional area of two different points in the pipe.

Applying Bernoulli's equation to two points in a pipe, yields the following equality.

$$P_1 + \frac{1}{2}\rho v_1^2 = P_2 + \frac{1}{2}\rho v_2^2 \tag{3.9}$$

Which, by applying the continuity equation can be rearranged as:

$$\Delta P = \frac{1}{2}\rho[(\frac{D}{d})^4 - 1]^2 \times \frac{Q^2}{A_1^2} \tag{3.10}$$

Where D/d is the ratio between pipe diameters and Q is flow rate.

Some of the mechanical configurations used in differential pressure flow measurement are the Venturi tube flow meter and the orifice plate flow meter shown in figure 3.21.

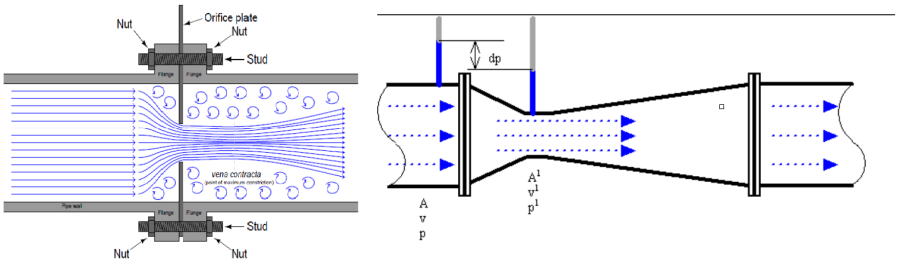

Figure 3.21: Differential pressure flowmeters. Orifice plate(left) and Venturi tube(right). Adapted from [48]

The orifice plate is the simplest although many considerations must be taken into account

for it to be properly sized. The Venturi tube sees less use for its added cost, but has the advantage of permitting regeneration of 80% of the pressure expended in the flowmeter.

In the presence of compressible fluids a expansability factor, ϵ must be added. It is assumed that pressure changes quickly enough as not to have any heat losses or work done, hence the expansion is considered isentropic and it only occurs longitudinally. For a Venturi flowmeter, it may be calculated as follows. [49]

$$\epsilon^2 = [(\frac{k\tau^{\frac{2}{k}}}{k})(\frac{1-(d/D)^4}{1-(d/D)^4\tau^{\frac{2}{k}}})(\frac{1-\tau^{\frac{k-1}{k}}}{1-\tau})]^{\frac{1}{1}} \tag{3.11}$$

Where k is the isentropic factor and $\tau = \frac{p_1 - \Delta p}{p_1}$ is the pressure ratio.

The expansability factor may be added to equation 3.10 by multiplication with its second term.

Another, simpler approach is to write the flow as:

$$Q = constant \times (\frac{\Delta P}{\rho})^{\frac{1}{2}} \tag{3.12}$$

And determine the constant trough calibration.

3.6.4 Electromagnetic Flowmeters

Magnetic flowmeters are sensors that measure a voltage induced by a fluid's flow through a pipe. These are obstructionless sensors with externally mounted transducers. Colloquially called magmeters, these sensors are comprised of a set of coils and electrodes mounted onto a pipe. A magnetic field is formed between the coils. This field forces the positive and negative charges of the fluid that flows through the sensor to separate, and thus, a potential difference is created between the electrodes and the sensor [48, 50].

To calculate flow from voltage the Faraday's law of electromagnetic induction is used.

$$E = constant \times B \times L \times v \tag{3.13}$$

Where B is magnectic flux density and L is self inductance. By maintaining a constant magnetic field the induced voltage becomes directly proportional the the velocity, which can be converted into volumetric flow by factoring in the area of the pipe's cross section, A.

$$Q = A \times v \tag{3.14}$$

Since these do not include any protrusions or obstructions in the pipe. They are a cost-effective solution for highly corrosive and abrasive fluids.

3.7 Conclusion

A selection of either previously used technologies in gasification and those that seemed most appropriate was assessed.

For all cases, the physical concepts behind their operation was succinctly addressed, with its strengths and weakness being put into perspective.

Concrete costs were not addressed as, for most cases, these values are highly dependent on situational characteristics. Qualitative comparisons were nonetheless addressed.

CHAPTER 4

Instrumentation System

A study of gasification was undertaken in Chapter 2 in order to ascertain the physical properties that would need to be measured to characterize the process. This was followed by a gross study of the technologies capable of quantifying these properties. In this Chapter the knowledge attained through these studies will be directed to the project at hand. The endeavor will be the definition of the most suited devices to form the instrumentation system of the project under development.

A high variability exists in the operating conditions of the different gasifier topologies. As so, it is not feasible to simply use previously used devices from the literature. The devised instrumentation systems in the literature will nonetheless be put into the perspective of the project at hand, and previously tested strategies will be preferred if they fit the scope of the project.

The gasifier under development is an Imbert downdraft gasifier, figure 4.1. Imbert is the name given to a gasifier with a constricted hearth area, named after its inventor, Jacques Imbert [15]. After construction, it will have a height of 754cm with 125cm of upper chamber diameter and a throat section diameter of 50cm.

Aside from the mechanical constraints, the functional parameters will have to be read, processed and written, going from the sensors to the actuators. This connection will be achieved with a microcontroller and the necessary signal conditioning.

The instrumentation system is represented by the block diagram in figure 4.2. The specific sensors and actuators will be exposed in subsequent sections, just as the chosen microcontroller.

4.1 Microcontroller

The chipKIT Max32 microcontroller [52] board from Diligent was chosen to be the centerpiece of the instrumentation system. This is a prototyping platform based around the Pic32MX795F512L microcontroller from Microchip presenting a core frequency of 80MHz, 512k of flash program memory and 128k of SRAM data memory. The development board possesses 16 analog channels connected to a 10-bit ADC, five PWM outputs, five 16-bit timers

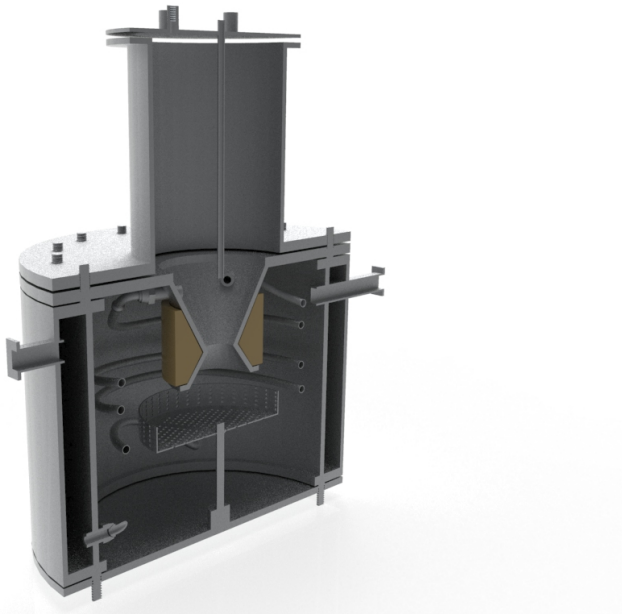

Figure 4.1: Imbert Downdraft gasifier.[1]

along with multiple SPI, I^2C and UART modules.

The broad array of functionalities of the chosen microcontroller should provide no restrictions to the selection of the instrumentation technologies. Besides, this microcontroller is widely used in the University of Aveiro and should facilitate the inlcusion of new people in the project, in case it is needed.

4.2 Pressure

Pressure inside the gasifier is affected by many factors such as the shape of the gasifier or the type of biomass used. At the moment, it is not possible to calculate the gasifier's operating pressure.

To counter this fact, the information present in [26] where the pressure profile of a downdraft gasification plant was measured at multiple points of its components. The gasifier developed in this study contained a higher throat diameter which indicates that the project's gasifier would have higher pressure drops than the one in the study. Therefore, a safety margin would have to be considered.

The values presented in this study showed pressure profiles of about 1.5kPa below atmospheric pressure, with pressure peaks of about 7kPa, above atmospheric pressure, at specific points in time of unstable gasifier operation. These values matched the range of the sensors used in gasifier control boards developed by ALL Power Labs. [53]. This and their low cost fostered the choice of the MPXV7007DP [54] piezoresistive, differential sensor.

[1] This image was created by other project members.

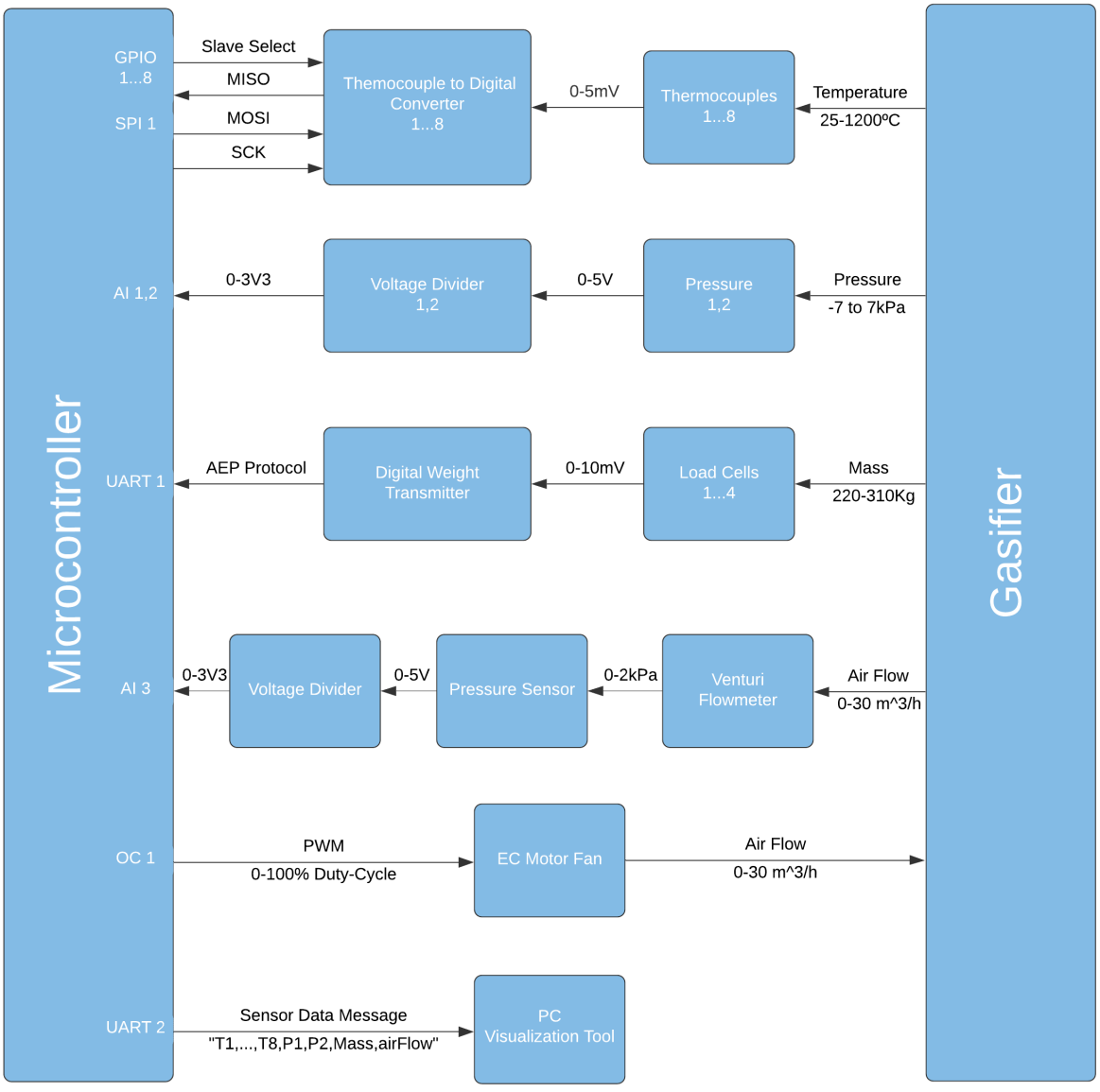

Figure 4.2: Instrumentation system block diagram. Created using Lucidchart [51].

These pressure sensors output a 0-5V DC signal. The signal conditioning for these sensors simply consists of a voltage divider to convert these into 0-3V3 DC making them compatible with the Max32.

4.3 Mass

Online measurements of the mass inside the gasifier are tightly constrained. This subsystem is expected to measure a variation of 90kg inside a 220Kg gasifier. Furthermore, the consumption of biomass was expected to round 22Kg/h. Because of this highly precise sensors are needed.

The chosen load cells were the CFI-150 [55] from Ascell. These load cells are supposed to support a maximum of 310Kg, however, to account for oscillations of the gasifier, a dynamic factor should be considered when sizing the rated capacity of the load cells. The default value used is 1.3, and no reason was found that justified deviation from this standard. The sensors would be installed in a three base configuration, each specifying a rated capacity of 150Kg, forming a total rated capacity of 450kg. This value is high enough to provide a safety factor while not overly hindering the accuracy of the measurements with non-repeatability of 0.01% and a creep error of 0.03%. Temperature is compensated in the range the sensors will be subject to and thus, was not considered in the calculations.

AEP transducers' TA5 digital weight transmitter [56] was used to connect the load cells to one of the microcontrolers UART. This IC possesses the capacity to internally perform the parallel of the load cells connected and includes low pass filtering of the signal, with an accuracy of 0.01%. Its output is a digital signal in the form of the dedicated AEP protocol [57].

With these characteristics, expected accuracy corresponds to the quadratic sum of the previously mentioned errors:

$$Espected\,Accuracy = \sqrt{0.01^2 + 0.03^2 + 0.01^2} = 0.031\% \tag{4.1}$$

Taking into account the system's rated capacity would imply an accuracy of approximately 140g.

$$Absolute\,Accuracy = Espected\,Accuracy \times Rated\,Capacity = 140g \tag{4.2}$$

As the expected biomass consumption rounds 6g/s, sampling time of the weighting system should not be inferior to, approximately:

$$Sampling\,Time > \frac{Absolute\,Accuracy}{Biomass\,Comsumption} = 23s \tag{4.3}$$

Meaning that for the change in biomass to surpass the measuring error, a minimum

sampling time of approximately 23 seconds should be used. This value is pertinent only to the mass measuring system, however, if the full system's sampling time is truncated to it, a control configuration like the one shown in figure 4.3 could be used.

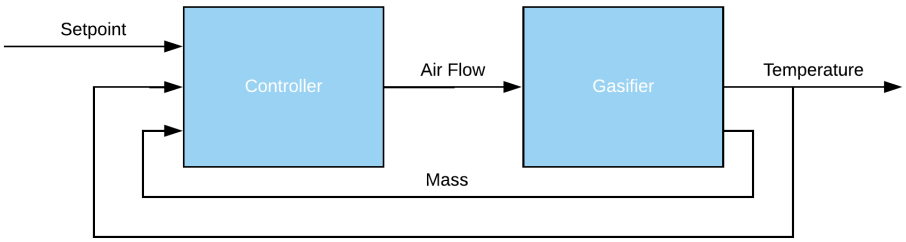

Figure 4.3: Control strategy proposal.

4.4 Fan

Initially, the air actuation subsystem was idealized to be formed static operating blower followed by a proportional control valve, that would be used to control the flow of air entering the gasifier.

The research exposed in Chapter 3 proved a need for the reconsideration of this decision. Properly sizing a valve was deemed to be too problematic for a project where the operating conditions are uncertain. Under sizing the valve would simply constrict the allowed flow rate, which will need to be experimentally tested, inevitably by trial and error in order to be optimized. Under sizing would also impose unnecessary pressure losses in the system which may result in motor failure. Over sizing, on the other hand, would hinder the already troublesome control of the gasifier, and result in unnecessary monetary costs.

With this in mind, the approach was replaced by a speed controlled fan, mainly for the higher margin of error. The equipment selected was the RG130/0800-361 radial fan [58].

This device incorporates an electrically commutated, EC, motor. More concretely, a DC brushless motor controlled by an embedded electronic circuit board, which is supposed to provide greater control and higher efficiency. This device is sold at a cost of 228.48€, in Farnell [59], which is even cheaper than a solenoid valve for the same flow rate [60]. The fan has a power consumption of 40W, being much more efficient that its DC and AC counterparts. The blower is able to force a flow rate of 30 m^3h^{-1} under a pressure of 3kPa, thus providing and comforting safety margin.

To fully control the air flow that goes into the gasifier, a fan is not sufficient. As changes in pressure profile will incur changes in the fan's operating point, air flow must also be measured in order to compensate for these variations. A subsystem must then be formed in order to control air flow as shown in figure 4.4.

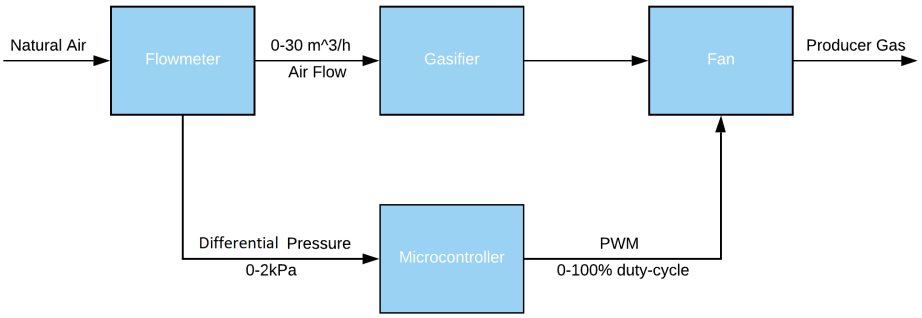

Figure 4.4: Air control subsystem.

4.5 Air flow

In order to simplify the selection of the flowmeter, it was decided that the quantity of gasifying agent would be measured at the entrance of the gasifier where both temperature and pressure would roughly match those of the atmosphere. As so, the main focus behind the sizing of the flowmeter was cost and durability.

Judging from the offers present in Endress+Hauser [61], one of the leading companies in industrial flow measurement, for the projects characteristics, sizing of a flowmeter could range from the cheapest thermal flowmeters, starting at around €1300, to the most expensive coriolis flowmeters, at around €8000 [61].

With this in mind a Venturi tube differential pressure flowmeter was chosen. The available resources permit in-house design and construction of the mechanical parts of the sensor majorly reducing its cost. Furthermore, this type of flowmeter has no moving parts making it durable.

The pressure sensor chosen to measure the differential pressure between the Venturi tube's outlets was the MPXV7002DP [62] which has a higher accuracy than its aforementioned counterpart, 2.5%, at the expense of a lower measuring range, -2kPa to 2kPa, for the same cost. The change was driven by the fact that the measurements of the air flow would be utilized to actuate the system unlike other sensors which are mostly used for surveillance purposes.

4.6 Temperature

The temperature inside a downdraft gasifier may reach values of up to 1200ºC. As so, type K thermocouples were used to measure it. This choice is dominant in the literature, being used in [23, 31, 63–65], among many others.

In order to connect the thermocouples to the microcontroller the MAX31855K amplifier [66] was utilized. This IC incorporates cold junction compensation and has a digital output with the SPI protocol specifying an accuracy of 2ºC. In [63, 67] this IC was sucessfully used

to connect the thermocouples to the microcontroller, corroborating its selection.

4.7 Development of a visualization tool

In order to allow efficient, real time, monitoring of the gasifier's operation a visualization tool was developed. Gasification is multi variable process with many parameters that need to be monitored and optimized. As so the need arises for a visualization capable of concurrently displaying these parameters. Such application should allow quick inferences about the gasifiers's current state whilst providing a way of analysing the overall gasification run and the relation between its different parameters.

4.7.1 Scope

The first step in the development of any visualization tool is the definition of the users and their subsequent needs. By the end of the software's development the following functionalities should be enabled:

- Monitoring of the gasifier's current state;
- Display of the operating parameters: temperature, mass, air flow and pressure;
- Concurrent analysis of the evolution of these parameters through the gasification run.

A gasification project may involve personnel from various areas such as chemistry, mechanics and eletronics. This implies a variable set of skills when it comes to data processing. With this is mind, the developed app should provide an accessible and efficient analysis tool for all of its users.

4.7.2 Implementation

The software was implemented using JavaScript, more specifically the d3.js library. This is a tool that allows the creation of dynamic visualizations featuring a broad array of personalising options. It is compatible with all recent browsers and has the advantage of supporting large data sets. Its main disadvantage is not having pre constructed visualizations although a large quantity of examples is available online.

The gasfier's ilustration was developed externally using the Inkscape software [68]. This software is a high level tool that supports the editing of SVG (Scalable Vector Graphics) files. It was used to divide a schematic of the gasifier into several, strictly labeled, SVG elements, pertaining the different sensor zones, facilitating their post processing in the tool's scope.

The real time updating of the data displayed is carried out by simply reloading the data set at specified time intervals. The complexity and size expected for the data sets did not justify

bolder approaches. The path of the data is described by the flowchart in figure 4.5. After the data from the sensors is read and converted to the appropriate units, data from all sensors is appended to a string, separated by commas. The formed message is then sent through one of the microcontroller's UART. This latter procedure is repeated at every sampling time, at a bare minimum. From the laptops perspective, a python script periodically checks the chosen serial port to read the sent message. The message is then appended to a csv (Comma-separated values) file where the data is stored. Finally the software loads the data set at specific instants, updating the visualization. As a batch gasification run may take a couple of hours, delays between transmissions should not be cumbersome to the user.

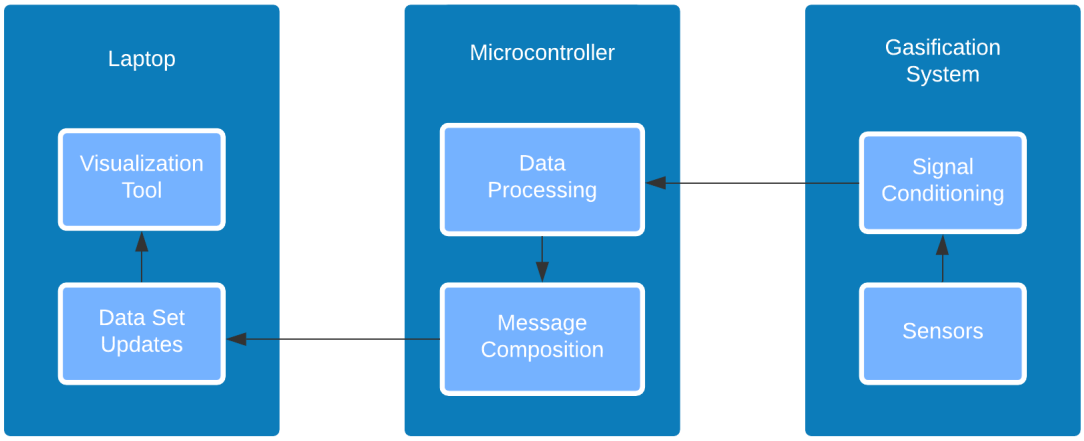

Figure 4.5: Data path flowchart. Created with Lucidchart [51]

4.7.3 Solution

The solution developed, shown in figure 4.6, consists of a dashboard containing an illustration of the gasifier, delimited by the areas monitored by each temperature sensor, three sectors displaying concrete values of the ongoing gasifier operation, and a customizable scatter plot of the evolution with time for the different quantities.

The gasifier illustration is used two purposes. The first is to allow overall determination of the gasifier's stability. When a gasifier reaches a stable sate of operation a gradient of temperature should be observable with the temperature monotonously rising when going from the pyrolysis zone into the combustion zone and then decreasing when nearing the reduction zone, as mentioned in section 2.5. The tool magnifies this gradient by coloring the areas pertinent to each temperature sensor with a color intensity computed with a color scale. The second purpose of this illustration is to act as a control panel of the data in the scatter plot as brushing is employed by clicking on a sensor respective zone to select the data displayed

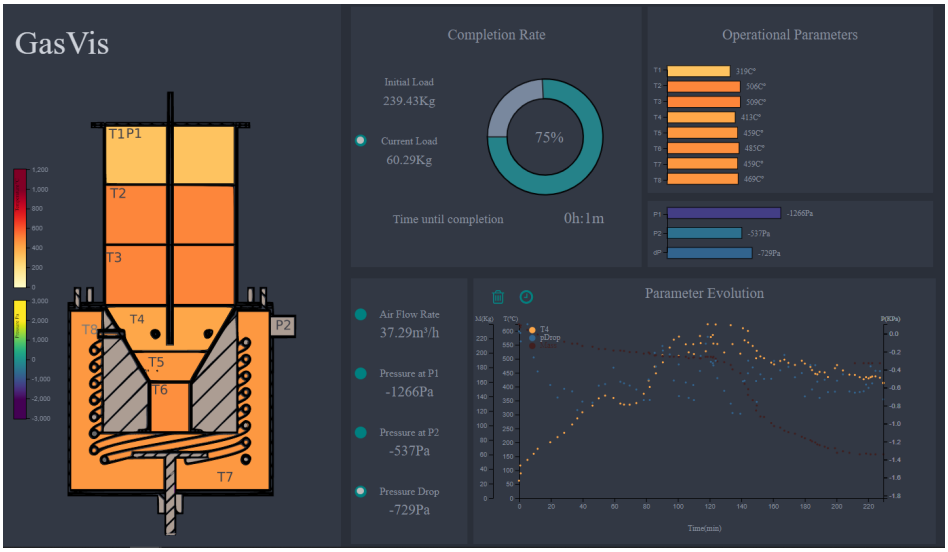

Figure 4.6: Visualization Tool.

on the scatterplot.

Despite of the ability of the chosen visualisation to providing a rapid overview of the system's state, color is not reliable in quantifying value. Because of this, the temperature distribution is also exposed in a bar chart. This approach makes it simpler to visualize the gradient of temperature along the height of the gasifier. The positioning of the sensors was not known at the time of developing this tool. In the future, the bar chart should be replaced by an histogram, substituting the categorical scale with the height of the gasifier.

The bars associated with pressure were separated from the rest as, unlike in the temperature case, there is no value in the sequentially of the bars.

The parameter evolution sector promotes the visualization of the system's properties with respect to time. Its contents can be easily toggled on or off, either by clicking on the picture, or through the use of conveniently placed buttons. This allows the analysis of a single parameter, or the concurrent analysis of the selected parameters, permitting the study of the relation between them.

Alongside the buttons, the current values of different parameters are displayed. The idea is that after the initial set up, for a normal gasification run, no further user input should be required.

In case the user wants to explore the ongoing run, or previously existing data, updates can be disabled, enabling the brushing functionality of the scatter plot, shown in figure 4.7.

Using this, the user may select a time lapse. The whole visualization will then be updated to show the average values in the selected window.

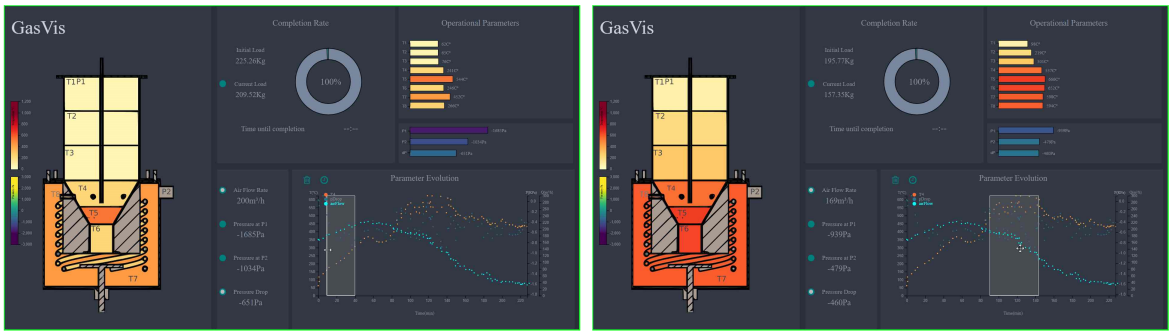

Figure 4.7: Visualization Tool, Brushing example.

4.8 Conclusion

A selection of sensors and actuators was proposed. This selection was based on previously used strategies when this information was available in the literature and compatible with the project at hand.

As mentioned in the beginning of the Chapter, it is nor possible at this point in time to fully predict the operating conditions of the gasifier. With this in mind, safety margins were always taken into account when sizing the different device specifications.

In spite of this, the proposal will still have to be tested in the real system as to realistically determine its suitability for the project.

A visualization app was developed to facilitate the monitoring of the gasifier's operation and its post operation analysis. The app was devised in a single iteration. As so, its implementation should be revisited after extended use to determine if it satisfies the user's needs.

CHAPTER 5

System Identification: Model Comparison

As asserted in Chapter 2, the performance of the gasification process can be influenced by many factors. As a result, gasifiers need to be designed either by analysing experimental data and/or by using mathematical or simulation based modelling [1].

A model is a topological or mathematical structure relating a set of input and output variables. Two major categories of systems exist: behavioural and physics based models. Physics based modelling, also known as white box modelling, describes a system through a set of physic equations that describe the interaction between the different system components, thus revealing the inner constitution of the system [69].

Behavioural, or black box modelling, describe a system without regard for its inner variables as only the system's response to predefined input signals, and these signals, are taken into account. This category is defined by a purely mathematical model carefully chosen and tuned to make the system's inputs match their corresponding outputs.

The main outcome differences between these approaches lies in generality and computational efficiency. Physics based models usually offer very good prediction and generalization abilities at the cost of high computational loads. Behavioural models, whilst being able to provide very high accuracy at high computational speed, suffer in terms of generality as they are utterly constrained by the information in the extraction signals. All information that isn't in these signals does not exist.

On one hand modelling has always played a key role both in applied gasification work as it is very effective in optimizing the operation of an existing gasifier. Models have been used to study the operation limits of the process and gain insight about the relation between performance and operating parameters whilst providing a low-cost way for exploration of the potential benefits, costs and risks associated with a gasification project [70, 71]. On the other hand, simulation is an extremely important tool for control system design. As explained in [72], for arbitrarily nonlinear plants, there is often no alternative to designing controllers by means of trial and error, using computer simulation.

This Chapter will consist of a literature review on the modelling approaches than have

been and currently are being used in the literature.

5.1 Thermodynamic equilibrium

Thermodynamic equilibrium models, commonly used to predict syngas composition in gasification systems, are based upon the application of the second law of thermodynamics to chemical reactions [9]. The usage of this law rests on the assumption that all specimens react completely over an indefinite period of time, with a reaction rate that is either constant or null. This amounts to saying that the concentration of species in a given reaction isn't dependent on time.

This assumption automatically makes this approach unsuitable if the endeavor is to obtain a dynamic model. Furthermore, it is nearly impossible to reach thermodynamic equilibrium in a gasification process. These will be, nonetheless, addressed in this dissertation for their prominence in the literature, justified by their simplicity and capability to promote inferences about biomass composition, syngas composition and other gasification parameters, thus making them a invaluable tool in a gasification project.

A commonly used procedure is to develop a general model and fine tune it with site specific correction factors [12]. Thermodynamic equilibrium models are mostly used in downdraft gasifiers, as this is the category that operates closest to equilibrium.

Equilibrium models can be divided into stoichometric and non stoichometric. The difference lies in the fact that in stoichometric models the reactions and species involved in the process are required to predict syngas composition whilst non-soichmoteric models predict syngas composition by minimization of Gibbs free energy. These approaches are, however, essentially equivalent as shown in [73].

Several assumptions are typically made when developing these models as shown in Appendix A. A description of the implementation of thermodynamic equilibrium models is also addressed in this appendix.

Underestimation of CH_4 and CO_2, just as overestimation CO and H_2 is a frequent problem plaguing these models. The major disadvantage with these models is the fact that they do not allow inferences about the shape of the gasifier, which constitutes a key aspect of its design.

5.2 Computational fluid dynamics (CFD)

Computational fluid dynamics models are based on the study and analysis of fluid flow, heat transfer, mass transfer, chemical reaction and related phenomena. They are described by set of equations representative of these processes that are solved using numerical methods in computer-based simulation, mostly accomplished using commercial software. The main point that sets these models apart from their counterparts is the emphasis given to fluid dynamics [12, 74].

When it comes to gasification, most literature refers to fluidized bed gasifiers, with CFD models being considered among the best developed models for this type of gasifier [14].

CFD models are intrinsically more appropriate to describe fuidized bed than fixed bed gasifiers [75, 76]. According to [77] all the CFD models in the literature make the assumption that particle are of a spherical shape and have a uniform distribution like in fluidized bed gasifiers but this is not the case for fixed bed gasification were wood chips and cylindrical pellets are used. In addition to high pressure-drop, non-uniform temperature and porosity distribution, fixed bed gasifiers also have mass transfer limitations by pore diffusion and external mass transport. Because of this, CFD models of fixed bed gasifiers should also be coupled with phenomena of non-uniform porosity distribution, particle shrinkage, swirl flow in the combustion zone and intra pellet mass transfer limitations on the reduction zone.

As stated in [78] , CFD models are still in a nascent stage to get a insight of the gasifier's performance.

In light of the above mentioned reasons and seeing as this dissertation is focused on a fixed bed, downdraft gasifier, no further research was done on CFD models. It should be noted, however, that there is significant ongoing work aimed at developing detailed CFD and kinetic models [1]. Furthermore, a great part of the equations developed for kinectic models, assessed in subsection 5.5, may also be used for CFD models.

5.3 Modelling with Simulink

Simulink is a block diagram environment, developed by Mathworks for multidomain simulation and Model-Based Design. Simulink is widely used in control theory and digital signal processing for simulaion and design [79].

Since the ultimate goal of this dissertation is the development of a temperature controller, it would be helpful to have a Simulink based plant model in order to design said controller.

In spite of this, to the best of the authors knowledge, only two dynamic models have been developed in the literature using Simulink.

One of them [8] is a very simplistic model of the gasifier's produced high heating values, HHV, as a function of air flow. This model was developed as a part of a larger gasification facility submodel and used to develop a grid frequency controller, thus not being usable in this dissertation.

The other was developed by T. Paes in [6] for an updraft gasifier aiming to develop a controller for temperature and outgoing mass flow. This model was developed by dividing the gasifier into equal slices of height, Δx, and modelling each slice individually and sequentially. Model structure was dependent on: concentration of element k in the gas flow, Y_k, concentration of the solid compound l, Y_l, gas temperature, T_g, temperature of solids, T_s, generation of elements, G_Y and generation of heat, G_h as is illustrated in figure 5.1.

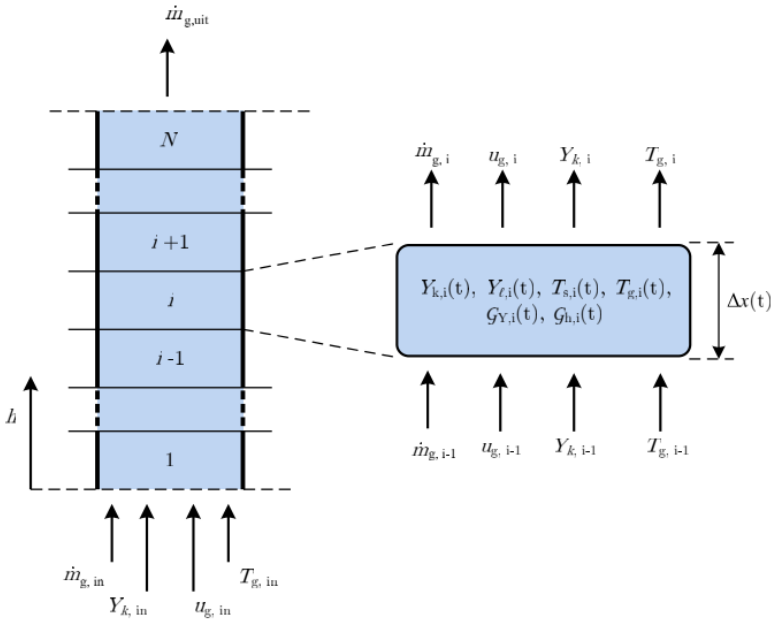

Figure 5.1: Simulink model architecture [6].

As the authors points out, although modelling gasification in simulink offers the possibility of easily doing tests and use the final model for online control, the formulation of a dynamic model becomes too large to remain practical. It should be noted than the developed model consisted of 40 slices of 2cm each. Furthermore, the development of the model was based on the monotonous decrease in temperature along the gasifier's height, which is only the case for updraft gasifiers and thus, is not suitable for this dissertation.

5.4 Kinetic Equations

As seen in section 5.2, thermodynamics are able to predict the composition of species at equilibrium or steady state. They don't, however, tell us anything about the dynamics that lead to that steady state. This is the field of chemical Kinetics [80].

Besides equilibrium gas composition, kinetic models are able to predict temperature and gas composition throughout the various gasifier zones as well as its evolution through time during non-steady state operations and startup. This implies that, in addition to reaction kinetics, detailed fluid dynamics modelling is required for the model to be accurate. Furthermore, models of particle size distribution, micro-scale mass transport and mixing inside the gasifier may still be included to further improve accuracy.

This accuracy and detail are, however, very difficult to achieve in practice due to the underlying complexity of modelling gas-solid-particulate fluid flows, gas-solid contacting process and microscopic evolution of particle distributions, among others [1].

Even for the simpler cases, variables factored in rate equations may incorporate: temperature, pressure, composition, phase state, ph, solvents, etc. The result is a very accurate but highly computational intensive model [14]. Because of this, many authors choose to model only key equations of the gasification process [1], while others choose to model the regions of the gasifier individually. A common approach is the use of a independent reduction zone model coupled with a general model of the remaining regions [9].

A simplified overview of the general model structure, and the definition of the ordinary differential equations it encompasses is addressed in Appendix B. This overview is based around the work developed in [10]. Comparison between the results attained, for molar concetration of different species, with the analysed model, experimental values of two different gasifiers and results obtained by another model present in the literature are shown in figure 5.2. The structure of kinectic models showcases a strong dependence between kinectic and fluid

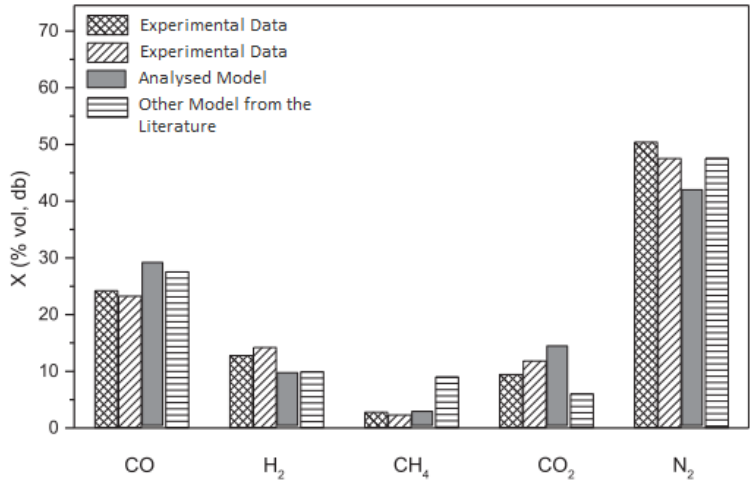

Figure 5.2: Comparison between molar concentration of species obtained by experimental measurements and kinectic models [10].

dynamics parts. Because of this, an increase in the detail in one part must be complemented by an equal increase in detail in the other, thus fostering a major increase in complexity [9].

If one desires to create a dynamic kinectic model, all of the ordinary differential equations would become partial differential equations instead. Such procedure was undertaken by Osgun Yucel et.al in [13]. This model incorporated, aside from the usual species conservation equations, the division of energy conservation equations assigning a different equation for solid phase, gas phase, inner wall and exit gas. Furthermore, it still included the effects of conservation of wood, conservation of char, conservation of moisture and conservation of mass for the exiting gas.

To solve the large amount of differential equations devised, the system is solved in a loop iterating over finite time steps. At every iteration, reaction rates are calculated followed by

transport and then temperature equations. Transport equations are solved using Matlab's routine Ode45, which implements Runge-Kutta method of order 4 with variable step size control. Energy equations however, are solved using a variable order method implemented by Matlab's ode15i. Figure 5.3 shows the results obtained for the evolution of injection temperature with time.

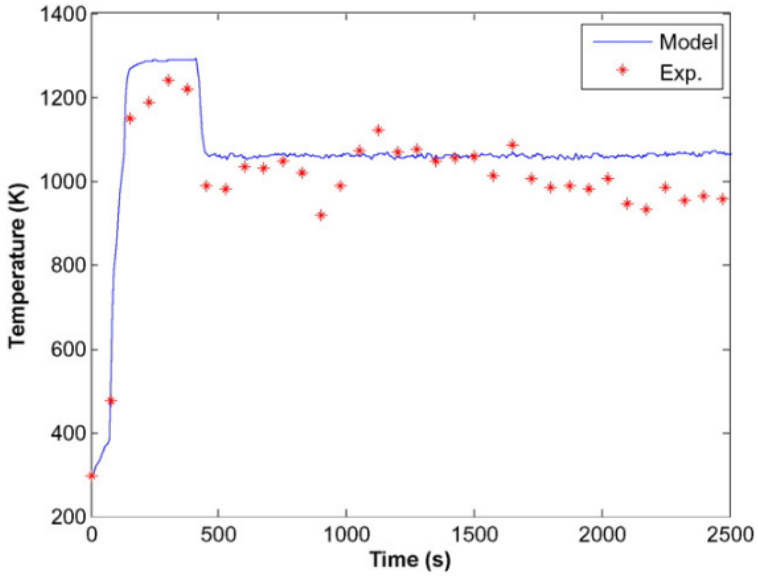

Figure 5.3: Evolution of temperature at injection point with time [13].

The author justifies the deviation between model and experimental values by explaining that, in the real case, air is drawn with vacuum while in the model, pressure in calculated continuously and air is drawn in to compensate vacuum difference.

5.5 Neural Networks

Artificial Neural networks are the result of men's attempt to mimic the behaviour of the human brain and establish it upon a machine. Neurons are the basic information processing element in the central nervous system, and thus, the basic processing unit in neural network models [81].

Conceptually, a neuron is an element that receives multiple inputs, multiplies them by weight factor, and uses the overall sum as an argument to an activation function. Biases are added at multiple points of the process as is depicted in figure 5.4 [82].

The behaviour of the neuron is mathematically described by the following equation.

$$y = b_0 + f(\sum_{k=1}^{n} x_k w_k + b_k) \tag{5.1}$$

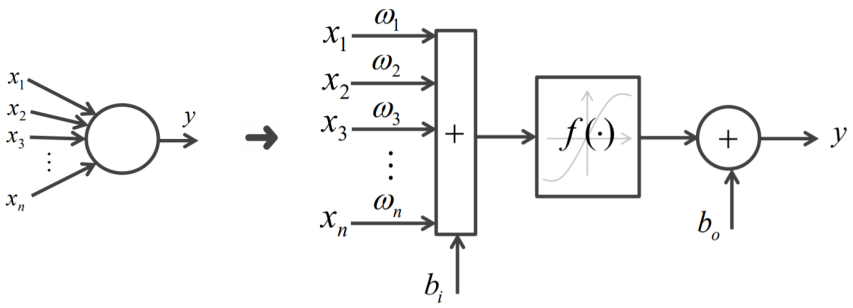

Figure 5.4: Neuron [69].

The activation function f may take many forms. The most common, shown in the figure 5.5 , are the hyperbolic tangent and the radial basis function, colloquially called sigmoid and gauss bell.

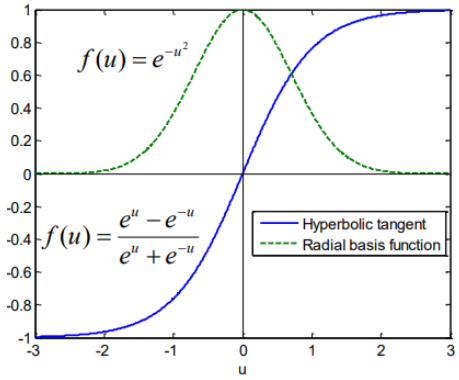

Figure 5.5: Neural network activation functions [13].

Several neurons can be grouped together and connected to form a neural network. Different structures may be formed, of which the simplest is the Artificial Neural Network, ANN, shown in figure 5.6.

The idea is to determine the network's weights and biases as to make a set of output data fit a set of input data. This process is known as model training or parameter extraction, depending on the context.

ANNs are not prepared for the modelling of dynamic systems. The simplest way of permitting this is to clone several ANNs, feed them with delayed versions of the input signals, and sum all the outputs. This is the concept of Time-Delayed Artificial Neural Networks, TDNN.

Recursivity may still be applied by simply adding the outputs and their delayed instances to the input of the network. As a great deal of information is stored in the system's outputs, doing this will most likely lead to a significant decrease in the number of neurons in the

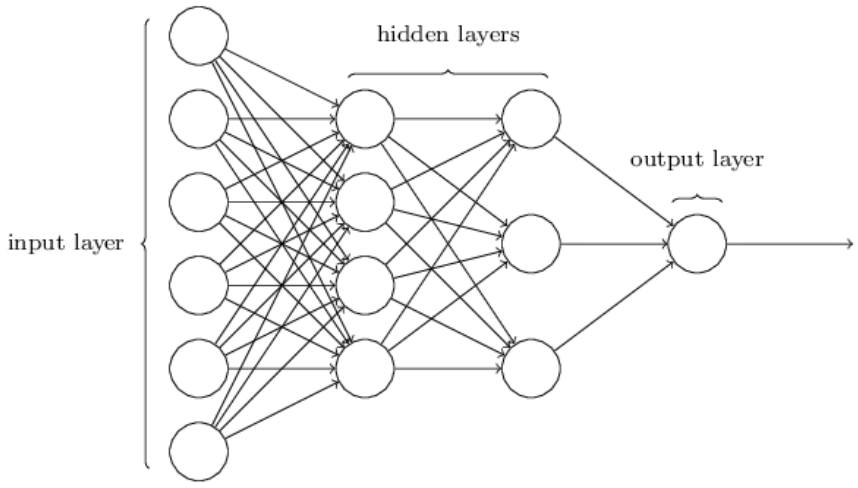

Figure 5.6: Neural network activation functions [13].

network [69].

5.5.1 Neural Networks in Gasification

As was explained in the previous Chapters, biomass gasification is very intricate process governed by a large number of operational parameters. As so, the development of physical model requires many idealizations and assumptions, resulting in a very simplified model, with little predictive capability. Because of this, the ability of universal approximattors, such as neural networks, to learn directly from input-output data makes them an appealing alternative to tackle this problem [83]. Furthermore, as these models constitute a direct mapping from input-output data, they still remain computationally efficient and thus, are appropriate for control purposes [84].

Most investigations on the use of neural networks have been conducted on fluidized bed gasifiers, with only a few investigations being made for downdraft, fixed bed, gasifiers. As Mikulandrik explains in [84], NARX neural network models seem to be a promising approach to describe non-linear systems with significant delays, where accumulation of mass and energy is considered. It should be noted that in fixed bed case, mass and energy accumulation is expected to be even higher than in its counterparts.

The major drawbacks of neural network models is that, as nonlinear in the parameters, black box models, the modeller cannot identify the most important parameters that influence prediction performance.

A nonlinear autoregressive with an exogenous input NARX, model constructs its output, $\hat{y}$ as combination of a finite number of past outputs and inputs, u [85].

$$\gamma(t) = [y(t-1), ..., t(t-na), u(t-1), ...u(t-nb)]^T \tag{5.2}$$

$$\hat{y}(t|\theta) = h(\delta(t), \gamma) \tag{5.3}$$

Where:

- na is number of output delays;
- nb is number of input delays;
- h is a set of nonlinear basis functions.

A NARXNN is the neural network's representative of a NARX model, which, for a single hidden layer with a single outputs, can be defined as:[86]

$$\hat{y}_t = \psi_2(\sum_{i=1}^{m} w_i^{(2)} \psi_1(X_{t-1}) + b^{(2)}) + e_k \tag{5.4}$$

$$X_{t-1} = \sum_{j=1}^{dx} w_{xj}^{(1)} x_{t-j} + \sum_{k=1}^{dy} w_{yk}^{(1)} y_{t-k} + b^{(1)} \tag{5.5}$$

Where:

- m is the number of sample in the dataset;
- $w_i^{(2)}$ are the weights between the hidden and the output layer;
- ψ_1 is the activation function of the hidden layer;
- ψ_2 is the activation function of the output layer;
- $b^{(2)}$ and $b^{(1)}$ are the bias terms in the output and hidden layer respectively;
- $w_{xj}^{(1)}$ and $w_{yk}^{(1)}$ are the weight terms of inputs and delayed outputs connected to hidden layer respectively.

In [87], several types of neural networks where used to predict syngas composition and calorific values in a fixed bed gasifier. The results demonstrated suitability of neural networks for prediction of gasification outputs as all the reviewed models showed a correlation coefficient, R^2, above 0.99. Among the tested networks, namely: feed-forward, cascade forward, Elman, and NARX, the latter showed the best results with an R^2 of 0.99869. It should highlighted, however, that these results were attained for one-step ahead prediction models, meaning that the models can only predict one time step into the future.

5.5.2 Choice of input parameters

Aside from the general structure, the definition of network's inputs remains undiscussed. In [87] this problem was addressed by comparing different choices of input variables through Principle Component Analysis.

The overall procedure of PCA can be described as:

- Compute the covariance matrix of the input variables as:

$$C = \frac{1}{m-1}\sum_{n=1}^{m}(x_n - \bar{x_n})((x_n - \bar{x_n}))^T \tag{5.6}$$

  Where $\bar{x_n} = \frac{1}{m}\sum_{n=1}^{m} x_n$ and m is the number of samples of each input

- Compute the eigendecomposition of C;
- Sort the resulting eigen values in decreasing order such that $\lambda_1 \geq \lambda_2 \geq ...\lambda_n$;
- Define the percentile cumulative energy captured by these principal component;

$$E(k) = \frac{\sum_{i=1}^{k}\lambda_i}{\sum_{i=1}^{N}\lambda_i} * 100 \tag{5.7}$$

- Define a threshold ζ and compute the final input vector:

$$p_n = [v_1, v_2, ..., v_k]x_n \quad \text{s.t} \quad E(k) < \zeta \tag{5.8}$$

  Where v_i is the correspondent eigenvector of the eigenvalue λ_i.

By following this procedure, the resulting input vector will contain at least ζ percent of the total energy in the dataset. Furthermore, as the columns of the resulting matrix are independent variables with minimal redundancy, multicollinearity problems between input vectors will be reduced.

In the previously mentioned study [87], ζ was set to 90%, and a collection of ER, fuel flow rate, temperatures at different points inside the gasifier and ultimate and proximate analysis of biomass. The results culminated in only 3 of the initial 16 input variables being present in the input matrix, which were not disclosed. The authors do, nonetheless, state that biomass properties, namely concentrations of: C, H, N, Moisture, Ash and Fixed Carbon are not present in the final input matrix. This is not unexpected as these inputs constitute vectors of constant values.

5.5.3 State of the art

Two neural networks downdraft gasifier models stand out in the literature. One of them is the third paper published by Mikulandric related to gasification modelling [84]. In this work several Multiple Input Multiple Output (MISO) NARXNN models, composed of 10 hidden layer neurons with hyperbolic tangent activation functions were developed to predict syngas composition and outlet gas temperature, figure 5.7. The model inputs were always

composed of Fuel flow rate, air flow rate and their respective delayed versions, aside from the delayed versions of the output. In spite of a very good one-step ahead prediction ability shown by the models, the author demonstrates a major deterioration of the model's accuracy for multistep-ahead predictions, as shown in figure 5.8.

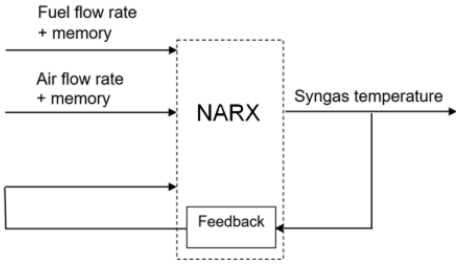

Figure 5.7: NARXNN model structure for temperature prediction [84].

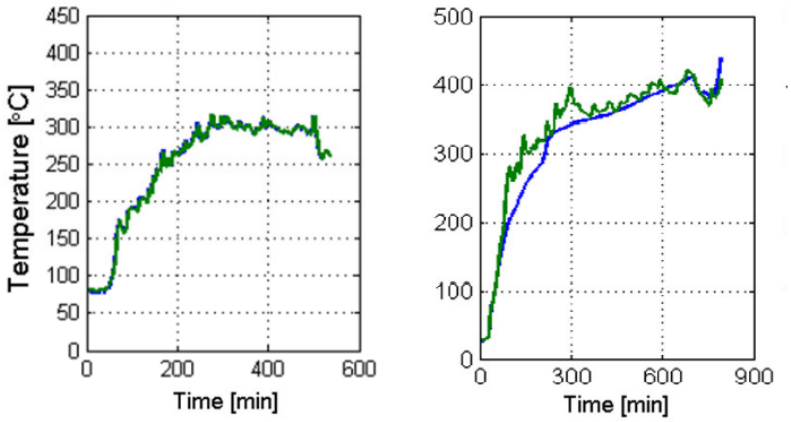

Figure 5.8: Example of one-step-ahead [84] (left), and multiple-step-ahead (right) temperature predictions [88].

This lead the author to the conclusion that NARXNN models can produce quality predictions if the measured values are used as history for the models input, however, for long term predictions the accumulation of error in consecutive predictions leads the model to become unstable and thus produce high prediction errors. The model was only considered useful for prediction horizons up to 5 minutes, which correspond to 10 samples for the sampling frequency used. In spite of this, the devised model was still able to provide good hourly predictions of temperature and syngas composition.

The second corresponds to the work done by F. Elmaz et.al in [86]. In this paper a NARXNN model was used to simultaneously predict throat temperature, syngas composition and calorific value. This model is composed of a hidden layer formed by 10 neurons with hyperbolic tangents as activation functions. Aside from delayed outputs, results from

proximate analysis of biomass and equivalence ratio were used as the network's inputs, as shown in figure 5.9.

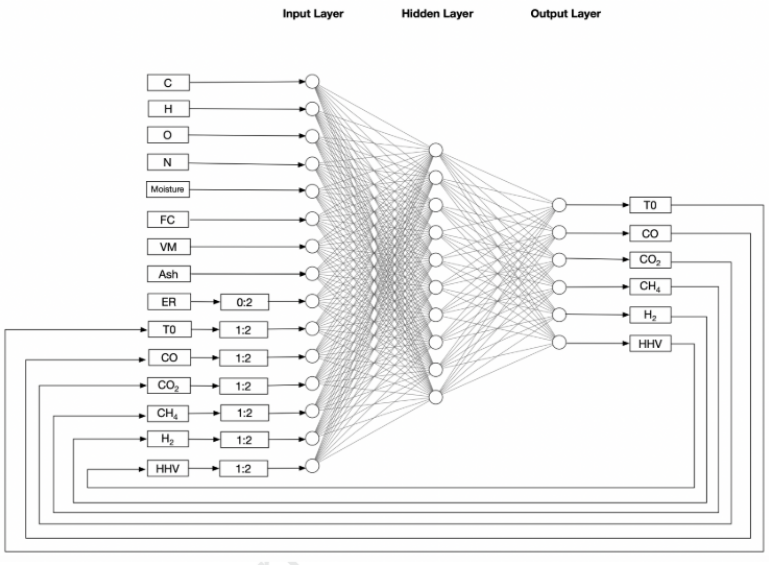

Figure 5.9: NARXNN model [84].

This work shows much better results for multiple step ahead predictions. Figure 5.10 exposes the results of the model's validation through rolling windows analysis. In this validation procedure the first 1000 points is used for parameter extraction with subsequent prediction of the next 100 points, the model is then retrained with all the previous points and used to predict the subsequent 100 points of data. This procedure is repeated until there are no more points left.

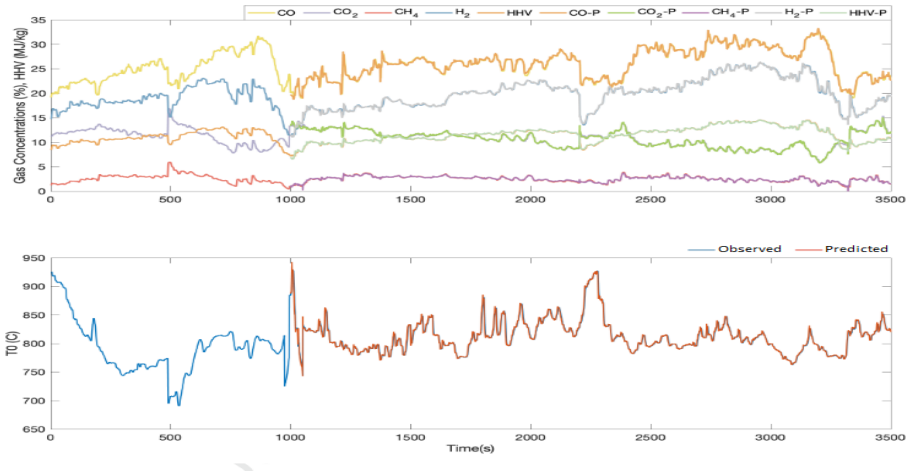

Figure 5.10: Rolling window analysys. Prediction starts at $t = 1000$ [86].

As can be seen from figure 5.10 the predicted points are almost impossible to differentiate

from observed points for all the system's outputs.

It should be noted that while in [84] a sampling rate of 30s was used, in [86], the data was sampled at intervals of 1s.

5.6 Conclusion

An exposition of the model architectures utilized in the literature was done with the goal of finding the adequate architecture to devise a dynamic simulation model. This would be used to simulate the behaviour of a downdraft gasifier under different conditions.

Ideally, a Simulink model would be the obvious choice for its potential utility in control system design. This choice was, however, considered unfeasible as the available literature showed that very limited research was undertaken with this category of models and that the tool itself is not fit for detailed description of the gasification process.

Themodynamic equilibrium, albeit the most used topology in the literature are based on many assumptions, thus undermining their potential. Although their performance can be improved by using coefficients for equilibrium constants or yield distribution, they are still plagued by poor results as many gasification reactions are simply too slow to reach equilibrium. These are very useful nonetheless, more so for downdraft gasifiers, and are advisable to run even if a more complex kinectic model is being developed [1].

CFD and kinectic models possess a higher predictive ability and simplify the study of more intricate design aspects. In order to optimize parameters like gasifier size, particle size distribution, feed-stock density, among others, a kinetic or CFD model is needed. These models, however contain kinetic and transport parameters that are hard to come by and will, at least to some degree, restrict its operation to a specific gasifier type and design.

The most recent literature has shown Neural Networks to be the most efficient architecture to model the outputs gasification process. These models foster the advantages of not needing extensive knowledge regarding the process at hand to be devised whilst still being able to accurately model the dynamic behaviour of the gasification outputs at low computational loads. These models are, however, next to useless in gasifier design optimization as it is very hard to correlate its inner workings with gasificaton parameters. Furthermore, the accuracy of the parameter extraction stage is dependent on the quality and quantity of experimental data, thus restraining its operating range.

In light of the aforementioned reasons and since, for this particular dissertation, the purpose of the model is to create a simulation environment with which a temperature controller may be designed, the only real options would be a dynamic kinectic model or a Neural Network. In spite of the rigorous and realistic testing that could be undertaken with a Kinectic model, the Neural Network topology was chosen. Kinetic modelling of dynamic systems are still in a very immature state of development and thus, to developed one such model with reasonable

accuracy would outweigh the purpose of this dissertation. Furthermore a Neural network model, due to its much higher computational efficiency, fosters a great potential for Model Predictive Control.

As so, at this point in time, a Neural Network model, with a NARX architecture, seems to be the best alternative to devise a dynamic simulation model.

CHAPTER 6

System Identification

In this Chapter, system identification of a gasification plant with a NARXNN model will take place. In order to do so, a general identification strategy will be implemented in Matlab.

The typical procedure in behavioural system identification is comprised of four lead actors, as described in figure 6.1 [89].

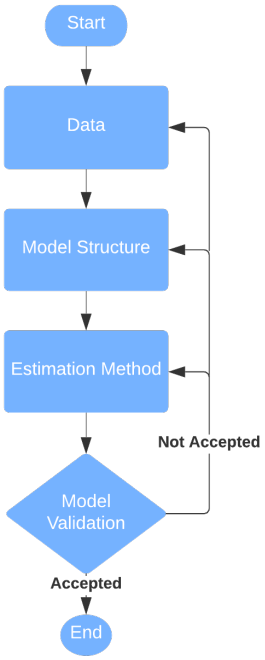

Figure 6.1: System identification lead actors.

The identification procedure starts off with the collection of data describing the system's operation. This task should be performed in an experimental manner. As described by L. Ljung and J. Schoukens in [85], "the result of the modelling process can be no better than what corresponds to the information contents in the data". This outlines the importance of the experiment to cover the model's intended use, in which, the power spectrum and the amplitude distribution should be properly set.

The choice of a model structure in a major problem in nonlinear system identification

with a very rich range of possibilities to chose from, like shown in Chapter 6. This choice is normally based on user's preference and system behaviour. For example, the system's behaviour dictates whether the non-linearity should be captured in a dynamic closed loop or not.

An important differentiation for this dissertation, is that of simulation and prediction models. A prediction model estimates the output of a system one-step-ahead at time k, using the system's input up to time k and real system measured outputs up to time k-1. These are central for modern control applications. On the other hand, there are simulation models where the previously measured outputs are disregarded, with previously predicted outputs being used instead. These are useful to test what happens in new situations, mimic physical systems, etc. Simulation models can, however, become unstable, and it is much harder to get small structural errors than it is for prediction models. A good prediction can fail completely to generate a reliable simulation [85].

The next step is the estimation method, which amounts to the selection of the model's parameters, θ, that best describes the observed data. These methods are based on a criterion of fit, that can be conceptually written as:

$$\theta_N = argmin_\theta \sum_{t=1}^{N} \parallel y(t) - \hat{y}(t|\theta) \parallel^2 \tag{6.1}$$

Where $y(t)$ are the system's observed outputs, and $\hat{y}(t|\theta)$ are the model's predictions. Squared error must be used or else positive and negative errors could cancel out each other. The choice of the criterion of fit should be based on the balance between noise disturbances and structural errors. If the first dominates, a statistically grounded choice should be employed. For the other case a weighting function can be added to enhance the models performance in the domain of interest, at the cost of reduced performance on the remaining domain [85].

The final step is the model's validation. Succinctly, it boils down to the question: "Does it solve our problem? and/or is it in conflict with either the data or prior knowledge?". In the not unlikely case of a negative answer, any of the previous step may have to be revisited. This is the reason why system identification is often seen as an iterative problem [85].

6.1 Gasifier Model

Unfortunately, due to delays in the project's development, it was not possible to collect the data needed to identify a model of the gasifier in development. To circumvent this issue data available in [86] was used. This data consists of the throat temperature profile of a GeK downdraft gasifier when actuated by changing the equivalence ratio inside the gasifer as shown in figure 6.2. The acquisition of this data was done by using the free software WebPlotDigitizer [90], an application that enables the extraction of data from images of

graphs, with parameterizable sampling rate and accuracy that were set to match those of the aforementioned paper.

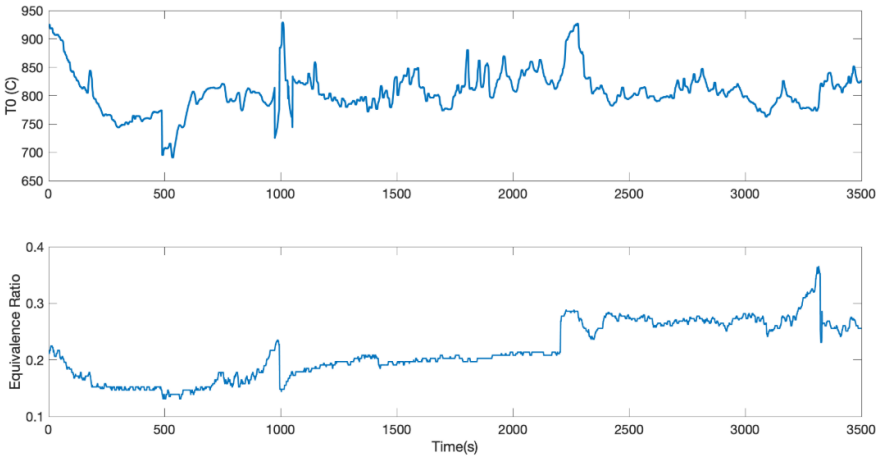

Figure 6.2: Identification data set. Throat temperature (top), equivalence ratio (bottom) [86].

The model's identification was the carried out using Matlab's Deep Learning toolbox [91]. This tool provides various neural network architectures allowing the choice between several embedded nonlinear optimization algorithms, activation functions and other options like regularization. The simplicity of this tool allows a simple and fast experimental process.

Since the data set does not include the gasifier's start up phase, the chosen validation function was the normalized mean squared error, NMSE, refer to equation 6.2.

$$NMSE = \frac{\sum_{t=1}^{m}(y(t) - \hat{y}(t|\theta))^2}{\sum_{t=1}^{m}(y(t) - mean(y))^2} \tag{6.2}$$

The minimization function used to extract the networks weights and biases was the Levenverg-Marquardt algorithm [92].

6.1.1 The Levenberg-Marquardt Optimization

Initially proposed by Kenneth Levenberg in 1941, and later improved by Donald Marquard in 1963 this method is described by the following steps [69]:

- Randomly select an initial solution for the values of parameters, θ_0;
- At every iteration k, the next solution is obtained by incrementing the current solution: $\theta_{k+1} = \theta_k + \delta$;
- Assume a linear approximation of the model $y = f(x, \theta)$, around the current solution, θ_k:

$$f(X, \theta_k + \delta) \approx f(X, \theta_k) + J\delta \tag{6.3}$$

Where X is a vector containing all the values in the extraction signal and J is the Jacobian matrix:

$$\begin{bmatrix} \frac{\partial f(x_1,\theta_k)}{\partial \theta_{k_1}} & \cdots & \frac{\partial f(x_1,\theta_k)}{\partial \theta_{k_{N'}}} \\ \cdots & \ddots & \cdots \\ \frac{\partial f(x_N,\theta_k)}{\partial \theta_{k_1}} & \cdots & \frac{\partial f(x_N,\theta_k)}{\partial \theta_{k_{N'}}} \end{bmatrix} \tag{6.4}$$

- The error function can now be estimated through:

$$\epsilon(\theta_k + \delta) \approx [y - (f(x, \theta_k) + J\delta)]^T [y - (f(x, \theta_k) + J\delta)] \tag{6.5}$$

- A damped minimization with respect to δ can now be achieved through the following linear equation:

$$(JJ^T + \lambda diag(JJ^T))\delta = J^T[y - f(x, \theta_k)] \tag{6.6}$$

  Where λ is updated at every iteration. Multiple update strategies may be employed.

The Levenberg-Marquardt method is seen as a good compromise between robustness and convergence speed, being the most commonly used method for the training of Artificial Neural Networks [92]. In spite of this, it is reliant on an arbitrary estimate of the initial solution. Consequently it may still suffer from a slow or wrongful convergence "when it must navigate a narrow canyon en route to a best fit", or when "the least squares function is very flat" [92].

6.1.2 Regularization

Regularization is a method used to prevent overfitting in the extraction data, and thus, improve the generalization ability of a model.

It consists of adding a regularization term to the optimizaion's cost function, not allowing the error to become to small. Besides increasing the unlikelihood of overfitting the extraction data, this technique also diminishes variance of the solutions.

The most common cost function used is the mean squared error, MSE.

$$MSE = \frac{1}{N} \sum_{i=1}^{N} (e_i^2) \tag{6.7}$$

In the system identification toolbox utilized in this work, it is altered to include a regularization term formed by the quadratic sum of the network's weights and biases, MSW.

$$MSW = \frac{1}{n} \sum_{j=1}^{n} w_j^2 \tag{6.8}$$

The final cost function, MSReg, then takes the form:

$$MSReg = \gamma * MSW + (1 - \gamma) * MSE \tag{6.9}$$

Where γ is a design parameter called performance ratio [93].

6.1.3 Structure Definition

Based on literature review undertaken in Chapter 6, it was decided that the network topology would be that of the NARXNN. The underlying model structure, however, was designed based on the procedure described in this section. The architecture was formed by one input, one output and one hidden layer with hyperbolic tangent activation functions, as done in [84, 86], which has been proved to be a global approximant. The ideal number of delays in both the inputs and outputs, just as the number of neurons in the hidden layer, were determined iteratively, as advised by Greg Heath [94].

The flowchart in figure 6.3 describes this process. The process requires the input of the iteration limits: number of trials, $numTrials$, maximum and minimum number of hidden layer neurons, $Hmax$ and $Hmin$ respectively, and maximum memory depth, $Mmax$. In order to minimize the bad start problem, present in the Levenberg-Marquardt algorithm, the process starts by iterating over a set number of trials, $numTrials$, with a fixed memory depth and number of neurons in the hidden layer. At each iteration of this inner loop, the initial parameter solution is randomized and subsequently optimized by the minimization algorithm. This procedure is carried out with the network in an open loop, or series-parallel configuration, meaning the delayed outputs fed into the network are real values taken from the extraction signals. For extraction of the network's parameters, the data set is first divided into three contiguous parts, where the first 70% of the data is used to update the weight's and biases, 15% for online validation whose error is monitored during extraction and 15% for model validation.

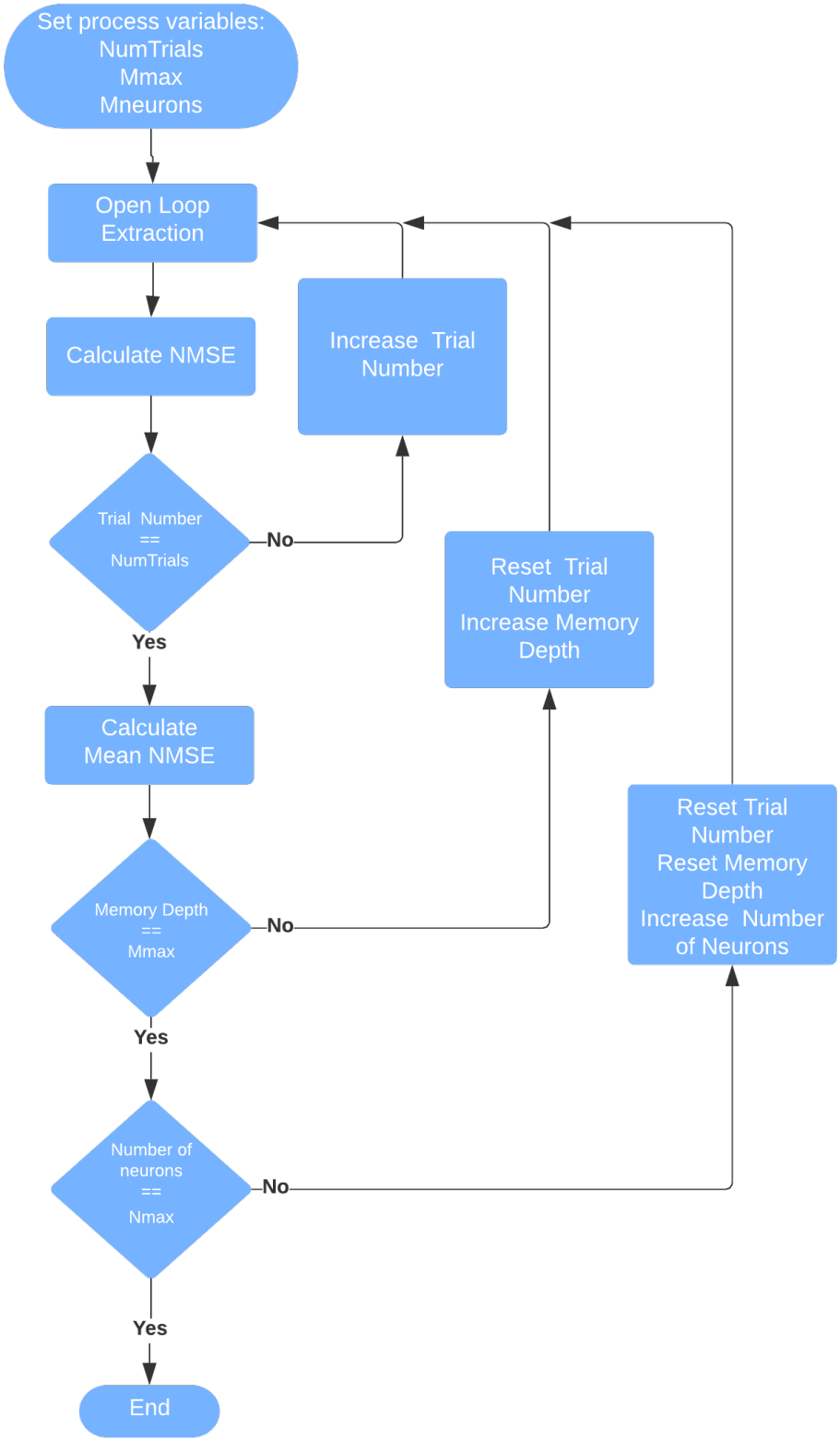

Figure 6.3: Iterative structure definition flowchart. Created using Lucidchart [51].

When the number of trials reaches its maximum, the structure's accuracy is calculated in terms of the mean value of validation NMSEs across the trials. This process is then repeated for all combinations of memory depth and number of hidden layer neurons.

The described procedure was realized with $numTrials$, $Hmin$, $Hmax$ and $Mmax$ set to 20, 5, 20 and 10 respectively. The results are shown in figure 6.4.

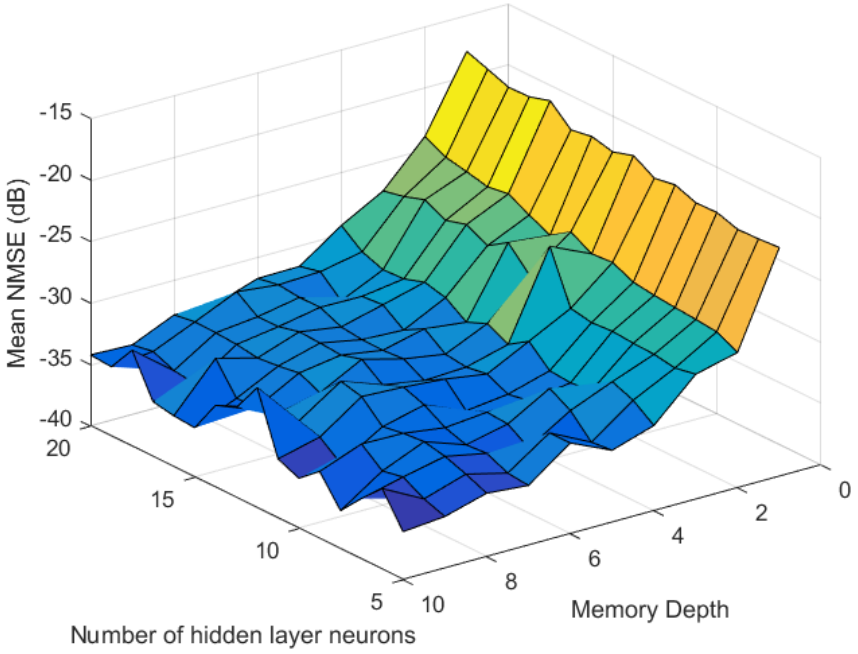

Figure 6.4: Structure comparison.

By analysing figure 6.4 it was decided that a memory depth of 4 with 10 neurons in the hidden layer would be a good compromise between complexity and accuracy.

6.1.4 Parameter extraction

In the parameter extraction step, the optimal structure was trained in a single loop akin to the inner loop of the previous procedure. The overall procedure is described by the flowchart in figure 6.5.

The difference is that, at each iteration, after doing the open loop extraction with randomized initial solutions, the network is converted into closed loop or parallel configuration, meaning its previous predictions are used as inputs.

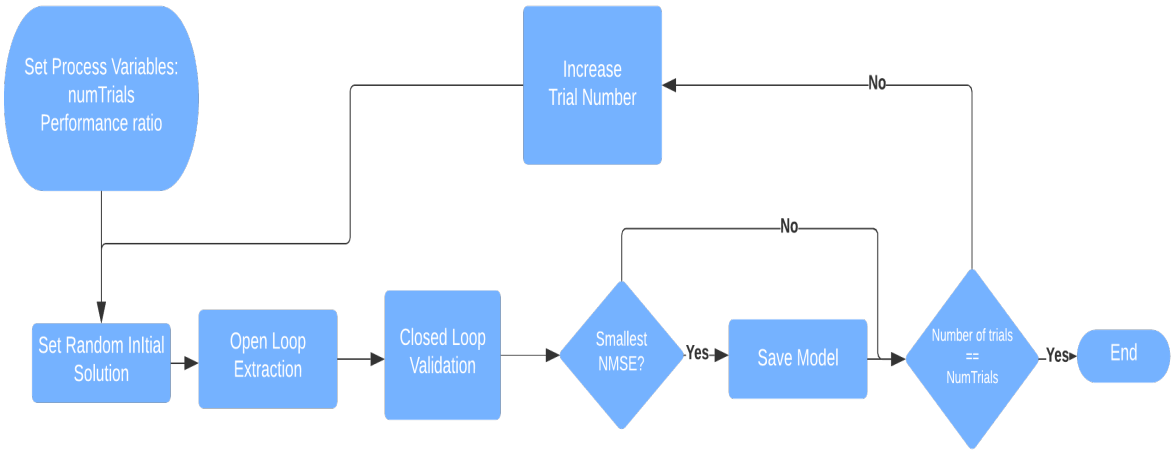

Figure 6.5: Parameter extraction flowchart. Created with Lucidchart [51].

The network's performance is then evaluated on both validation and extraction data in terms of its NMSE. The end result is the weights and biases that led to the smallest overall NMSE.

During the extraction, the number of trials was set to 100 while a regularization performance ratio of 0.3, set by trial and error, was used in order to diminish the variance of the solutions. Open and closed loop results are shown in figure 6.6.

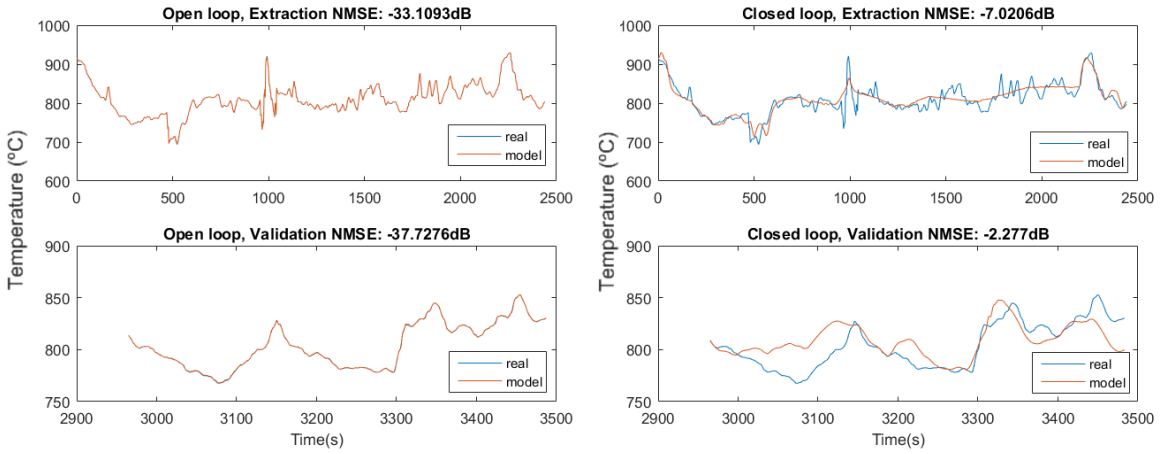

Figure 6.6: Extraction results.

The deterioration presented between open loop and closed loop performance correlates to the analysis done by Mikulandric [84]. As he explains, the accumulation of error between consecutive predictions induces a major decrease in closed loop performance. The final results are, however, lacking in comparison to those shown in [86]

Analysing the auto correlation of residuals of the open loop predictions, figure 6.7, shows

correlation values throughout the lag space above the confidence level, which indicates the presence of structural errors.

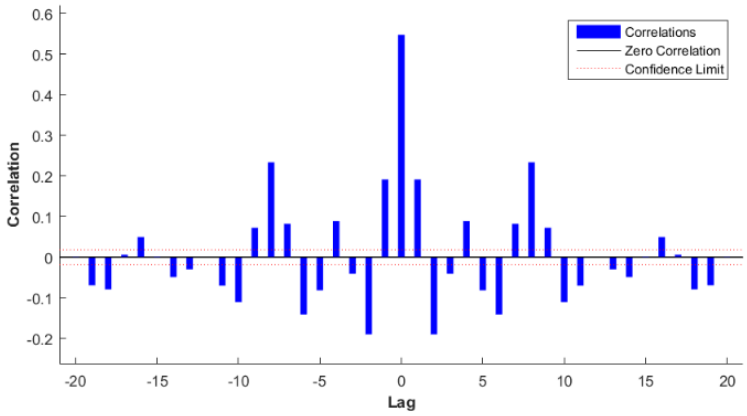

Figure 6.7: Auto correlation of residuals.

Further tests have been done in order to evaluate the prediction ability of the model. Figure 8.8 shows the deterioration of the NMSE with the prediction horizon. In order to developed this analysis, the network's states are first updated, in open loop, with real data from time $k - memory\,depth$ up to time k. Afterwards the network is converted into close loop and used to calculate the next k-step-ahead predictions, where $k = prediction\,horizon$.

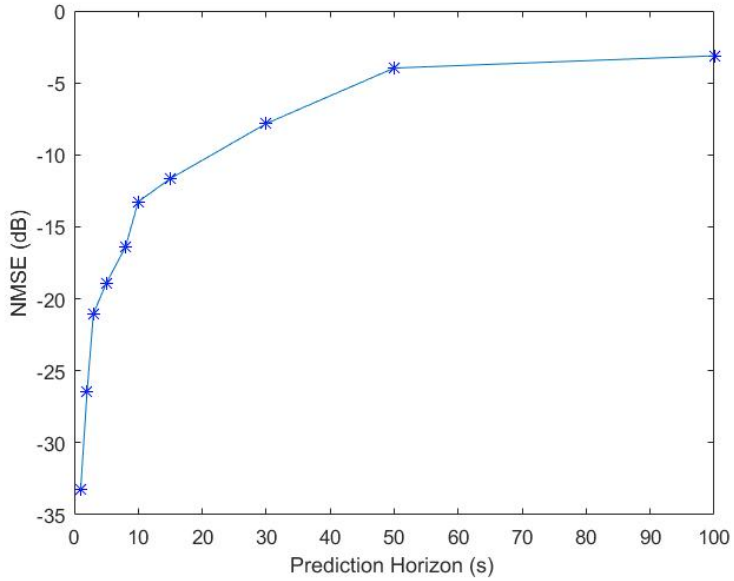

Figure 6.8: Evolution of model error with prediction horizon.

A closer look at the results for a prediction horizon of 5 is given in figure 6.9.

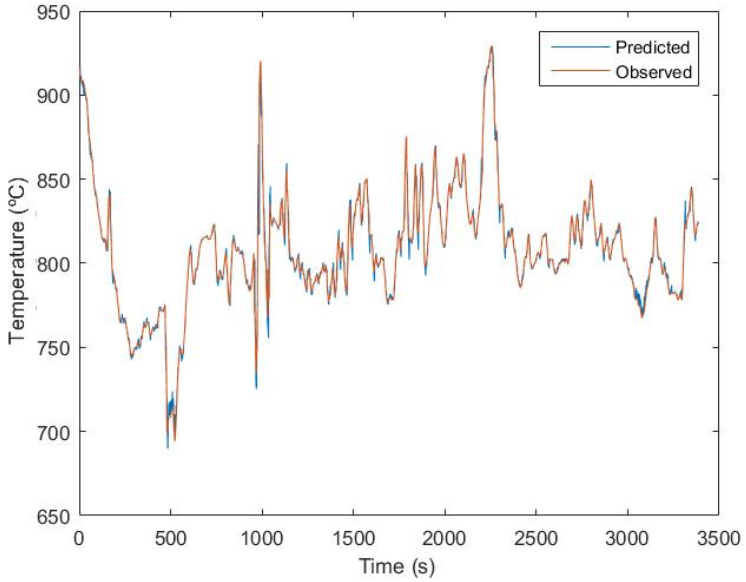

Figure 6.9: Comparison between observed and predicted values for a prediction horizon of 5.

It can be seen that despite the deterioration of the NMSE value the model is still able to capture the behaviour of the system. Furthermore, the mean value of absolute error, 1.7ºC, is below the measurement uncertainty present in the data, 2ºC.

6.2 Conclusion

The results obtained prove that the devised model has a good potential as a prediction model for online control with small prediction windows.

Its simulation counterpart shows a big deterioration in predictions ability. In spite of this the model is still able to provide good average temperature predictions, as it clearly follows the trend in the data.

The devised model will be used as a simulation model, as it constitutes the best available option. Later, when the real gasifier is operational, the system's identification should be revisited featuring a more deliberate choice of extraction signals, which was not possible at the time of writing this dissertation.

CHAPTER 7

Temperature Control

Based on the literature review undertaken for this dissertation it can be concluded that very few studies focus on control of the downdraft biomass gasification process outputs.

This Chapter will start with a revision of such studies.

7.1 Literature review

Although a small number of control related studies have been developed, several types of controller design have been tested ranging from the simplistic ON/OFF controller to the more sophisticated Model Predictive Control.

A simple strategy for maintaining stable gasifier operation would be the gasifier controller unit developed by P. Kamble [67]. This simplistic approach resumed itself to actuating the gasifier with an ER of 1 for reduction temperatures below 400^{o}C and an ER of 0.3 for reduction temperatures above that value.

Another possibility for controller design is that of fuzzy logic controllers. This constitutes an appealing approach as it is based on the implementation of human heuristic knowledge into a control system [7]. This procedure does not necessarily lead to more stable gasification performance, however [67]. One such controller was developed in [7] to control temperature and CO/CO_2 ratio by manipulating air flow and grate shaking frequency of a downdraft gasifier. The set of heuristics was developed by using a static model of the gasifier. The results showed good temperature control but were only tested on a very simplistic 1st order, SISO, temperature model.

PID control was employed by the same author in [63, 95] where the controlled system proved to have better performance than when actuated manually, albeit only tested on a second order, SISO, transfer function model. The author concludes nonetheless that in order to further improve performance, intelligent control techniques would have to be implemented.

In [31] a novel control strategy was employed. This strategy consisted of a feedback loop where the differential temperature between combustion and reduction zone was controlled by indirectly actuating ER through the fuel feed rate. This was achieved through a simplification of the complex reaction dynamics with first order correlations between different process

variables. This strategy was tested for more than 70h of continuous operation of a downdraft gasifier. It culminated in a significant decrease in the oscillatons of differential temperature, from ±200 to ± 50 °C (figure 7.1), flow rate, from 16 ± 6.5 to 12 ± 1.8 L/min, composition of main gas components, LHV, from 6.2 ± 3.1 to 5.7 ± 1.6 MJ/Nm3, and tar content, from 8.0 ± 9.7 to 7.5 ± 4.2 g/Nm3.

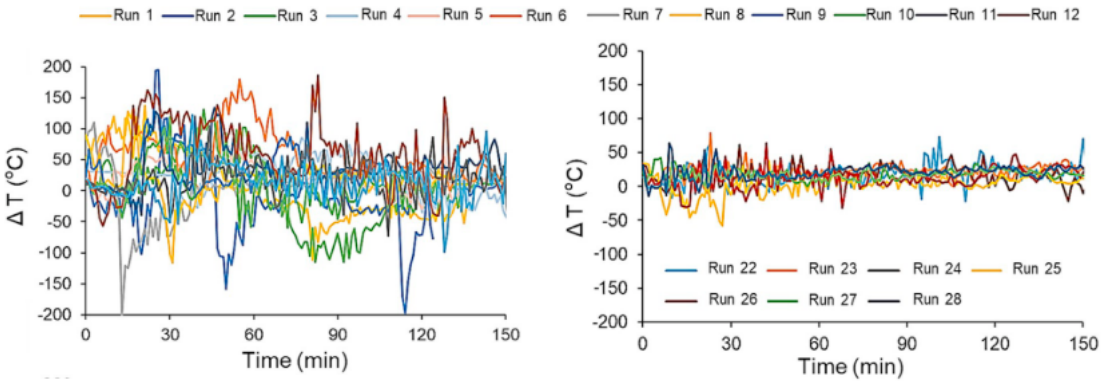

Figure 7.1: Comparison between uncontrolled, left, and controlled, right, differential temperature using a novel control strategy [31].

The work done by F. Elmaz and O.Yucel [86], already heavily referenced in Chapter 5 and 6, presented several Model Predictive Controllers, developed using second order polynomials to control the outputs of the developed NARXNN model. The controllers devised were able to control all of outputs with precision lesser than that of the measuring error, as shown in figure 7 for the case of H_2.

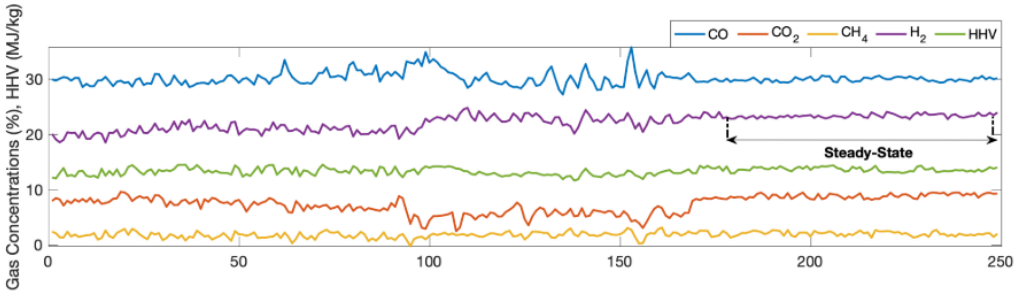

Figure 7.2: H2 concentration control with Model Predictive Control [86].

In the following sections a Model Predictive Controller will be designed by utilizing the NARXNN model devised in the previous Chapter.

7.2 Generalized Predictive Control

Over the years, Model Predictive Control has become a first choice control strategy in the industry as it is intuitive and can explicitly handle multivariate systems with constraints [96].

The overall procedure of MPC is always the same [97]. At every sampling instant k, the horizon of control variables are calculated online.

$$U(k) = \begin{bmatrix} u(k|k) \\ \vdots \\ u(k+N_u-1|k) \end{bmatrix} \tag{7.1}$$

Where N_u is the control horizon and and the notation $u(k+i|k)$ represents the value of u at iteration $k+i$ calculated at iteration k.

The increments of the control variable are defined as:

$$\Delta U(k) = \begin{bmatrix} u(k|k) - u(k-1|k-1) \\ u(k+1|k) - u(k|k) \\ \vdots \\ u(k+N_u-1|k) - u(k+N_u-2|k) \end{bmatrix} \tag{7.2}$$

Generalized Predictive Control, utilized in this dissertation, is a category of MPC that aims to calculate the set of control variables u that minimize the cost function described in equation 7.3 [82, 97],

$$J(k,u) = \sum_{p=1}^{N} (y^{sp}(k+p|k) - \hat{y}(k+p|k, u(k+p|k)))^2 + \lambda \sum_{p=0}^{N_u-1} (\Delta u(k+p|k))^2 \tag{7.3}$$

subject to

$$u(k+p|k) = u(k+N_u-1|k),\ p = N_u, ..., N \tag{7.4}$$

$$u_{min} < u(k) < u_{max} \tag{7.5}$$

Where the first term of the equation consists of the difference between the preset set-point trajectory and the model predicted outputs along the prediction horizon N, λ is a weighting coefficient that penalizes changes in the control signal.

These signals are represented in figure 7.3. The first sample of the calculated control horizon is then applied to the system, with the remaining being discarded.

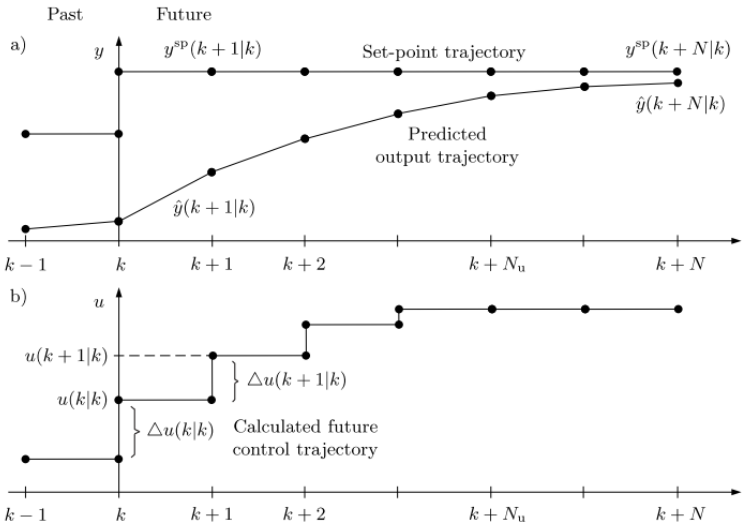

Figure 7.3: Signals in MPC [97].

7.3 Controller Development

The GPC algorithm was implemented in Matlab by coupling the Deep Learning toolbox [91], used for the system's identification, and the Optimization Toolbox [98].

Equation 7.3 may be rewritten in matrix form, more suitable for implementation in Matlab, as shown in equation 7.6 [82].

$$\begin{aligned} J(k,U(k)) &= [R(k)-\hat{Y}(k)]^T[R(k)-\hat{Y}(k)] + \lambda\Delta U^T\Delta U \\ &= E(k)^T E(k) + \lambda\Delta U^T\Delta U \end{aligned} \tag{7.6}$$

Where:

$$\begin{aligned} R(k) &= [y^{sp}(k|k),...,y^{sp}(k+N|k)]^T \\ \hat{Y}(k) &= [\hat{y}(k|k),...,\hat{y}(k+N|k)]^T \\ E(k) &= R(k)-\hat{Y}(k) \end{aligned} \tag{7.7}$$

For the purpose of this dissertation no predicted output restrictions are required. As so, minimization of equation 7.6 subject to input restrictions may be posed as a bounded nonlinear optimization problem and solved with the Trust-Region-Reflective algorithm implemented by the Optimization Toolbox function *lsqnonlin* [99].

Trust Region Reflective

The minimization problem is stated as [100]:

$$min(f(x)),\, x \in \mathcal{F} = \{x : l \leq \ x \leq u\} \tag{7.8}$$

Where l and u are the lower and upper bounds of the search space. These bounds may include infinite components, not limiting the search in that direction.

First, a vector $v(x)$ formed by the distance to the bound at which anti-gradient points to, is defined as follows:

$$v(x)_i = \begin{cases} u_i - x_i, & g_i < 0 \, and \, u_i < \infty \\ x_i - l_i, & g_i < 0 \, and \, l_i > -\infty \\ 1 & otherwise \end{cases} \tag{7.9}$$

Where $g = \nabla f(x)$ is the gradient of cost function to be minimized, f(x).

Next, matrix D is defined as:

$$D(x) = diag(v(x)^{1/2}) \tag{7.10}$$

At this point the problem can be reformulated as a diagonal system of nonlinear equations by writing.

$$D^2(x)g(x) = 0 \tag{7.11}$$

The newton step, p, for this system satisfies:

$$(D^2 H + diag(g)J_v)p = -D^2 g \tag{7.12}$$

Where H is the Hessian matrix of $f(x)$ and J_v is the diagonal Jacobian matrix of $v(x)$. In case the Hessian matrix is not known, H may be replaced by $J^T J$, with J being the Jacobian matrix of f.

Now a trust region problem must be formulated as:

$$min\, p, m(p) = \frac{1}{2} p^T B p + g^T p, \quad s.t \quad \left\| D^{-1} p \right\| \leq \Delta \tag{7.13}$$

With

$$B = H + D^{-1} C D^{-1} \tag{7.14}$$

Where Δ is the size of the trust region.

The newton improvement ratio (ρ) can now be calculated with:

$$\rho = \frac{f(x+p) - f(x) + \frac{1}{2}(D^{-1}p)^T C D^{-1} p}{m(p)} \tag{7.15}$$

This procedure is repeated at every iteration of the optimization problem until convergence.

The new solution $x = x + p$ is tested to see if a better solution as been found and kept if the result is positive. After this, the size of the trust region, Δ, is adjusted as a function of the improvement ratio, ρ. It should be noted that the solution using Newton steps exposed here is not an exclusive solution with another prominent way of solving the trust region problem being the so called "Steighaug Conjugate Gradient Method" that will not be presented here. For a more detailed description see the paper [101].

The reflective part of the algorithm only interferes when the newton step tries to overstep a bound. In this scenario, the newton step solution is fist restricted to lay within the bounds, then a reflected newton step is computed as:[102]

$$p_r(x) = \begin{cases} p & x \neq i \\ -p & x = i \end{cases} \tag{7.16}$$

Where $l(i)$ or $u(i)$ corresponds to the bound that had been overstepped. This solution is then compared to its contestants and kept if it provides better results.

In order to solve the minimization problem a initial solution must be provided. This solution may be randomly generated or handpicked. The common approach in MPC algorithms is to set the initial solution equal to the previous control sequence, or equal to a time shift of the previous solution. In this dissertation all of the solutions were tested, which proved to have indistinguishable results. As so the latter solution was implemented, with the last value of the control sequence being set as $U(pH) = U(pH - 1)$.

7.4 Results

In this Chapter, the devised model will be used both for the controller's predictions and for the simulation of the plant, as no better option was available. The resulting controller will nevertheless constitute a good starting point for the project and the developed framework will serve as a foundation for future work.

There is no established way of tuning the prediction and control horizon of an MPC [103]. For this endeavor a non-parametric solution was developed. The solution consists of a Matlab script that plots both these horizons concurrently with previous plant outputs at every iteration of the simulation, as shown in figure 7.4.

In the case that these horizons are properly set, the plant's output and input trajectories should mimic those predicted by the controller. In the opposite case, the predicted horizons should frequently change [104]. In spite of this, sub-optimal solutions with a small control horizon were preferred, as increasing this variable forces an exponential increase in the

optimization's search space and thus, a major increase in the computational load.

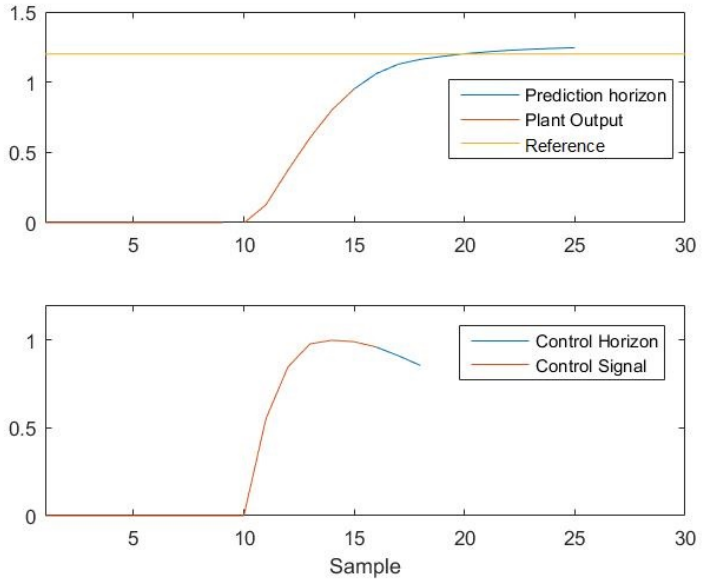

Figure 7.4: Simulation example for a prediction horizon of 10 and a control horizon of 3.

Figure 7.5 shows the behaviour of the controller for prediction horizons of 3 (left) and five (right). In spite of the resemblance of predicted and plant outputs it can bee seen that, some time after stabilization, the plants output diverges from the set-point. This was solved by increasing the prediction horizon. A weighting coefficient, λ in equation 7.6, of 100 was used.

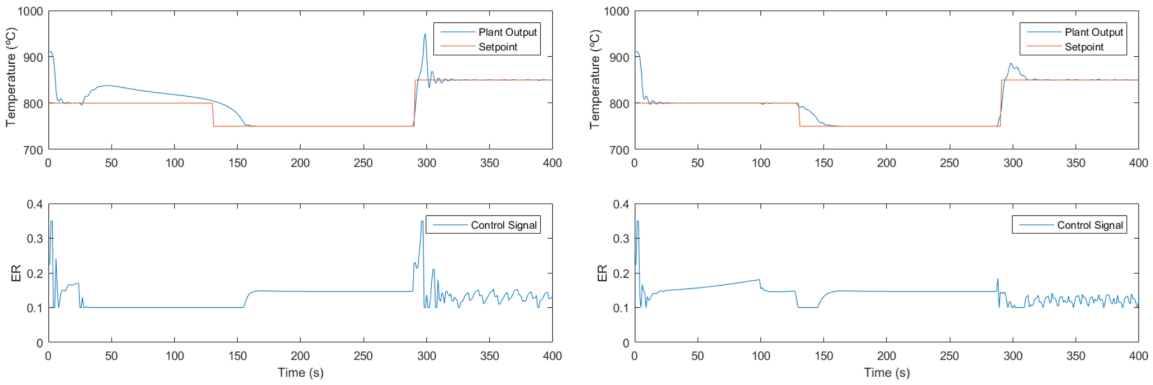

Figure 7.5: Controlled simulation with a prediction horizon of 3 (left) and 5 (right).

During the simulation the input signal was restricted to limits existing in the extraction data $[0.1; 0.35]$. Furthermore, the plant's temperature was always initialized to match the initial temperature of the data. Start-up of the gasifier is normally forced by external heat sources that were not represented in the extraction data. As so, it would be too unrealistic to run a simulation with null initial conditions.

In an attempt to decrease the fluctuations in the control signal for the third variation of the set point, 850ºC, several values were tested for the weighting coefficient, ranging from 0 up to 10000, but no improvements were seen, so the value of 100 was kept.

After tuning of its parameters, the controller was tested under step disturbances in the input variable[1]. Figure 7.6 shows the behaviour of the controlled system when subject to a continuous disturbance of 10% of the maximum input signal's amplitude, at time instant 40.

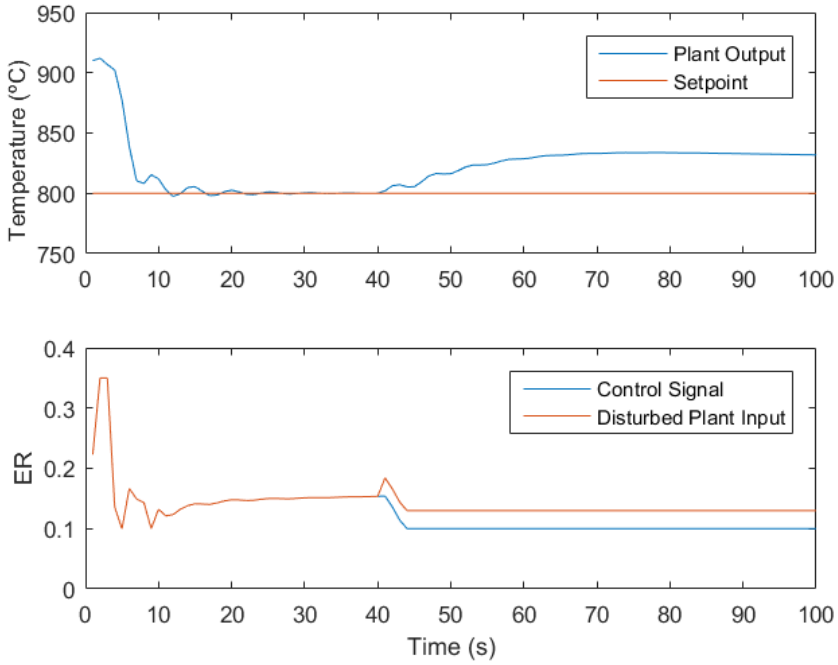

Figure 7.6: Controlled simulation with a prediction horizon of 5, under disturbances.

As can be seen, when the disturbance is applied, the system is forced into the saturation limit and is unable to correct the steady state error. This problem will be addressed in the next section.

7.5 Disturbance Rejection

During calculation of the prediction horizon, it is necessary to acknowledge that the model is not perfect and the process may be affected by unmeasured disturbances [105].

This issue may be solved by the inclusion of a disturbance model in the model's predictions, as defined in equation 7.17.

$$\hat{y}(k+p|k) = y(k+p|k) + d(k) \tag{7.17}$$

[1] In the control loop a disturbance in the form of a step shaped signal is added to the control signal after its calculation.

Where $d(k)$ is the disturbance term.

The most typical approach is to assume that the disturbance is constant over the prediction horizon and is determined as the difference between the observed value of process' output and the model's predicted value at sampling instant $k-1$, equation 7.18 [97].

$$d(k) = y_{obs}(k) - y(k|k-1) \tag{7.18}$$

By including the disturbance estimation, the MPC algorithm has integral action even if the model is not perfect.

Figure 7.6 shows the homologous experiment undertaken in figure 7.5 with the inclusion of the described disturbance model.

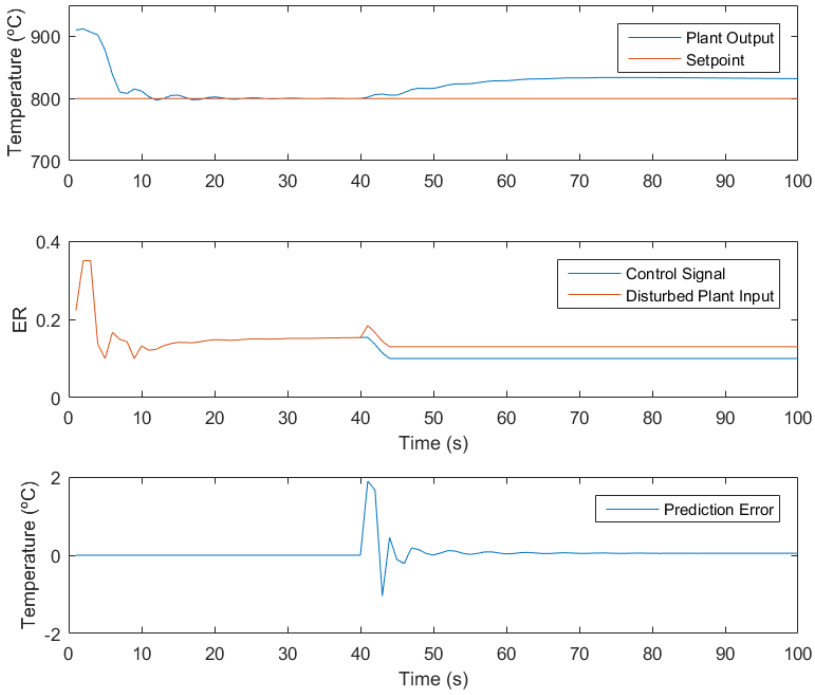

Figure 7.7: Controlled simulation with a prediction horizon of 5, under disturbances.

As can be seen, the inclusion of the disturbance model provides no enhancement to the controller's performance. As under these conditions its does not seem possible for the controller to correct the deviations imposed by the disturbance, a simulation with broader constraints was done, figure 7.8.

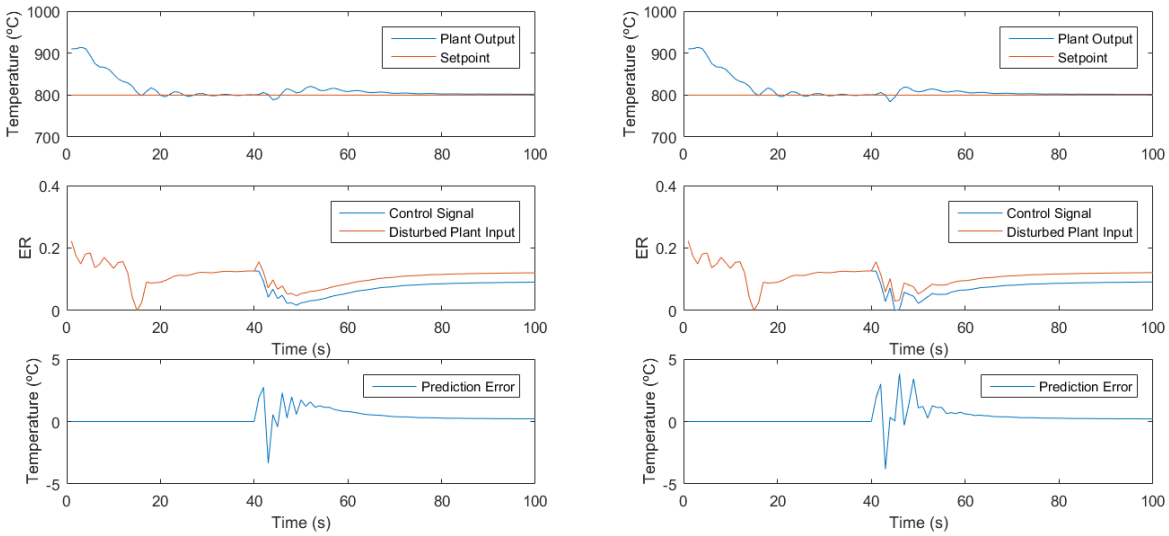

Figure 7.8: Controlled simulation under disturbance with laxer constraints without disturbance model, left, and with disturbance model, right.

With the actuator limits amplified to $[0; 1]$ the controlled system is able to to follow the reference trajectory even without a disturbance model. When one is added its response to disturbances becomes slightly faster and more aggressive, with the overshoot decreasing from 21.1ºC to 19.3ºC.

The results indicate that future data extractions should include broader limits in the actuation signal.

By analysing the prediction error plots across figure 7.8 it may be seen that in spite of the step shaped disturbance imposed on the input signal the prediction error does not have a step shaped characteristic. As was explained, the disturbance model used assumes that the disturbance is constant along the prediction horizon, which is clearly not the case, specially in the initial moments after the disturbance is imposed.

For this reason the disturbance model was replaced by a 3rd order Nonlinear Auto-Regressive Neural Network model, NARNN. It should be noted that the choice of a neural network topology was based solely on the existence of an already established identification framework developed on Chapter 6. Furthermore the added complexity is akin to single iteration of the minimization algorithm.

This model, composed of four hidden layer neurons with hyperbolic tangent activation functions, had it's coefficients tuned to prediction error data shown in figure 7.8 (left). Disturbance estimates can now be calculated across the whole prediction horizon as described in equation 7.19.

$$D = \begin{bmatrix} \hat{d}(k+1) = \Psi(d(k), ..., d(k-3)) \\ \hat{d}(k+2) = \Psi(\hat{d}(k+1), ..., d(k-2)) \\ \vdots \\ \hat{d}(k+N) = \Psi(\hat{d}(k+N-1), ..., \hat{d}(k+N-4)) \end{bmatrix} \tag{7.19}$$

Where d(k) is the prediction error calculated with equation 7.18, Ψ is the neural network's function, $\hat{d}$ are the NARNN model disturbance estimates that will be added to the controller model's predictions.

Figure 7.9 shows the results attained with the NARNN disturbance model.

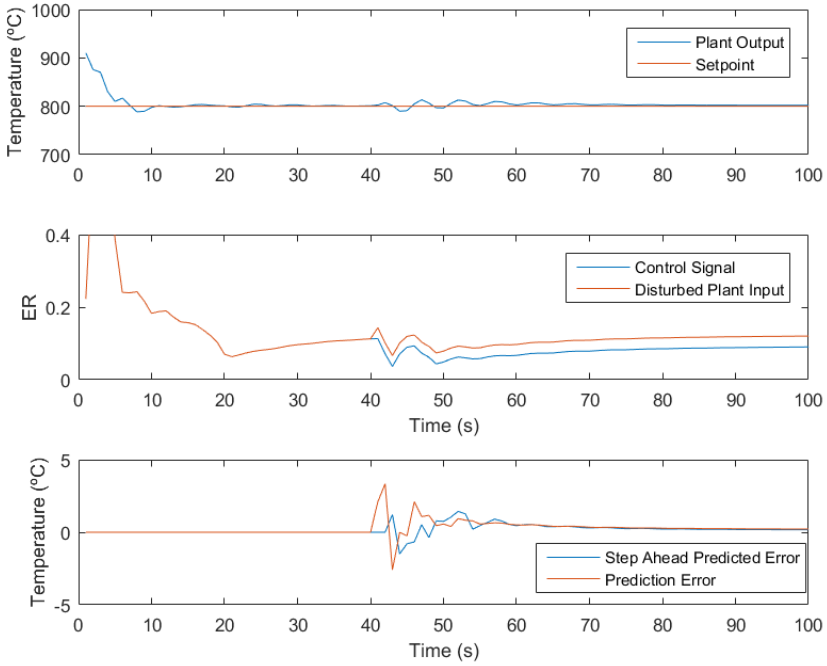

Figure 7.9: Controlled simulation under disturbances with a NARNN disturbance model.

As can be seen, the disturbance predictions do not mirror the prediction error in the instants after the disturbance is imposed. They are, however, able to mimic its fluctuating behaviour to some extent, and closely resemble their targets in the remaining time windows.

This approach provided a decrease in the overshoot from 21.1ºC to 13.4ºC outperforming the simpler disturbance model and justifying the deviation from the constant disturbance approach.

7.6 Conclusion

A Model Predictive Controller was developed to control the outputs of the previously devised model. For the lack of a better option, the same model was used for prediction and simulation.

The controller was able to stabilize temperature at the desired set-points, under the extraction data saturation limits.

When subject to input disturbances the controller was forced into the lower saturation limit. To account for this, the limits of the actuation signals had to be expanded beyond those of the extraction data. This procedure allowed the controller to compensate the presence of input disturbances. Disturbance models were nonetheless applied, with and without the assumption of a constant disturbance over the prediction horizon. Both approaches fostered a decrease in overshoot with the latter showing the best performance, from 21.1^{o}C to 13.4^{o}C.

CHAPTER 8

Conclusions

This dissertation tackled several problems of the initial stage of a gasification project. Its outcome constitutes a solid ground for the project's development.

A study of the gasifier's operating principles was undertaken which revealed the complex phenomenon that is gasification. This study was then complemented with the study of instrumentation technologies that could expose the operational parameters of the system to be developed. Two relevant points stood out along this phase. First, the selection of the air control subsystem where the initial design using electrically actuated valves proved to be unfeasible and had to be replaced by a speed controlled fan. Second, it was found that actuating air flow would be insufficient to properly control the system's temperature, leading to the design of a weighting system capable of acquiring online mass measurements of the products inside the gasifier. Afterwards, a visualization tool was developed to interactively display the information present in the sensors and make the gasifier's behaviour transparent to the user.

Propelled by the unavailability of the real system nor an established gasification simulator, this dissertation coursed into the development of a gasification model that would be used as a basis for controller design. With this goal a literature review with a focus on gasification modelling was done. The review consisted of a critical analysis of the different model architectures used in the literature. By the end, it was clear that physical modelling of the gasifier's dynamic behaviour was still in a very immature stage of development and neural network modelling came out as the best topology to achieve this goal.

Behavioural modelling, a thematic in which neural network modelling is incorporated is highly dependent on the existence of quality data describing the modeled system. Regardless, due to the current unattainability of such data, data available in the literature was used. A system identification framework was implemented using MathWorks's "*DeepLearningToolbox*". The model attained through this procedure proved to have great potential as a prediction model, presenting a validation NMSE of -37.919dB. When converted into a simulation model, a deterioration to the models accuracy was seen, both on extraction and validation data, with an NMSE of -7.02dB and -2.277dB respectively. In spite of this deterioration, very good average temperature predictions were achieved, with the model clearly

following the overall trend of the data.

A Model Predictive Controller was developed in Matlab by combining the prediction functionalities of the "Deep Learning Toolbox" with the nonlinear optimization capacities of the "Optimization Toolbox". For lack of a better option, the controller was devised utilizing the same model for prediction and simulation. The controller was able to stabilize temperature at all of the desired set-points. The model was then tested under input disturbances. In this experiment, the operating range of the control signal, set to match that of the extraction data, 0.1 to 0.35 ER, proved insufficient for the controller to be able to correct the error caused by the disturbance. To account for this, the saturation limits of the control signal were amplified to 0-0.4 ER. In these conditions the devised model was able to correct the disturbance, revealing the need to include broader limits in the extraction signals. Two disturbance models were then developed, one assuming prediction errors are constant along the prediction horizon and one with full prediction of the error along the horizon. The latter approach showed better performance, being able to decrease to overshoot from 21.1ºC to 14.4ºC, while the simpler approach was able to decrease the overshoot to 19.3ºC.

8.1 Future work

The high variability, even among its categories, of a gasification project makes it very hard to accurately design an instrumentation system. As so, the most important step after the gasifier prototype is available is the validation of the proposed devices. This must, however, be preceded by the implementation of the microcontroller code and the necessary printed circuit boards. Special care should then be taken to calibrate the Venturi flowmeter. Finally, a controller should be devised in order to maintain the desired air flow rate by actuating the fan. It should be noted that the fan's operating point will change with the pressure drops inside the gasifier, which will vary during operation.

The system identification done in the dissertation was developed using data available in the literature. This limited the possibilities of the work done. As the project's gasifier is available, careful procedures should be undertaken in order to attain quality extraction data. The extraction data should contain, as possible, uniform frequency and amplitude distribution that covers the gasifiers intended use. Furthermore, the sampling frequency of the system will have to be selected. As referred in Chapter 7, the equivalence ratio should be varied beyond the optimal values presented in the literature. After this is done, PCA analysis, addressed in Chapter 5, could be used to determine the most influential parameters and reduce collinearity between data vectors. At this point, having done a careful selection of the actuation signals, it should be possible to differentiate linearities, non-linearities and noise, following the procedures explained in [85], which will help validating the model.

After the data collection step, the identification procedures assessed in Chapter 6, should

be applied to the extracted data. In case structural errors are present, with the model's performance deteriorating when fed its own predictions, a weighted extraction should be done. Starting at the study done in the proposed extraction, the cost function of minimization problem should be customized to include frequency weighting. While this procedure will most likely decrease the overall accuracy of the model, it will increase its accuracy at frequencies of interest.

With a model of the prototype gasifer, the Model Predictive Controller should be tuned using the developed framework, which should prove to be trivial task. Disturbances should be addressed first with the simpler disturbance model. The more complex model should only be used in the case that the previous does not perform well enough. The disturbance rejection strategy developed in [105] and used in [82] could also be tested in order to improve the response to disturbances. Finally the controller should be implemented in the microcontroller, according to the platforms restrictions, and tested in the real system,

The devised software was implemented in a single iteration. Only through continuous use and the consequent user feedback will it be possible to determine the right information that should be displayed at a given time. As so, after extended usage of the software, its development should be revisited to see if it still matches he user's needs. The functionality of changing air flow rate during operation should also be implemented.

References

[1] S. Safarian, R. Unnþórsson, and C. Richter, "A review of biomass gasification modelling", *Renewable and Sustainable Energy Reviews*, vol. 110, pp. 378–391, 2019. DOI: 10.1016/j.rser.2019.05.003.

[2] R. Fernanda, S. Valter, M. Miguel, B. António, B. Paulo, *et al.*, "Using Biomass Gasification for Small Scale Power Generation Systems: Specifications of the Conceptual Framework", *2019 8th International Conference on Renewable Energy Research and Applications (ICRERA)*, 2019.

[3] ——, "Small scale power generation Unit using Biomass gasification: The SUBe Project", *2019 8th International Conference on Renewable Energy Research and Applications (ICRERA)*, 2019.

[4] H. Roesch, "Downdraft Gasification of Various Biomass Feedstocks for Energy Production", 2011, Florida State University Libraries.

[5] M. R. Costa, "Projecto de um gasificador de biomassa", 2009, Universidade de Aveiro. [Online]. Available: http://ria.ua.pt/bitstream/10773/660/1/2010000393.pdf.

[6] T. Paes, "Modeling for control of a biomass gasifier", 2005, Technische Universiteit Eindhoven.

[7] S. Gandhi, T. Kannadasan, and R. Suresh, "Biomass Downdraft Gasifier Controller Using Intelligent Techniques", *IntechOpen*, p. 13, 2012. DOI: http://dx.doi.org/10.5772/57353.

[8] Y. Muñoz, A. Ospino, C. Robles, and C. Arizmendi, "Implementation of a frequency control in a biomass gasifier system", *International Journal of Electrical and Computer Engineering*, vol. 9, no. 1, pp. 66–77, 2019, ISSN: 20888708. DOI: 10.11591/ijece.v9i1.

[9] O. D. Sánchez, "Modelamiento termodinámico de la gasificación de bambú y cuesco de coco en un gasificador de lecho fijo escala piloto.", p. 153, 2018, Universidad Nacional de Colombia. [Online]. Available: bdigital.unal.edu.co/63681/.

[10] A. Chaurasia, "Modeling, simulation and optimization of downdraft gasifier: Studies on chemical kinetics and operating conditions on the performance of the biomass gasification process", *Energy*, vol. 116, pp. 1065–1076, 2016, ISSN: 03605442. DOI: 10.1016/j.energy.2016.10.037.

[11] A. P. Labs, "How gasification works", [Online]. Available: http://www.allpowerlabs.com/gasification-explained, (accessed: 17.6.2020).

[12] S. Ferreira, E. Monteiro, P. Brito, and C. Vilarinho, "A holistic review on biomass gasification modified equilibrium models", *Energies*, vol. 12, no. 1, pp. 1–31, 2019, ISSN: 19961073. DOI: 10.3390/en12010160.

[13] O. Yucel and M. A. Hastaoglu, "Kinetic modeling and simulation of throated downdraft gasifier", *Fuel Processing Technology*, vol. 144, pp. 145–154, 2016, ISSN: 03783820. DOI: 10.1016/j.fuproc.2015.12.023.

[14] M. P. Arnavat, "Performance Modelling and Validation of Biomass Gasifiers for Trigeneration Plants", 2011, Universitat Rovira. [Online]. Available: www.tesisenxarxa.net.

[15] T. Golden, B. Reed, and A. Das, "Handbook of Biomass Downdraft Gasifier Engine Systems", *SERI . U.S. Department of Energy*, no. March, p. 148, 1988. DOI: 10.2172/5206099.

[16] H. Knoef, R. Harald, G. Andreas, and R. M. Thomas, *Handbook Biomass Gasification*. BTG biomass technology group B.V, Meppel, 2005.

[17] P. Basu, "Combustion and gasification in fluidized beds. CRC Taylor & Francis.", 2006, Referenced in [83].

[18] K. B. Sutar, S. Kohli, and M. R. Ravi, "Design, development and testing of small downdraft gasifiers for domestic cookstoves", *Energy*, vol. 124, pp. 447–460, 2017, ISSN: 03605442. DOI: 10.1016/j.energy.2017.02.076.

[19] C. Diyoke, N. Gao, M. Aneke, M. Wang, and C. Wu, "Modelling of down-draft gasification of biomass – An integrated pyrolysis, combustion and reduction process", *Applied Thermal Engineering*, vol. 142, pp. 444–456, 2018, ISSN: 13594311. DOI: 10.1016/j.applthermaleng.2018.06.079.

[20] I. Narváez, A. Orio, J. Corella, and M. Aznar, "Gasification with air in an atmospheric bubbling fluidized bed: effect of six operational variables on the quality of the produced raw gas.", *Industrial & Engineering Chemistry Research*, 1996, Referenced in [83].

[21] W. Doherty, A. Reynolds, and D. Kennedy, "The effect of air preheating in a biomass CFB gasifier using ASPEN Plus simulation", *Biomass and Bioenergy*, vol. 33, no. 9, pp. 1158–1167, 2009, ISSN: 09619534. DOI: 10.1016/j.biombioe.2009.05.004.

[22] F. M. Guangul and S. A. Sulaiman, " Mitigation of the bridging problem in biomass gasification by a novel approach.", *Asian journal of scientific research*, 2013.

[23] M. G. A. Rubio and K. Jaojaruek, "Small-scale shaking single-stage downdraft biomass gasifier", *Proceedings of the 2016 International Conference on Cogeneration, Small Power Plants and District Energy, ICUE 2016*, no. September, pp. 1–5, 2016. DOI: 10.1109/COGEN.2016.7728949.

[24] S. Capper, Z. Khan, P. Kamble, J. Sharp, and I. Watson, "Progression towards Online Tar Detection Systems", *Energy Procedia*, vol. 142, no. December, pp. 892–897, 2017, ISSN: 18766102. DOI: 10.1016/j.egypro.2017.12.143.

[25] T. Milne, N. Abatzaglou, and R. Evans, "Combustion and gasification in fluidized beds. CRC Taylor & Francis.", 1998, National Renewable Energy Laboratory. Referenced in [1].

[26] L. M. Dion, "Biomass Gasification for Carbon Dioxide Enrichment in Greenhouses by", no. February, pp. 1–138, 2011, McGill University.

[27] C. Higman, "Syngas Database: 2017 Update", *Global Syngas Technologies Council*, vol. 7, no. 1, 2017, ISSN: 2045-2322. DOI: 10.1038/s41598-017-01767-4.

[28] J. Kiel, "Biomass gasification Beyond State of the Art", *ECN TNO*, vol. 21, no. 1, 2018, ISSN: 03027511.

[29] A. Molino, S. Chianese, and D. Musmarra, "Biomass gasification technology: The state of the art overview", *Journal of Energy Chemistry*, vol. 25, no. 1, pp. 10–25, 2016, ISSN: 20954956. DOI: 10.1016/j.jechem.2015.11.005.

[30] R. J. Bender, J. P. Tomasi, and B. M. Novisky, "Independent vector control system for gasification furnace", 2011, Patent Application Publication.

[31] W. P. Chan, A. Veksha, J. Lei, W. D. Oh, X. Dou, *et al.*, "A novel real-time monitoring and control system for waste-to-energy gasification process employing differential temperature profiling of a downdraft gasifier", *Journal of Environmental Management*, vol. 234, no. October 2018, pp. 65–74, 2019, ISSN: 10958630. DOI: 10.1016/j.jenvman.2018.12.107.

[32] LearnENGINEERING, "Brushed, brushless and induction motors", 2018. [Online]. Available: https://learnengineering.org/, (accessed: 20.6.2020).

[33] Tameson, "Solenoid valves", [Online]. Available: https://tameson.com/solenoid-valve-types.html, (accessed: 24.2.2020).

[34] P. Skousen, "Valve Handbook", vol. 101, no. 1988, pp. 1–436, 2004. DOI: 10.1002/pi. [Online]. Available: https://www.facebook.com/pages/Ebooks-Chemical-Engineering/238197077030.

[35] C. MGA, "Indirect solenoid valves", [Online]. Available: https://www.mgacontrols.com/products/valves/solenoid-valves/indirect-acting-solenoid-valves/, (accessed: 24.2.2020).

[36] Wermac, "Indirect solenoid valves", [Online]. Available: http://www.wermac.org/valves/valves_butterfly.html, (accessed: 24.2.2020).

[37] T. F. Control, "What is a needle valve", [Online]. Available: http://www.tc-fluidcontrol.com/about-us/blog-posts/what-is-a-needle-valve/, (accessed: 24.2.2020).

[38] Tameson, "Needle valves – function and selection criteria", 2019. [Online]. Available: https://www.engineeringclicks.com/needle-valves/.

[39] J. Monsen, "Part i: An insider's guide to valve sizing & selection", 2015. [Online]. Available: https://www.flowcontrolnetwork.com/instrumentation/flow-measurement/article/15562033/part-i-an-insiders-guide-to-valve-sizing-selection, (accessed: 24.2.2020).

[40] ——, "Part ii: An insider's guide to control valves & process variability", 2015. [Online]. Available: https://www.flowcontrolnetwork.com/instrumentation/flow-measurement/article/15562038/part-ii-an-insiders-guide-to-control-valves-process-variability, (accessed: 24.2.2020).

[41] ——, "Part iii: An insider's guide to installed gain as a control valve sizing criterion", 2015. [Online]. Available: https://www.flowcontrolnetwork.com/valves-actuators/article/15562236/part-iii-an-insiders-guide-to-installed-gain-as-a-control-valve-sizing-criterion, (accessed: 24.2.2020).

[42] ——, "Part iv: Keys to effective valve sizing & selection", 2015. [Online]. Available: https://www.flowcontrolnetwork.com/valves-actuators/article/15562441/part-iv-keys-to-effective-valve-sizing-selection, (accessed: 24.2.2020).

[43] P. Fonseca, "Sistemas de instrumentação electrónica", 2007, Universidade de Aveiro.

[44] Avnet, "Pressure Sensors : The Design Engineer ' s Guide.", pp. 1–3, 2019.

[45] M. Bao, "Micro mechanical transducers : pressure sensors, accelerometers and gyroscopes", no. 2, 2000.

[46] Variohm, "Load cells", [Online]. Available: https://www.variohm.com/, (accessed: 4.6.2020).

[47] AND, "How to Use Load Cells", pp. 1–6, 2012. [Online]. Available: https://www.aandd.jp/products/weighing/loadcell/introduction/pdf/6-1.pdf.

[48] D. W. Spitzer, *Industrial Flow Measurement*. International Society of Automation, 1990, ISBN: 1-55617-243-5.

[49] D. Stewart, H. Reader, and R. Peters, "Derivation of an expansability factor for the V-Cone meter", *Flow Measurement 2001 - International Conference*, 2000.

[50] Emerson, "Magnetic flow meters", [Online]. Available: https://www.emerson.com/en-us/automation/measurement-instrumentation/flow-measurement/about-magnetic.

[51] S. I. Lucid, "Lucidchart see more. know more. do more.", [Online]. Available: https://www.lucidchart.com/pages/landing, (accessed: 30.6.2020).

[52] Digilent Inc., "chipKIT™ Max32™ Board Reference Manual", 2011. [Online]. Available: http://www.digilentinc.com/Data/Products/CHIPKIT-MAX32/chipKIT%20Max32%7B%5C_%7Drm.pdf.

[53] G. Homsy, "ALL Power Labs GCU Manual", vol. 23, p. 11, 2009.

[54] I. Freescale Semiconductor, "MPXV7007DP Integrated Silicon Pressure Sensor On-Chip Signal Conditioned , Temperature Compensated and Calibrated", 2012.

[55] Ascell, "CFI-IP68 Datasheet", 2000.

[56] Vetec, "TA5 Digital Weighing transmitter Datasheet. ", [Online]. Available: http://digitalweighing.blogspot.com/2010/09/strain-gauge-how-does-it-work.html.

[57] AEP Transducers, "Optoinsulated RS232/RS485 Digital Transmitter TA5 Operating Manual", 2004.

[58] EBM, "RG130/0800-3612 Datasheet ", 2018.

[59] Farnell, "Rg130/0800-3612", [Online]. Available: https://de.farnell.com/ebm-papst/rg130-0800-3612/radialgebl-se-115m3-h-230v/dp/1781452, (accessed: 24.2.2020).

[60] Tameson, "Proportional valves and controllers", [Online]. Available: https://tameson.com/valves/solenoid-valve/proportional//connection_size-45x45_mm/, (accessed: 24.2.2020).

[61] Endress+Hauser, [Online]. Available: https://www.engineeringclicks.com/needle-valves/.

[62] NXP, "MPXV7002 Integrated Silicon Pressure Sensor On-Chip Signal Conditioned, Temperature Compensated and Calibrated", 2017.

[63] P. Vijay Daniel, A. Sanjeevi Gandhi, and R. Suresh, "Design and standardization of temperature measurement system for biomass downdraft gasifier", *Proceedings of IEEE International Conference on Innovations in Electrical, Electronics, Instrumentation and Media Technology, ICIEEIMT 2017*, vol. 2017-Janua, pp. 337–342, 2017. DOI: 10.1109/ICIEEIMT.2017.8116862.

[64] P. Kamble, Z. Khan, S. Capper, J. Sharp, and I. Watson, "Improving downdraft gasifier stability by robust instrumentation and control systems", *Energy Procedia*, vol. 142, pp. 2214–2217, 2017, ISSN: 18766102. DOI: 10.1016/j.egypro.2017.12.591.

[65] R. Mikulandrić, D. Lončar, D. Böhning, R. Böhme, and M. Beckmann, "Artificial neural network modelling approach for a biomass gasification process in fixed bed gasifiers", *Energy Conversion and Management*, vol. 87, pp. 1210–1223, 2014, ISSN: 01968904. DOI: 10.1016/j.enconman.2014.03.036.

[66] Maxim Integrated, "MAX31855 Cold-Junction Compensated Thermocouple-to-Digital Converter Datasheet", pp. 1–13, 2015. [Online]. Available: https://datasheets.maximintegrated.com/en/ds/MAX31855.pdf.

[67] P. Kamble, Z. Khan, M. Gillespie, J. McCalmont, I. Donnison, *et al.*, "Robust instrumentation and control systems for gasification of biomass", *European Biomass Conference and Exhibition Proceedings*, vol. 2018, no. 26thEUBCE, pp. 516–520, 2018, ISSN: 22825819.

[68] Inkscape, "INKSCAPE Draw freely ", [Online]. Available: http://digitalweighing.blogspot.com/2010/09/strain-gauge-how-does-it-work.html.

[69] T. Cunha, "Slides da Unidade Curricular de "Identificação de Sistemas"", 2018, Universidade de Aveiro.

[70] P. Basu, "Combustion and gasification in fluidized beds.", *CRC press*, 2006, Referenced in [1].

[71] T. K. Patra and P. N. Sheth, "Biomass gasification models for downdraft gasifier: a state-of- the-art review.", *Renew Sustain Energy*, 2015, Referenced in [1].

[72] W. S. Levine, M. Otter, and F. E. Cellier, "Software for Modeling and Simulating Control Systems", *Control System Fundamentals*, pp. 419–432, 2019. DOI: 10.1201/9781315214030-22.

[73] S. Jarungthammachote and A. Dutta, "Thermodynamic equilibrium model and second law analysis of a downdraft waste gasifier. ", *Energy*, 2007, Referenced in [12].

[74] H. Versteeg and W. Malalasekera, "An Introduction to Computational Fluid Dynamics, 2nd ed.", *Prentice Hall: London*, 2007, Referenced in [12].

[75] M. Oevermann, S. Gerber, and F. Behrendt, " Euler Lagrange simulati n of wood gasification in a bubbling fluidized bed reactor.", *Particuology*, 2009, Referenced in [87].

[76] T. Ismail and M. Sala, " Eulerian cfd model on fluidized bed gasifier using coffee husks as fuel. ", *Applied Thermal Engineering*, 2016, Referenced in [87].

[77] A. Sayigh, "5.05 - biomass co-firing. ", *Oxford: Elsevier*, 2012, Referenced in [87].

[78] S. Mahapatra, "Experiments and Analysis on Wood Gasification in an Open Top Downdraft Gasifier", *Indian Institute of Science Bangalore, India*, 2016.

[79] H. Hans, "Introduction to Simulink", pp. 175–208, 2007, Telemark University College. DOI: 10.2514/5.9781600861628.0175.0208.

[80] L. P. Oliveira, D. Hudebine, D. Guillaume, and J. J. Verstraete, "A Review of Kinetic Modeling Methodologies for Complex Processes", *Oil and Gas Science and Technology*, vol. 71, no. 3, 2016, ISSN: 19538189. DOI: 10.2516/ogst/2016011.

[81] G. Madan and R. Dandina, *Neuro-control Systems: Theory and Applications*. IEEE, 1993.

[82] J. Antunes, "Control of nonlinear systems with neural networks", 2019, Universidade de Aveiro.

[83] M. B. de Souza, L. Couceiro, A. G. Barreto, and C. P. B. Quitete, "Neural Network Based Modeling and Operational Optimization of Biomass Gasification Processes", *Gasification for Practical Applications*, no. February 2017, 2012. DOI: 10.5772/48516.

[84] R. Mikulandrić, D. Böhning, and D. Lončar, "Modelling of temperature and syngas composition in a fixed bed biomass gasifier using nonlinear autoregressive networks", *Journal of Sustainable Development of Energy, Water and Environment Systems*, vol. 8, no. 1, pp. 145–161, 2020, ISSN: 18489257. DOI: 10.13044/j.sdewes.d7.0263.

[85] J. Schoukens and L. Ljung, "Nonlinear System Identification: A User-Oriented Road Map", *IEEE Control Systems*, vol. 39, no. 6, pp. 28–99, 2019, ISSN: 1941000X. DOI: 10.1109/MCS.2019.2938121. arXiv: 1902.00683.

[86] F. Elmaz and Ö. Yücel, "Data-driven identification and model predictive control of biomass gasification process for maximum energy production", *Energy*, vol. 195, p. 117 037, 2020, ISSN: 03605442. DOI: 10.1016/j.energy.2020.117037.

[87] F. Elmaz, Ö. Yücel, and A. Y. Mutlu, "Predictive modeling of biomass gasification with machine learning-based regression methods", *Energy*, vol. 191, 2020, ISSN: 03605442. DOI: 10.1016/j.energy.2019.116541.

[88] R. Mikulandrić, D. Böhning, R. Böhme, L. Helsen, M. Beckmann, *et al.*, "Dynamic modelling of biomass gasification in a co-current fixed bed gasifier", *Energy Conversion and Management*, vol. 125, pp. 264–276, 2016, ISSN: 01968904. DOI: 10.1016/j.enconman.2016.04.067.

[89] L. Ljung, *System Identification: Theory for the User*. 1987, ISBN: 9783319042282.

[90] A. Rohatgi, "Webplotdigitizer web based tool to extract data from plots, images, and maps", [Online]. Available: https://automeris.io/WebPlotDigitizer/, (accessed: 4.6.2020).

[91] MathWorks, "Deep learning toolbox design, train, and analyze deep learning networks", [Online]. Available: https://www.mathworks.com/products/deep-learning.html, (accessed: 4.6.2020).

[92] M. K. Transtrum and J. P. Sethna, "Improvements to the Levenberg-Marquardt algorithm for nonlinear least-squares minimization", *ResearchGate*, 2012.

[93] Matlab, "Improve shallow neural network generalization and avoid overfitting", [Online]. Available: https://www.mathworks.com/help/deeplearning/ug/improve-neural-network-generalization-and-avoid-overfitting.html, (accessed: 4.6.2020).

[94] G. Heath, "How to decide size of neural network like number of neurons in a hidden layer & number of hidden layers?", [Online]. Available: https://www.mathworks.com/matlabcentral/answers/72654-how-to-decide-size-of-neural-network-like-number-of-neurons-in-a-hidden-layer-number-of-hidden-lay, (accessed: 4.6.2020).

[95] P. V. Daniel and A. S. Gandhi, "Enhanced Conventional PID controller for Temperature Control in Woody Gasifier using Searching Algorithms.", *International Journal of Innovative Technology and Exploring Engineering (IJITEE)*, no. 4, pp. 438–442, 2019.

[96] R. K. Al Seyab and Y. Cao, "Nonlinear model predictive control for the ALSTOM gasifier benchmark problem", *IFAC Proceedings Volumes (IFAC-PapersOnline)*, vol. 16, no. 8, pp. 69–74, 2005, ISSN: 14746670. DOI: 10.3182/20050703-6-cz-1902.01587.

[97] M. Ławryńczuk, *Studies in Systems, Decision and Control 3 Computationally Efficient Model Predictive Control Algorithms A Neural Network Approach*. Springer, ISBN: 9783319042282.

[98] MathWorks, "Optimization toolbox solve linear, quadratic, integer, and nonlinear optimization problems", [Online]. Available: https://www.mathworks.com/products/optimization.html, (accessed: 4.6.2020).

[99] ——, "Lsqnonlin solve nonlinear least-squares (nonlinear data-fitting) problems", [Online]. Available: https://www.mathworks.com/help/optim/ug/lsqnonlin.html, (accessed: 4.6.2020).

[100] N. Mayorov, "Trust region reflective algorithm", [Online]. Available: https://nmayorov.wordpress.com/2015/06/19/trust-region-reflective-algorithm/, (accessed: 4.6.2020).

[101] M. A. Branch, T. F. Coleman, and Y. Li, "Subspace, interior, and conjugate gradient method for large-scale bound-constrained minimization problems", *SIAM Journal of Scientific Computing*, vol. 21, 1999, ISSN: 10648275. DOI: 10.1137/S1064827595289108.

[102] MathWorks, "Constrained nonlinear optimization algorithms", [Online]. Available: https://www.mathworks.com/help/optim/ug/constrained-nonlinear-optimization-algorithms.html, (accessed: 4.6.2020).

[103] E. F. Camacho and C. Bordons, *Model Predictive Control in the Process Industry*. Springer London, 1995.

[104] J. Rossiter, "Generalized predictive control/ model predictive control", [Online]. Available: https://www.youtube.com/watch?v=ahQFWHUotYg&list=PLs7mcKy_nInGiG2er-vTC--VinZX9Cjlw, (accessed: 10.5.2020).

[105] Alireza, H. Sadjadian, A. Khaki-Sedigh, and A. Jazayeri, *Disturbance Rejection in Neural Network Model Predictive Control*, 2. IFAC, 2008, vol. 41, pp. 3527–3532, ISBN: 9783902661005. DOI: 10.3182/20080706-5-kr-1001.00596.

[106] M. La Villetta, M. Costa, and N. Massarotti, "Modelling approaches to biomass gasification: A review with emphasis on the stoichiometric method. ", *Renewable and Sustainable Energy Reviews*, 2017, Referenced in [12].

[107] J. Smith, "Chemical engineering kinetics ", *London: McGraw Hill*, 1891, Referenced in [10].

[108] S. Ergun, "Fluid flow through packed columns ", *Industrial & Engineering Chemistry Research*, 1952, Referenced in [10].

APPENDIX A

Appendix A

A.1 Thermodynamic Equilibrium Model Assumptions

The several assumptions made in equilibrum modelling were resumed and enumerated in [106]:

- Steady state;
- Reactions reach the equilibrium state (infinite residence time);
- Homogeneous mixing with uniform pressure and temperature;
- Kinetic and potential energies are neglected;
- Perfect gas behavior of the gas phase;
- Pyrolysis is considered a single step reaction producing gas, tar and char;
- Gasifying medium is enough to convert all carbon of the biomass;
- The gasifier operates at constant pressure and temperature;
- The reactor is considered adiabatic
- The produced gas does not contain oxygen;
- Nitrogen is considered as inert;
- Solely major species compose the produced gas (CO, H2, CO2, CH4, N2 and H2O);
- Tar is not modeled in the gas phase;
- Ashes are not considered in energy balances.

A.2 Stoichometric Approach

The main products of gasification are formed by H_2, CO, CO_2, CH_4, H_2O and N_2. The overall reaction of gasification can be defined as:

$$CH_xO_yN_z+wH_2O+m(O_2+3.7N_2) \rightarrow n_1H_2+n_2CO+n_3H_2O+n_4CO_2+n_5CH_4+n_6N_2 \quad \text{(A.1)}$$

Where:

- n_1 to n_6 are stoichometric coefficients;
- $CH_\alpha O_\beta N_\gamma S_\delta$ is the biomass' composition;
- x is the molar moisture amount in biomass;
- y is moles or air.

Some variations of this formula exist which try to incorporate other elements, e.g, the amount of N_2 in the gasifying agent may be featured as variable, tar content can be portrayed as a molecule by including C_6H_6 or $CH_{1.003}O_{0.33}$ in the reaction [9] or biomass composition may include sulfur. All coefficients can be obtained by ultimate analysis.

Mass balance equations, for equation A.1, may be written as follows:

$$C : n_2 + n_4 + n_5 = 0 \quad \text{(A.2)}$$

$$H : 2n_1 + 2n_3 + 4n_5 = x + 2w \quad \text{(A.3)}$$

$$O : n_2 + n_3 + 2n_4 = y + w + 2m \quad \text{(A.4)}$$

$$N : 2n_6 = z + 7.52m \quad \text{(A.5)}$$

The resulting systems has more variables than equations and therefore cannot be solved. The solution for this is to add the equilibrium constant definition pertaining to some of the most important linearly independent reactions. The common choices are: the boudouard (eq2.6), water-gas (eq2.7), methane formation (eq2.9), water-gas shift (eq2.8) and methane reforming reactions (eq2.10).

Given a reaction:

$$aA + bB \Longleftrightarrow cC + dD \quad \text{(A.6)}$$

the equilibrium constant Kc is defined as follows:

$$K_c = \frac{C_C^c C_D^d}{C_A^a C_B^b} \quad \text{(A.7)}$$

Where C refers to concentration of a species at equilibrium.

Only two reactions are needed to solve the system and they should be chosen taking into account the composition of the biomass used.

Combining the two sets of equations, syngas composition for a given equivalence ratio may be calculated.

The final step is the calculation of gasification temperature. By considering the process is adibiatic, this is achieved trough the energy balance equation shown below. .

$$\sum_i n_i[h^0_{f,i} + \Delta H^T_{298}]_{i,reactants} = \sum_i n_i[h^0_{f,i} + \Delta H^T_{298}]_{i,products} \tag{A.8}$$

Where:

- $h^0_{f,i}$ is the enthalpy of the formation of species i;
- H_i is the standart enthalpy of formation at temperature i.

Considering the enthalpy of formation of O_2, H_2 and N_2 are zero at ambient temperature, the energy balance and the gasification reaction may be combined to form:

$$h^0_{f,biomass} + w(h^0_{f,H_2O} + h_vap) = n_2 h^0_{f,CO} + n_3 h^0_{f,H_2O} + n_4 h^0_{f,CO_2} + n_5 h^0 f, CH_4 + n_6 h^0_{f,N_2} + \Delta T(n_1 c_{p,H_2} + n_2 c_{p,CO} n_3 c_{p,H_2O} + n_4 c_{p,CO_2} + n_5 c_{p,CH4} + n_6 c_{p,N_2}) \tag{A.9}$$

Where:

- h_{vap} is the enthalpy of the vaporization of water;
- c_p is the specific heat;
- ΔT is the difference between gasification and ambient temperature.

A.3 Non-Stoichometric Approach

This method starts differing from the previously described one past the definition of the overall gasification reaction. As so, the same mass balance equations are used. None of the more specific chemical reactions are used in this method, hence the name non- stoichometric. This makes this subcategory of models especially useful when all the equations that describe the gasification process are not known. The atom balance of the reactants is the basis for the calculation of syngas composition, and so, biomass with unknown molecular formula can also be handled.[12]

As mentioned in the beginning of this Chapter, this category solves the mass balance systems by factoring in the minimization of Gibbs free energy, G_{total}, which is given by:

$$G_{total} = \sum_{i=1}^{N} n_i \Delta G^0_{fi} + \sum_{i=1}^{N} n_i RTln(\frac{ni}{\sum ni}) \tag{A.10}$$

Where ΔG^0_{fi} is the standard Gibbs free energy of formation of species i, at its normal pressure and N is the number of species involved.

And we can define the number of atoms, A, in species j as:

$$A_j = \sum_{i=1}^{N} a_{i,j} n_i, j = 1, 2, 3, ...K \tag{A.11}$$

The objective now is to minimize G_{total} and that can be achieved trough several algorithms, among which, Lagrange multipliers is known to provide satisfactory results.

The following Lagrange function, L, can be written:

$$L = G_{total} - \sum_{j=1}^{K} \lambda_i (\sum_{i=1}^{N} - A_i) \tag{A.12}$$

The extreme point may then be calculated by replacing G_{total} in equation 12 with equation 10, and setting the partial derivative to zero.

$$\frac{\partial L}{\partial n_i} = 0 \leftrightarrow \frac{\Delta G^0_{f,i}}{RT} + \sum_{i=1}^{N} ln(\frac{n_i}{n_{total}}) + \frac{1}{RT} \sum_{J=1}^{K} \lambda_i (\sum_{i=1}^{N} a_{ij} n_i) = 0 \tag{A.13}$$

The equation may be solved iteratively by setting an initial temperature.

A.4 Arrhenius Equation

Another frequent practice is the use of the Arrhenious equation to solve the mass balance system. This equation features the incorporation of temperature and Gibbs energy in the calculus of the equilibrium constants. By doing this the need to use energy balance equations in stoichometric models is forfeit.[9]

It can be defined as:

$$K_C = e^{\frac{-\Delta G^0_T}{RT}} \tag{A.14}$$

Where R is the universal gas constant and ΔG^0_T is the Gibbs free energy of formation. The rate constant may then be replaced into equation A.7 in order to solve the equation. The mass balance system previously shown would now require three gasification reactions instead of two the accommodate the addition of the Temperature unknown.

APPENDIX B

Appendix B

B.1 Kinectic Model Implementation

The reaction rate, $mol\,l^{-1}s^{-1}$ is the amount of substance that forms per unit of time and volume in a chemical reaction.

A high concentration of species will lead to a higher amount collisions, hence the dominant factor in reaction rate is the reagent concentration. Any of the aforementioned variables may be factored in the calculus of reaction rates. The most common is temperature which can be incorporated with the Arrhenius equation, equation A.14, resulting in the following rate law definition.

$$r = k(T)C_A^m C_B^n \tag{B.1}$$

where:

- K(T) is the equilibrium constant calculated by the Arrhenius equation;
- C_A and C_B are the concentration of the reaction reagents;
- m and n are reaction orders dependent on the reaction mechanism.

Many reactions take place in heterogeneous systems rather than in a single homogeneous phase. In these cases it is best to define reaction rate in terms of the surface area available for the reaction, and mass transfer.

For gasification systems reaction rates of heterogeneous reactions calculated as descibred by Smith [107] using the following equation:

$$r = \frac{C_i}{\frac{1}{k_m a_p} + \frac{1}{k_j}} \tag{B.2}$$

where:

- k_m is the mass transfer coefficient;

- a_p is the surface area;
- k_j is the enthalpy of reaction j.

Rate equation should be written for all, or a subset of the the chemical equations present in gasification, described in Chapter 2.

The next step is the definition of a system of governing equations. In order to showcase this procedure, an example of the simplest, time-independent and one dimensional case developed by A.Chaurasia [10] for a downdraft two-stage hot-rod reactor will be analysed.

Assuming a cilindrical reactor with cross sectional are A_r and considering a thin cross section Δz along the length, z, of the gasifier, the mass balance of species can be written as:

$$C_{i(z+\Delta z)} A_r v_{g(z+\Delta z)} - C_{i(z)} A_r v_{g(z)} = R'_i A_r \Delta z \tag{B.3}$$

Where:

- C_i is the molar concentration of species i, $mol\, m^{-3}$;
- $v_{:}g$ is the superficial gas velocity, $m\, s^{-1}$,
- R'_i is the net rate of production of species i by chemical reactions, $mol\, m^{-3}\, s^{-1}$.

Using equation B.3 the conservation equations are written as differential equations for each of the modeled species. An example conservation equations is shown for the concentration of H2, C_{H_2}, in equation B.4.

$$v_g \frac{1}{a} \frac{\partial C_{H_2}}{\partial z} = -C_{CO_2} \frac{\partial v_g}{\partial z} - 2r_1 + r_2 + r_3 - 2r_4 \tag{B.4}$$

Where:

- v_g is superficial gas velocity, ms^{-1};
- r_1 to r_4 are reaction rates of the combustion reaction (eq2.5), water-gas shift (eq2.8), water-gas (eq2.7) and methane formation (eq2.9) respectively.

It should be noted that the plus or minus sign anticipating each reaction reaction denotes that the species is, respectively, a product or reagent of the reaction, and the constant by which it is multiplied denotes its stoichometric coefficient in the reaction.

Assuming $\Delta z \xrightarrow{0}$, energy balance may be described by the following equation.

$$(v_g \sum_i C_i c_{pi}) \frac{\partial T_g}{\partial z} = -\sum_j r_j \Delta H_j - v_g \frac{\partial P}{\partial z} - P \frac{\partial v_g}{\partial z} - \sum_i R'_i c_{pi} T_g - \frac{4 h_{gw}}{D_r} (T_g - T_w) \tag{B.5}$$

Where:

- $v_{:}g$ is the superficial gas velocity, $m\,s^{-1}$;
- C_i is the molar concentration of species i, $mol\,m^{-3}$;
- c_{pi} is the specific heat of species i, $J\,kg^{-1}\,K^{-1}$;
- T_g is the gas' temperature, K;
- r_j is the reaction rate of reaction j, $mol\,m^{-3}\,s^{-1}$;
- ΔH_j Is the enthalpy of reaction j, units are variable and not specified in the paper;
- P is pressure, Pa;
- R'_i is the net rate of production of species i by chemical reactions, $mol\,m^{-3}\,s^{-1}$;
- h_{gw} is the gas/wall heat transfer coefficient, $W\,m^{-2}\,K^{-1}$;
- Dr is the reactor diameter, m;
- T_w is the gasifier's walls temperature,K.

To solve B.5 the expressions for $\frac{\partial P}{\partial z}$ and $\frac{\partial P}{\partial z}$ are needed.

The dependency of the pressure gradient with superficial gas velocity was defined in [108] trough the following correlation.

$$-\frac{\partial P}{\partial z} = \frac{150\mu(1-\epsilon)^2}{d_p^2\epsilon^3}v_g + \frac{1.75C_g(1-\epsilon)^2}{d_p^2\epsilon^3}v_g^2 \tag{B.6}$$

Where:

- μ is viscosity, $k_G\,m^{-1}\,s^{-1}$;
- ϵ is porosity;
- d_p is particle diameter, m;
- C_g is the sum of the different species' concentration, $mol\,m^{-3}$;
- v_g is the superficial gas velocity, $m\,s^{-1}$.

The gradient of superficial gas velocity is descibed by eq6.23.

$$\begin{aligned}\frac{\partial v_g}{\partial z} = \frac{1}{C_gR_g + \sum_i C_ic_{pi}}\Bigg[&-\frac{\sum_j r_j\Delta H_J}{Tg} - \frac{\partial P}{\partial z}\left(\frac{v_g}{T_g} + \frac{v_g\sum_i C_ic_{pi}}{P}\right)\\ &+\frac{\sum_i C_ic_{pi}\sum_i R'_i}{C_g} - \sum_i R'_ic_{pi} - \frac{4h_{gw}(T_g - T_w)}{D_rT_g}\Bigg]\end{aligned} \tag{B.7}$$

Where:

- v_g is the superficial gas velocity, $m\,s^{-1}$;
- C_g is the sum of the different species' concentration, $mol\,m^{-3}$;
- R_g is the universal gas constant, $J\,mol^{-1}\,K^{-1}$;
- C_i is the molar concentration of species i, $mol\,m^{-3}$;
- c_{pi} is the specific heat of species i, $J\,kg^{-1}\,K^{-1}$;
- r_j is the reaction rate of reaction j, $mol\,m^{-3}\,s^{-1}$;
- ΔH_j Is the enthalpy of reaction j, units are variable and not specified in the paper;
- T_g is the gas' temperature, K;
- P is pressure, Pa;
- R_i' is the net rate of production of species i by chemical reactions, $mol\,m^{-3}\,s^{-1}$;
- h_{gw} is the gas/wall heat transfer coefficient, $W\,m^{-2}\,K^{-1}$;
- Dr is the reactor diameter, m;
- T_w is the gasifier's walls temperature,K.

Finally the system formed by all of the conservation equations, energy balance, superficial gas velocity gradient and pressure gradient must by solved by a differential equation solver.